

# Evaluating Human Electromagnetic Exposure in a UAV-aided Network

Thomas Detemmerman

Student number: 01707806

Supervisors: Prof. dr. ir. Wout Joseph, Prof. dr. ir. Luc Martens

Counsellors: Dr. ir. Margot Deruyck, German Dario Castellanos Tache

Master's dissertation submitted in order to obtain the academic degree of  
Master of Science in Information Engineering Technology

Academic year 2019-2020



## Acknowledgement

I would like to thank Prof. dr. ir. Wout Joseph, Prof. dr. ir. Luc Martens and Dr. ir. Margot Deruyck for providing me access to their capacity based deployment tool which allowed me to complete my research regarding electromagnetic exposure but also for helping me to map the road of my research. Further I would like to express my gratitude to MPhil German Dario Castellanos Tache who followed up my weekly progress by providing answers to questions or problems I had and gave me extensive feedback and suggestions to the results I booked. I would also like to show my deepest appreciation towards mrs Carine Lambrecht and miss Anke Blommaert for taking a second - and even a third - eye on the linguistic part of this document but also for the general mental support during this journey making this entire degree possible, allowing me to stand where I am today.

*The author(s) gives (give) permission to make this master dissertation available for consultation and to copy parts of this master dissertation for personal use. In all cases of other use, the copyright terms have to be respected, in particular with regard to the obligation to state explicitly the source when quoting results from this master dissertation.*

# Evaluating Human Electromagnetic Exposure in a UAV-aided Network

by Thomas Detemmerman

Master's dissertation submitted in order to obtain the academic degree of Master of Science in  
Information Engineering Technology industriële wetenschappen: informatica  
Academiejaar 2019-2020

Supervisors: Prof. dr. ir. Wout Joseph, Prof. dr. ir. Luc Martens  
Counsellors: Dr. ir. Margot Deruyck, MPhil. German Dario Castellanos Tache  
Faculty of engineering and architecture  
Ghent University

## Abstract

Society relies more than ever on the availability of wireless networks. Due to the mobility of a UAV, a UAV-aided network is able to provide this necessary access in case the existing terrestrial network gets damaged. However, the public is concerned about the potential health effects of the electromagnetic radiation caused by these networks. Therefore, mobile devices and base stations have to comply to strict legislation enforced by the government.

This research investigates how different scenarios influence power consumption, electromagnetic exposure and specific absorption rate. These different scenarios are defined by various flying heights, number of UAVs available and population densities. Further, also an analysis on the difference between a realistic microstrip patch antenna and a fictional equivalent isotropic radiator is performed. Thereafter, the network will be optimized towards goals like electromagnetic exposure of the average user or power consumption of the entire network; which results in conflicting requirements.

To accomplish this goal, a capacity based deployment tool will be used which simulates an entire UAV-aided network. In this way, all important sources for electromagnetic radiation, like all user equipment and all flying base stations, will be considered.

It looks from the results that a power consumption optimized network with a fixed flying height of 80 metres is the recommended approach for the city centre of Ghent. A microstrip patch antenna with a sufficiently large aperture angle is a good starting point. However, different antenna array configurations still have to be investigated.

## Keywords

deployment tool, electromagnetic exposure, LTE microstrip patch antenna, power consumption, radiation pattern, specific absorption rate (SAR), UAV, unmanned aerial base stations

# **Evaluatie van de electromagnetische blootstelling van de mens in een netwerk van drones**

door

Thomas Detemmerman

Masterproef ingediend tot het behalen van de academische graad van Master of Science in de  
industriële wetenschappen: informatica  
Academiejaar 2019-2020

Promotoren: Prof. dr. ir. Wout Joseph, Prof. dr. ir. Luc Martens

Begeleider: Dr. ir. Margot Deruyck, MPhil. German Dario Castellanos Tache

Faculteit Ingenieurswetenschappen en architectuur

Universiteit Gent

## **Samenvatting**

TODO: Ook updaten op plato TODO: Translate

## **Trefwoorden**

LTE, electromagnetische blootstelling, energieverbruik, drone, femtocell, microstrip patch antenna, stralingspatronen, specific absorption rate (SAR)

# Evaluating Human Electromagnetic Exposure in a Unmanned Aerial Vehicle (UAV)-aided Network

Thomas Detemmerman

Supervisor(s): Prof. dr. ir. Wout Joseph, Prof. dr. ir. Luc Martens

**Abstract**—Society relies more than ever on the availability of wireless networks. Due to the mobility of a UAV, a UAV-aided network is able to provide this necessary access in case the existing terrestrial network gets damaged. However, the public is concerned about the potential health effects of the electromagnetic radiation caused by these networks. Therefore, mobile devices and base stations have to comply to strict legislation enforced by the government.

This research investigates how different scenarios influence power consumption, electromagnetic exposure and specific absorption rate. These different scenarios are defined by various flying heights, number of UAVs available and population densities. Further, also an analysis on the difference between a realistic microstrip patch antenna and a fictional equivalent isotropic radiator is performed. Thereafter, the network will be optimized towards goals like electromagnetic exposure of the average user or power consumption of the entire network; which results in conflicting requirements.

To accomplish this goal, a capacity based deployment tool will be used which simulates an entire UAV-aided network. In this way, all important sources for electromagnetic radiation, like all user equipment and all flying base stations, will be considered.

It looks from the results that a power consumption optimized network with a fixed flying height of 80 metres is the recommended approach for the city centre of Ghent. A microstrip patch antenna with a sufficiently large aperture angle is a good starting point. However, different antenna array configurations still have to be investigated.

**Keywords**—deployment tool, electromagnetic exposure, LTE microstrip patch antenna, power consumption, radiation pattern, specific absorption rate (SAR), UAV, unmanned aerial base stations

## I. Introduction

SOCIETY is constantly getting more and more dependent on wireless communication. On any given moment, in any given location, an electronic device can request to connect to the bigger network, starting from small Internet of Things (IoT) up to self-driving cars.

Also in exceptional and possibly life threatening situations, the public relies on the cellular network despite the fact that the network might be severely damaged and not properly functioning anymore. One solution for a fast temporarily deployable back-up network is to use UAVs. A base station can be attached to these flying UAVs to support the network over a limited area. This approach is also useful in case of an unexpected increase in traffic. For example during the terrorist attacks at Brussels Airport, mobile network operators saw all telecommunications drastically increasing causing moments of contention. Some operators even decided to temporarily exceed the exposure limits in order to handle all connections [1]. Electromagnetic exposure caused by these networks can however not be neglected. Research shows how excessive electromagnetic radiation can cause diverse biological side effects [2], [3]. It becomes clear that electromagnetic exposure is a key value when designing a UAV-aided network and should def-

initely not surpass the limits predefined by the government.

UAV-aided networks can, thanks to their mobility, easily be repositioned towards a certain goal. Several papers explain how a network can be optimized towards different goals like power consumption. However, very limited research has been done where a UAV-aided network is optimized towards electromagnetic exposure. While several publications exist, discussing how the electromagnetic exposure can be calculated, most of them only consider a limited number of sources; e.g. only base stations or only the user's mobile device. Papers who cover electromagnetic exposure from all the different sources and convert it into a single value are rather limited.

This research proposes a method to optimize the network towards electromagnetic exposure and power consumption when considering all four sources of radiation in a telecommunications network, being: the user's own phone, the base station that is serving this user, all devices from other users in the network and all other active base stations that are not serving this user. In this way, the contribution of each source towards the total electromagnetic exposure can easily be identified.

The behaviour of the electromagnetic exposure and power consumption of the network will be analysed by applying the tool in different scenarios by using different types of antennae, various flying height and population densities. Values like Specific Absorption Rate (SAR), electromagnetic exposure and power consumption will give insight in how the network behaves so the network could be optimized accordingly.

To make this research possible, an existing capacity based deployment tool developed by the WAVES research group at Ghent University is extended for the specific purpose. This planning tool describes a fully configured UAV-network which is a suitable starting point for this research.

## II. State of the Art

### A. Electromagnetic exposure

Users in a telecommunication network are exposed to various sources of electromagnetic radiation, expressed in  $V/m$ . Once the exposure is absorbed by the human body, we speak of the specific absorption rate (SAR) which is expressed in  $W/kg$ . All these values are subjected to limitations enforced by the government. This research is based in Ghent, a Flemish city in Belgium where the 2.6 GHz frequency band, an individual antenna cannot exceed 4.5  $V/m$  and the cumulative sum of all fixed sources has its

maximum at 31 V/m [4], [5]. The maximum whole body SAR-values for a mobile device over a 10 g tissue ( $SAR_{10g}$ ) is defined at  $2W/kg$  [6].

Several papers calculate exposure originating from specific sources [7], [8], [9], [10] where some convert the up-link (UL) radiation into localized specific absorption rates [9], [10]. With the advent of 5G, paper [11] describes how the localized SAR-values are achieved from all different sources. Finally, [12] describes how the electronic radiation can be converted into whole body SAR values.

In a realistic network, some users are calling while others are using other types of telecommunication services like browsing the web. Therefore, all absorbed electromagnetic exposure should be expressed in whole body SAR while still covering all sources.

## B. Optimized UAV-aided networks

A UAV knows several applications. It was originally mainly used to support the military for surveillance and remote attacks without endangering pilots [13]. However, UAVs have recently become more accessible by the general public due to decreasing costs. This allowed UAVs to be researched for various applications.

A UAV equipped with a femtocell base station antenna is called a Unmanned Arial Base Station (UABS) which brings several advantages like mobility and rapid deployment. However, it brings also challenges like limited weight of the payload and sparse power supply.

Kawamoto et al. introduced in [14] a WiFi network with the support of UAVs while considering resource allocation and antenna directivity. Gangula et al. illustrates in [15] how UAVs can be used as a relay for Long-Term Evolution (LTE) and Zeng et al. proposes in [13] a tutorial in 5G-and-beyond wireless systems where challenges like energy consumption, mobility and antenna direction are discussed. In [16], Deruyck et al. designed a capacity based deployment tool for UAV-aided emergency networks for large-scale disaster scenarios where an ideal flying height of 100 m is suggested. This was expanded in [17] with a performance evaluation of the direct-link backhaul of this tool where a slightly lower flying height of 80 metres is recommended.

Mozaffari et al. provides in [18] guidelines on how to optimize and analyse UAVs equipped for wireless communication equipment. A research area that has been excessively studied is the location solution optimization problem where networks are designed in such a way that certain goals like minimal power consumption or shortest flying distance are achieved [19], [20], [21], [22]. These optimizations can be done through different implementation methods like exact algorithms or machine learning [18], [23].

Research where network is optimized towards electromagnetic exposure is rather limited. Deruyck et al. discusses in [8] how a terrestrial network can be optimized towards either a minimal exposure or minimal power consumption of the entire network. However, to the best of the author knowledge, no research has been done where a UABS-network has been optimized towards electromagnetic exposure.

## C. Technologies

For the deployment of the network, the more robust UAV from [16] will be used (details in table II) and will be operating in the 2.6 GHz bandwidth. Since the users are assumed to experience a constant electromagnetic exposure without interruptions, frequency division duplex is used.

The onboard antenna of the UAV will act as the gateway between the UE and the backhaul network. However, determining which antenna to use and how to position it, can be challenging. The radiation pattern from the antenna can be influenced by the UAV [24]. Also the fact that the UAV will hover above the user makes traditional 2D modelling insufficient. A 3D-model which accounts for both elevation and azimuth directivity will be required [13].

The easiest radiation pattern is a hypothetical isotropic radiator which radiates equally in all directions. Antennae that radiate equal quantities for a certain plane are called omnidirectional antennae [13] and several UABSs use antennae like monopoles, dipoles and wing antennae [25], [26], [27], [28]. Another type of antennae are directional antennae which save energy by focussing the electromagnetic energy where it is needed. One type that has excessively been researched in various array-configurations is a microstrip patch antenna [29], [30], [31]. These provide several advantages compared to traditional antennae [32], [33] like lightweightness and being low in cost, causing them to be more aerodynamic.

A basic microstrip antenna consists of a ground plane and a radiating patch, both separated by a dielectric substrate. Several variations exist like microstrip patch antennae, microstrip slot antennae and printed dipole antennae which all have similar characteristics [32], [33]. They all are thin, support dual frequency operation and they all have the disadvantage that they will transmit at frequencies outside the aimed band which is also known as spurious radiation. The microstrip patch and slot antenna support both linear and circular polarization while the printed dipole only supports linear polarization. Further, the fabrication of a microstrip patch antenna is considered to be the easiest of the considered patch antennae [32].

Figure 1 shows a microstrip patch antenna constructed out of an aluminium patch and a teflon substrate. The microstrip patch antenna is pointing towards the ground since the UAV will be flying above the user.

## III. Methodology

### A. Electromagnetic Exposure

#### A.1 Total Electromagnetic Exposure

The total whole body SAR ( $SAR_{10g}^{wb, total}$ ) of a user can be calculated by a simple sum of individual SAR values from the different sources and is based on [11]. This formula assumes that the users are holding their device next to their ear and therefore investigates localized SAR for head and torso area. However for this case, this would result into incorrect conclusions since the position of the device relative to the user is unknown. The position of the phone can

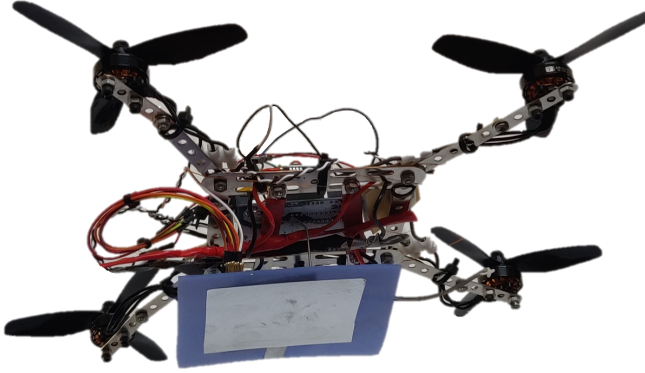


Fig. 1: Image of a microstrip patch antenna attached to the bottom of a UAV.

be next to the head but also in front of the user. The induced electromagnetic radiation will therefore be expressed in function of the entire body.

$$\begin{aligned} SAR_{10g}^{wb,\text{total}} = & SAR_{10g}^{wb,\text{myUE}} + SAR_{10g}^{wb,\text{myUABS}} \\ & + SAR_{10g}^{wb,\text{otherUE}} + SAR_{10g}^{wb,\text{otherUABSS}} \end{aligned} \quad (1)$$

The first parameter,  $SAR_{10g}^{wb,\text{myUE}}$ , indicates the absorbed electromagnetic radiation by the whole body originating from the user's own device. Despite that the UL radiation is destined for the serving UABS, a portion of that radiation is directly absorbed by its user, due to the omnidirectional nature of the mobile's antenna. The second parameter,  $SAR_{10g}^{wb,\text{myUABS}}$ , represents the downlink (DL) radiation caused by the UABS that is serving the user. As the third parameter, we have the  $SAR_{10g}^{wb,\text{otherUE}}$  which is radiation caused by other people's devices. The radiation of these devices is once again destined for a specific UABS but again, a portion of that UL radiation will also be absorbed by our user. Finally,  $SAR_{10g}^{wb,\text{otherUABSS}}$  represents the DL radiation by the other UABSSs to which our user is exposed to but not served by. An illustration is given in figure 2. The green arrow stands for near-field radiation, the others represent far-field radiation.

#### A.2 Electromagnetic Radiation from a Single Source

Calculating far-field exposure in a certain point needs to be done for all UABSSs and UE, except for the device present in that specific point which will be near-field radiation and has to be calculated differently. The exposure  $E$  of a single user  $u$  from a single radiator  $i$  can be calculated as follows.

$$E_i(u)[V/m] = 10^{\frac{RRP(u)[dBm] - 43.15 + 20 * \log(f[MHz]) - PL(u)[dB]}{20}} \quad (2)$$

Calculating the real radiation power (RRP) for a certain user  $u$ , requires first the equivalent isotropic radiation power (EIRP)-value to be calculated [7], [8]. This is achieved by adding the transmission power  $P_{tx}$  to the

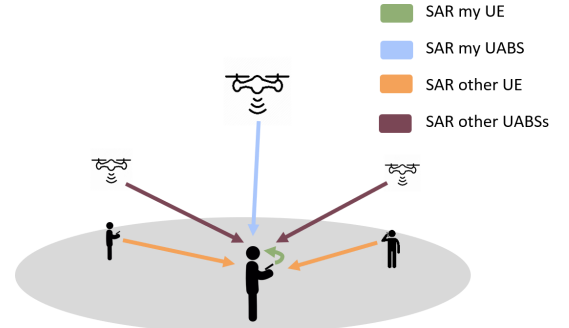


Fig. 2: Illustration of the network that shows how the average user (here shown in the center) is influenced by different types of sources.

transmitter gain  $G_t$  and thereafter subtracting the feeder loss  $L_t$ . This formula needs to be expanded to also account for attenuation from the used antenna. This value depends on the angle between this user and the antenna's main beam. The attenuation from an equivalent isotropic radiator is always zero. This leads to the following formula.

$$\begin{aligned} RRP[dBm] = & P_{tx}[dBm] + G_t[dbi] - L_t[dB] \\ & - \text{attenuation}(u)[dB] \end{aligned} \quad (3)$$

The used frequency in formula 2 is denoted as  $f$  and is expressed in MHz. Since LTE is used, this value will be 2600 MHz.

At last, formula 2 requires the path loss  $PL$ . In order to calculate this, an appropriate propagation model — of which several exist — is required. The Walfish-Ikegami model is used since it performs well for femtocell networks in urban areas [16].

#### A.3 Combining Exposure

The total electromagnetic exposure  $E_{tot}$ , in a certain spot, originating from different sources can be calculated with formula 4.  $E_i$  stands for the electromagnetic exposure from source  $i$  and  $n$  stands for all far-field radiators of a certain category which will either be UABSSs or UE from other people.  $E_{tot}$  will be calculated for each location where a user is positioned.

$$E_{tot}[V/m] = \sqrt{\sum_{i=1}^n (E_i[V/m])^2} \quad (4)$$

#### A.4 Converting electromagnetic radiation into SAR-values

Formula 1 expects that the radiation is expressed in whole body SAR-values. To make this calculation possible, a distinction has to be made between near-field SAR ( $SAR^{wb,nf}$ ) and far-field SAR ( $SAR^{wb,ff}$ ).  $SAR_{10g}^{wb,\text{myUABS}}$  is a form of near-field radiation, all the other types are far-field radiation.

Converting the electromagnetic radiation is done with a conversion factor which is based on Duke of the Virtual

Family. Duke is a 34-year old male with a weight of 72 kg, a height of 1.74 m and body mass index of 23.1 kg/m [12]. Research shows that the conversion factor for WiFi in the far-field is  $0.0028 \frac{W/kg}{W/m^2}$  and  $0.0070 \frac{W/kg}{W}$  for the near-field [12]. Since WiFi, at a frequency of 2400 MHz, is very close to LTE, at 2600 MHz, it is assumed in [12] that this value is also applicable for LTE. Calculating SAR from far-field radiation is done as follows.

$$S[W/m^2] = \frac{(E_{tot}[V/m])^2}{337} \quad (5)$$

$$SAR_{10g}^{wb,ff}[W/kg] = S[W/m^2] * 0.0028 \left[ \frac{W/kg}{W/m^2} \right] \quad (6)$$

The constant in equation 6 converts the power flux density  $S$  to the required  $SAR_{10g}^{ff,wb}$ . To make this possible, the electromagnetic radiation from formula 4 should first be converted to the power flux density with formula 5.

The SAR caused by near-field radiation is calculated by multiplying the constant with the used transmission power  $P_{tx}$  of the User Equipment (UE) which results to the following formula.

$$SAR_{10g}^{wb,nf} \left[ \frac{W}{kg} \right] = 0.0070 \left[ \frac{W/kg}{W} \right] * P_{tx}[W] \quad (7)$$

The power of the UE can be calculated using equation 8 [12].

$$\begin{aligned} P_{tx}^{UE} &= \min\{P_{max}[dBm], \\ &P_{pusch}[dBm] + \alpha * PL[dB] + 10\log(M) + \sigma\} \end{aligned} \quad (8)$$

### B. Microstrip Patch antenna

A microstrip patch antenna is chosen because it allows easy production but more important, it has a low weight and has a thin profile causing it to be very aerodynamic which is useful when attaching it to a drone [32].

The dimensions of the antenna depend on the frequency it is operating at and the characteristics of the used substrate. The antenna will be radiating at a centre frequency  $f_0$  of 2.6 GHz. Each substrate has a dielectric constant  $\epsilon_r$  representing the permittivity of the substrate that depends on the used material. Substrates with a high dielectric constant and low height reduce the dimensions of the antenna while a lower dielectric constant with a high height improves the performance of the antenna [33], [34]. In this research, a substrate like glass is chosen because of the higher dielectric constant of  $\epsilon_r = 4.4$  compared to materials like Teflon with only a dielectric constant of  $\epsilon_r = 2.2$  [33]. Doing this in combination with an antenna height of 2.87 mm will decrease the dimensions of the entire antenna surface. This comes in handy since drones only have limited space available.

The dimensions of the radiating patch can be calculated with the formulas from [33], [34]. Doing so will result in a radiating patch of 35.09 mm by 26.55 mm and a ground-plane of at least 52.40 mm by 43.80 mm. The microstrip patch antenna as illustrated in fig. 3 will result in the radiation pattern of fig. 4.

description	symbol	value
centre frequency	$f_0$	2600 Hz
dielectric constant	$\epsilon_r$	4.4
height of the substrate	$h$	0.00287 m

TABLE I: Overview of configuration parameters.

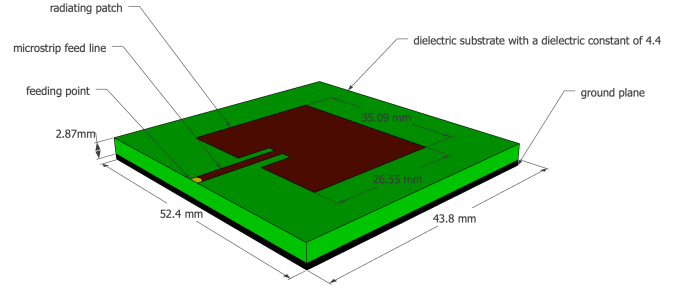


Fig. 3: Design of the microstrip patch antenna.

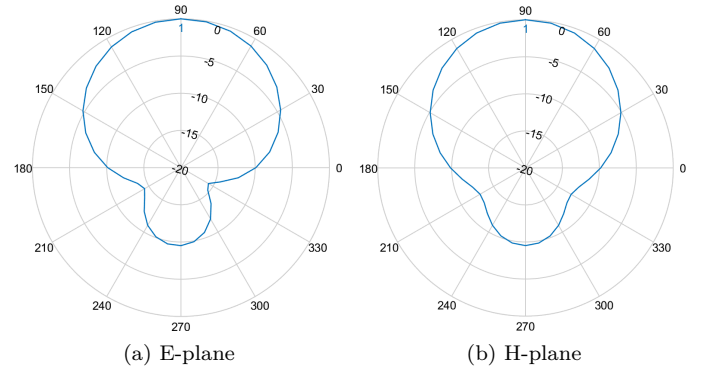


Fig. 4: Radiation patterns generated by the used microstrip patch antenna.

### C. Optimizing the network

Deruyck et al. discusses in [8] how a terrestrial telecommunication network either can be optimized towards electromagnetic exposure of an individual or towards power consumption of the entire network. However, an increasing transmission power of an antenna comes with an increasing electromagnetic exposure. This is not the case considering both values for an entire network. In fact, the authors from [8] prove that both become inversely equivalent. The reason why the network behaves like this is because it is often cheaper to increase the exposure of an already active base station than activating a new one. This leads to the following fitness function which is based on [8].

$$f = w * \left( 1 - \frac{E_m}{E_{max}} \right) + (1 - w) * \left( 1 - \frac{P}{P_{max}} \right) * 100 \quad (9)$$

Formula 9 returns a fitness value which represents the performance of the entire network.  $w$  is the importance factor of electromagnetic exposure ranging from 0 to 1, boundaries included. A  $w$  set to 0 means that electromag-

netic exposure is not important. Such network will therefore be called a power consumption optimized (PwrC. Opt.) network. Likewise, a  $w$  set to 1 means that minimizing exposure is top priority and will result in an exposure optimized (Exp. Opt.) network.  $P_{max}$  is the power consumption of all UABSs, both active and inactive, when radiating at the highest level possible while  $P$  is the effective power used by the current designed network. This will be the power required for the flying drones themselves and their antennae.  $E_m$  will be the weighted exposure of the average user for the current designed network and  $E_{max}$  the weighted average of the electromagnetic exposure when all antennae are at their highest power level.

When optimizing the network, it is not only important to consider the average exposure of all users, but also to limit high extremes [8]. A weighted average will be used not only considering the median but also the 95 percentile from all users' DL exposure using formula 10. Since both values are considered to have equal importance, the weight factors  $w_1$  and  $w_2$  will both have an equal importance of 50%.

$$E_m = \frac{w_1 * E_{50} + w_2 * E_{95}}{w_1 + w_2} \quad (10)$$

## D. Simulation Tool

### D.1 Main Algorithm

First, a description of the area has to be provided to the tool. This is done with so-called shape-files. These files contain a complete description about the shape of the buildings. Thereafter, users are uniformly distributed over the area and a temporary UABS is positioned above each user. Now, the decision algorithm needs to decide which of these UABSs can actually remain and how hard each one should be radiating. Once the decision algorithm is done, the tool checks whether the number of online UABSs does not exceed the capacity of the facility where the UABSs are stored. If this is the case, the UABSs covering the least amount of users will be removed.

### D.2 Decision Algorithm

Solving the network is done by the decision algorithm and starts by calculating the path loss between all users and between users and UABSs. Thereafter, the algorithm iterates over each user and tries to connect that user to each UABS. This connection is not always possible. A UABS might be saturated with users and will not be able to cover yet another one or maybe the user is so far away that in order to cover that user, the UABS would have to exceed its maximum allowed input power. If however a connection is possible, the user will be connected to that UABS and the fitness function (eq. 9) is applied. This is repeated for each UABS. Only the connection which results in the best fitness value for the entire network will be used. Doing so will make sure that, given the currently designed network, the user is optimized. In other words, each user is optimized and not the entire network. It is however

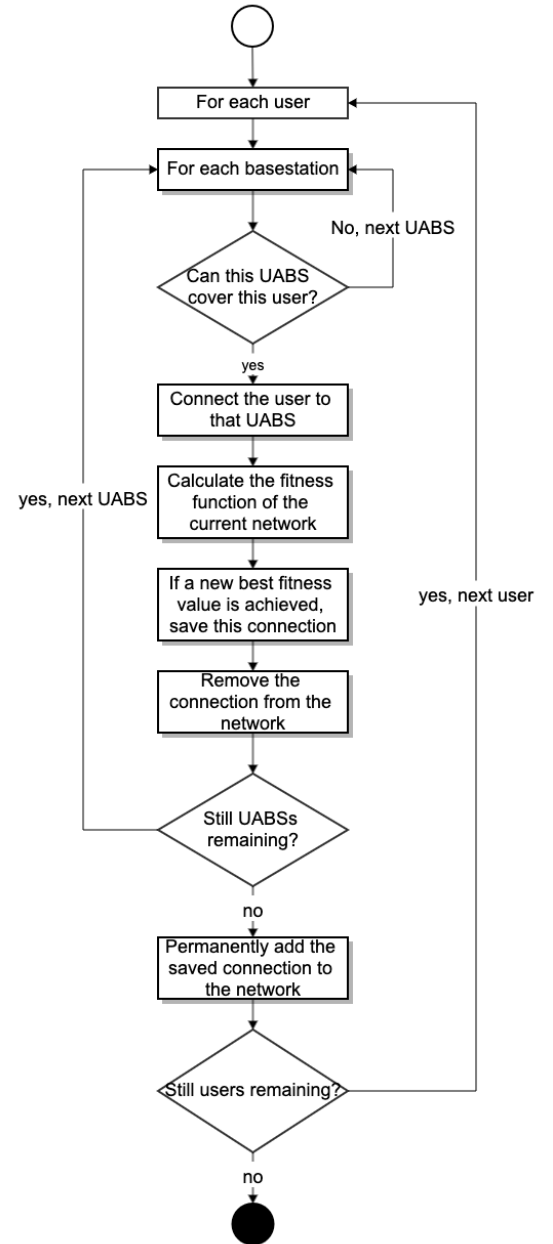


Fig. 5: Flowchart of the decision algorithm.

assumed that the average network will be optimized as well. Thereafter, the tool shifts to the next user. When the last user has been processed, the network is fully designed for an unlimited number of drones and the result is returned to the main algorithm for further processing. The flowchart of this algorithm is given in figure 5.

## IV. Scenarios

The default configuration is given in table II and is always applicable unless mentioned otherwise.

Three main scenarios will be investigated. The first one has only one user and one UABS present in the network. SAR, electromagnetic exposure, power consumption and antenna transmission power are investigated at different

Broadband cellular network	
Technology	LTE
Frequency	2.6 GHz
Power offset ( $P_{pusch}$ )	-120 dBm
Path loss compensation ( $\alpha$ )	1
Correction value	0 dBm
Number of used resource blocks	100
Femtocell antenna	
Maximum $P_{tx}$ antenna direction	33 dBm downwards (az: 0°; el: 90°)
Gain	4 dBm
Feeder loss	2 dBm
Implementation loss radiation pattern	0 dBm EIRP or microstrip patch
Flying altitude	100 m
UAV	
UAV power	13.0 A
Average UAV speed	12.0 m/s
Average UAV power usage	17.33 Ah
UAV battery voltage	22.2 V
UE Antenna	
Height	1.5m from the floor
Gain	0 dBm
Feeder loss	0 dBm
Radiation pattern	EIRP
Quantity in network	224

TABLE II: Overview of default configuration values.

flying heights.

In a second scenario, the network is expanded for multiple users while still considering only one UABS. The scenario is divided into two cases. One with a variable flying height but with a fixed number of 224 users as is average on an usual day at 5 p.m. in Ghent [16]. In the other case, the number of users varies but the flying height is set to 100 metres [16]. The power consumption, electromagnetic exposure and specific absorption rate are investigated for each case.

The third scenario is quite similar to the previous scenario. The same two cases are investigated, but now an unlimited number of UABSs is available.

Each case from each scenario consists out of four possible configurations. There are two possible antennae, namely EIRP and microstrip patch antenna, which can both be applied in a PwrC. Opt. network or an Exp. Opt. network.

It is important to note that all measured values are strictly limited to the sources mentioned in the previous section and thus only cover data traffic between UE and UABSs. Any other potential sources like backhaul links will not be covered. An overview of the simulation configuration scenarios is presented in figure 6

Antenna type	Optimization strategy	
	Exposure optimized	Power consumption optimized
	Equivalent isotropic radiator	EIRP Exp Opt
Microstrip patch antenna	Microstrip Exp Opt	Microstrip PwrC Opt

Fig. 6: Matrix with the four possible configurations

## V. Results

As explained in the previous section, four configurations will be investigated in three different scenarios. The flying height and number of users, are evaluated by monitoring the power consumption, electromagnetic exposure and SAR-values. The electromagnetic radiation and SAR are measured for the weighted average user using equation 10 with both  $w_1$  and  $w_2$  set to 50%. Each result is averaged over 20 simulations.

### A. One User and One UABS

The results show that for a varying flying height, a logarithmic relationship exists between the  $P_{tx}$  and the flying height. This is mainly caused by the logarithmic scale in which the decibels of the  $P_{tx}$  are expressed. Each time the flying height becomes too large to cover, the  $P_{tx}$  increases with one dBm. When using the default configuration, with a maximum  $P_{tx}$  of 33 dBm, a UABS can fly up to 387 m before losing connection in a free line of sight (LOS) scenario.

This scenario is investigated with a microstrip patch antenna using power consumption optimization. However, the chosen optimization strategy does not really matter because the decision algorithm decides which user needs to be connected to which UABS. Since only one UABS is available, both optimization strategies will behave identical. Further, also the used antenna will not make any difference. The user is namely positioned in the perfect centre of the main beam where there is no attenuation experienced for both antennae.

When investigating this scenario at different flying heights, we notice that the UL radiation increases exponentially while the DL radiation remains constant at 10 nW/kg during the entire time. The reason that the DL radiation remains constant is because of power control which makes sure that no more power is used than strictly necessary. We can therefore confirm that the electromagnetic exposure is a constant fraction of power and distance. The UL radiation starts very low but surpasses the DL radiation around 80 metres.

### B. Increased Population with one UABS

#### B.1 Variable Flying Height

A PwrC. Opt. network has higher exposure compared to an Exp. Opt. network; a behaviour that was already proven by [8]. However, for this scenario, a PwrC. Opt. network will not necessarily result in a lower power con-

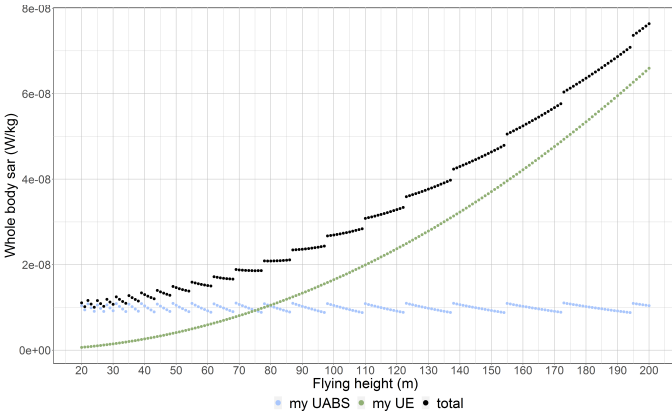


Fig. 7: This figure shows how SAR values from different sources are influenced by different flying altitudes.

sumption. For example, at 100 metres, an EIRP Exp. Opt. network exposes the average user to  $1.5 \text{ mV/m}$  less but requires  $20 \text{ mW}$  more. To understand this, the behaviour of the deployment tool needs to be understood first. A PwrC. Opt. network will result in a few high powered UABSSs because increasing the input power of an antenna costs less than activating a new UAV. Likewise, an Exp. Opt. network generates a lot of low powered UABSSs because the lower the power of the antenna, the lower the exposure. This has the consequence that the cover radius is less and therefore requires more UAVs which costs more energy. When only a limited amount of UABSSs are available, like only one in this scenario, the tool will only keep UABSSs which cover the most users. Therefore, the power consumption in a PwrC. Opt. network is often higher.

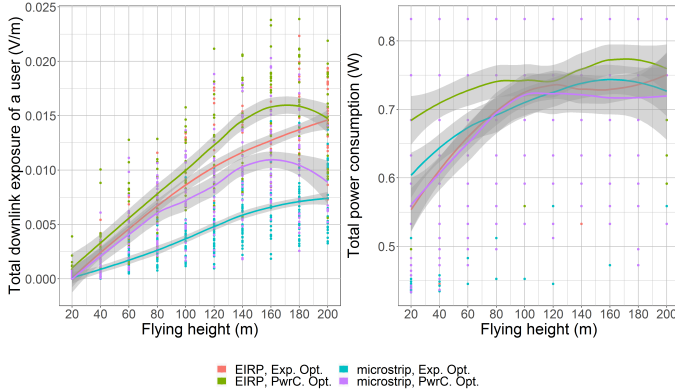


Fig. 8: Fig. (a) show how the flying height influences the downlink electromagnetic radiation of the average user and fig. (b) the power consumption of the entire network for the only UABS available in the network.

Further, figure 8 also show that the exposure increases with higher flying altitudes because there is a lower probability of having non line of sight (NLOS) links by obstructing buildings. This has as consequence that more users become covered. Increasing the flying height from 20 to 100 metres improves the coverage between 1% and 2% for

all four configurations. The increasing electromagnetic radiation is however not unlimited. A microstrip PwrC. Opt. network is at his highest point around 162 metres and an EIRP PwrC. Opt. is at his highest at 195 metres. This decline starts later for exposure optimized networks and is situated outside the investigated flying range. The decreasing electromagnetic radiation at high flying altitudes is not caused by the obstructing buildings but by the distance in general.

Figure 9 shows the whole body  $SAR_{10g}$  for the weighted average user, deducted from all electromagnetic sources. When investigating the three different sources, we see that the  $SAR^{myUABS}$  shows the same curve as it did with the electromagnetic exposure in figure 8.a. This is normal behaviour considering that equation 6 is able of converting the DL exposure to SAR by simply multiplying with a constant. During the entire time is  $SAR^{myUABS}$  the most dominant factor followed by the near-field radiation from the user's own device. The far-field radiation from other UE barely has influence. As an illustration, when the UABS flies at 140 metres, the average user in an EIRP PwrC. Opt. network will experience around  $2.1 \text{ nW/kg}$  from the UABS and around  $0.2 \text{ nW/kg}$  from his own device. The exposure from other UE can be neglected with  $0.03 \text{ pW/kg}$ . A low but plausible value considering that most UE are not radiating anything since they are uncov-

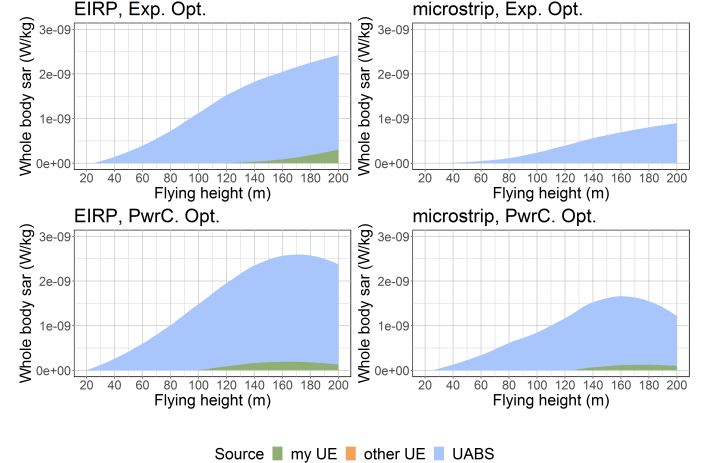


Fig. 9: Each figure corresponds with a certain configuration and shows how the SAR from different sources are influenced by an increasing flying height.

## B.2 Variable Number of Users

The number of covered users increases linearly compared to the number of users present in the network as shown in figure 10.b. It illustrates how an equivalent isotropic radiator is able to reach more users compared to a microstrip patch antenna. Just like an power consumption optimized network is able to reach more users than an exposure optimized network. For example, with 600 users, 5 to 7 additional people can be covered when replacing a

microstrip patch antenna with an equivalent isotropic radiator and changing an exposure optimized network with an power consumption optimized network will cover one or two additional users.

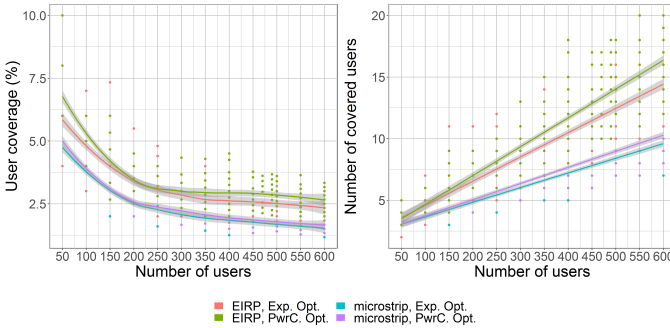


Fig. 10: The influence of increasing traffic on the user coverage.

Figure 11.a is influenced by 10.a. When less users are covered, the exposure of the average user will decrease as well. For example, in an EIRP PwrC. Opt. network, 50 users have a 6.75% coverage which corresponds with a weighted average exposure of  $18 \text{ mV/m}$  while 600 users with 2.75% coverage only have  $9 \text{ mV/m}$ . Further, figure 11.b is directly influenced by figure 10.b. When the UABS has to cover more users, the probability that some of these users have a worse path loss is higher. The UABS solves this problem by increasing the power consumption. Increasing the population from 50 to 600 will require between 0.05 and 0.1 W more. For this scenario, no clear difference in power consumption exists between the four configurations.

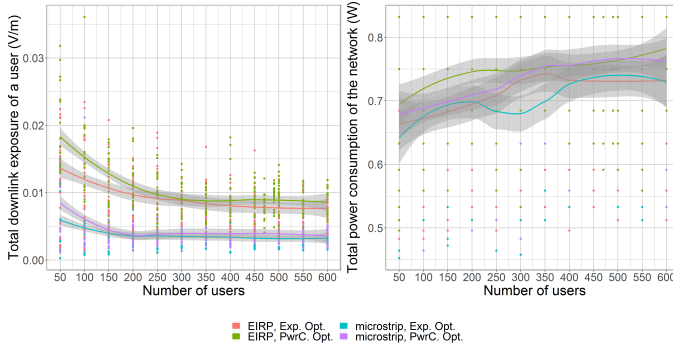


Fig. 11: These two figures show how various sizes of population influence the downlink electromagnetic radiation of the average user (left) and power consumption of the entire network (rights) for one UABS available in the network.

The SAR coming from the user's own device is on average zero since most users are uncovered. Figure 13 shows the exposure for the covered user just below the UABS. Scenario I already showed that the SAR from the user's own device is only influenced by the flying height and is also confirmed by the results in fig. 13 where constant  $SAR^{myUE}$  is measured of  $0.15 \mu\text{W/kg}$ . The SAR from the

UABS experiences a slight increase of  $0.005 \mu\text{W/kg}$ . When the population grows, more users will be near the UABS. The UABS will likely decide to cover these users as well as visible in figure 12. These users might have a slightly worse path loss because of obstructing buildings or somewhat bigger distance. The UABS reacts to this by increasing his power consumption causing an increase in the DL SAR for the central user. The far-field radiation from UE is very low as mentioned before and therefore added separately in figure 12.b. It shows that the SAR from other UE increases from zero to  $0.15 \mu\text{W/kg}$ . This is normal behaviour considering that around the central user more and more people become available of which some will be connected to the UABS and therefore also emitting radiation.

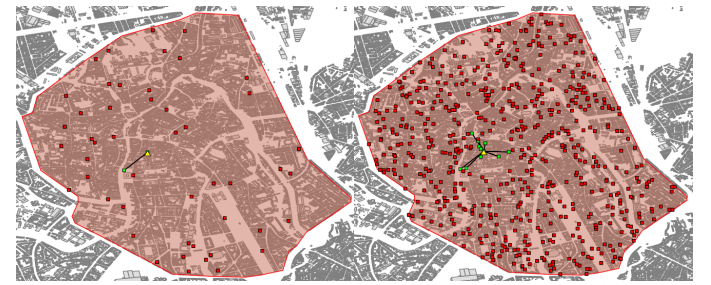


Fig. 12: Overview of which users are connected to the UABS. The map on the left is for 50 active users while the map on the right considers 600 active users.

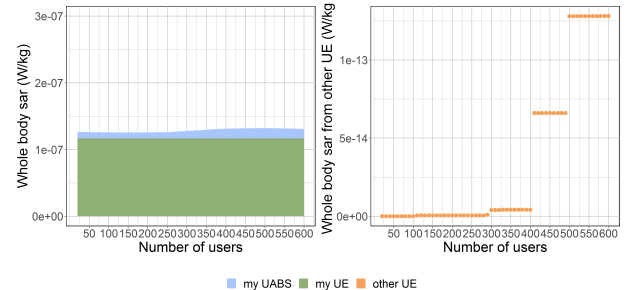


Fig. 13: SAR-values for the user who is directly beneath the only UABS available.

### C. Unlimited Number of UABSS

#### C.1 Variable Flying Height

The same scenario as in the previous section is investigated. Only now, an unlimited number of UABSS is available. The results prove that the different optimization strategies work as intended. A PwrC. Opt. network has indeed a lower power consumption but therefore result in higher electromagnetic radiation. On the other hand, an Exp. Opt. network will reduce the electromagnetic exposure by using more UAVs and thence also increase the network's power consumption. This conclusion was already made in [8] and is supported by these results. For example, when comparing both optimization strategies for the

same equivalent isotropic radiator and the same default flying height, we see that the power consumption optimized network requires 51 W and therefore exposes its users to 15 mV/m. When optimizing towards electromagnetic radiation, the exposure drops to 11.5 mV/m but at a cost of a higher power consumption of 54 W.

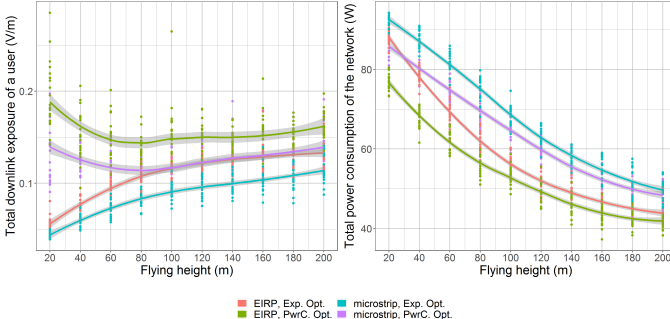


Fig. 14: These two figures show how the flying height influences the downlink electromagnetic radiation of the average user (left) and power consumption of the entire network (right) for an unlimited number of drones.

The exposure in figure 14 shows that an Exp. Opt. network increases logarithmically while the PwrC. Opt. network rather has a concave relationship with the flying height, and has its lowest point at around 70 metres.

Figure 15.a shows that the optimal coverage is achieved at a low flying height of 40 metres with around 99% coverage. However, there is a downside to this. Figure 15.b shows that the number of required UAVs increases when the flying altitude becomes lower; a behaviour which was also determined in [16]. For example, an microstrip Exp. Opt. network and an EIRP PwrC. Opt. network require respectively 84 and 64 UABSSs at a flying altitude of 200 m which increases respectively to 211 and 162 UABSSs at a much lower flying altitude of 20 m.

Figure 16 shows how each source contributes to the total SAR. A first consequence of raising the flying altitude from 20 to 200 metres is the increase SAR from the user's own device situated with 89 and 141 nW/kg; a behaviour

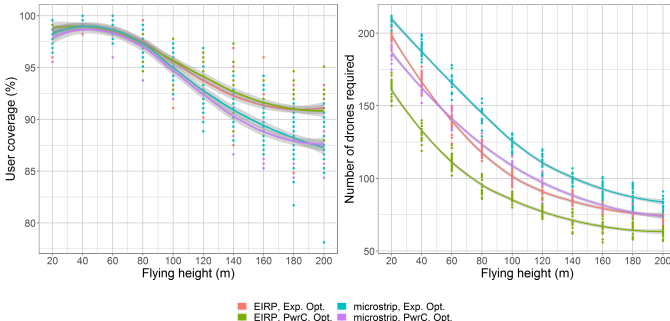


Fig. 15: This graph shows how much UAVs are required at different flying heights while trying to achieve a 100% coverage.

also explained in the first scenario. Figure 16 shows that once the flying altitude surpasses the NLOS of the buildings, around 70 to 80 metres, the SAR from the serving UABS remains more or less constant for all configurations. The  $SAR^{myUABS}$  varies for these higher flying heights around 160 nW/kg for microstrip PwrC. Opt. networks and around 98 nW/kg for microstrip Exp. Opt. and EIRP PwrC. Opt. networks. An EIRP Exp. Opt. network is situated around 47 nW/kg. These higher flying altitudes will also result in an increase in electromagnetic radiation from other UABSSs. Raising the flying altitude from 20 to 200 metres will increase the the  $SAR^{otherUABS}$  between 115 and 140 nW/kg for EIRP antennae and between 54 and 74 nW/kg for microstrip patch antennae for both optimization strategies.

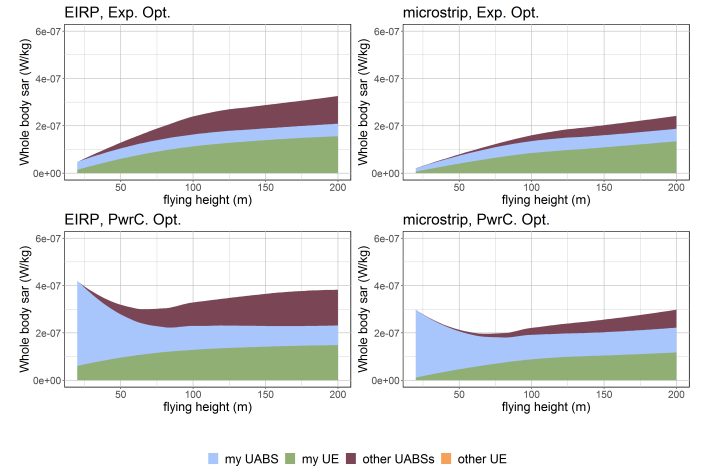


Fig. 16: Each chart corresponds with one of the four possible configurations. The contribution of each source towards the total SAR for a varying flying height is shown.

## C.2 Variable Number of Users

The second evaluated parameter of scenario III is a variable number of users while the flying height is fixed to 100 metres. Figure 17.a shows how the tool tries to reach a 100% coverage. The percentage of covered users is slightly less for smaller networks. For only 50 users, an average coverage of around 93% is achieved while a network with 600 users has a coverage of around 97%. Figure 17.b shows how the tool requires more UAVs for these large populations. The difference in optimization strategy is very little for a small amount of people but increases very quickly. When the population increases from 50 to 600 users, 200 more UABSSs are required by a microstrip Exp. Opt. network around 130 more UABSSs for an EIRP Exp. Opt. network or a microstrip PwrC. Opt. network and 110 more UABSSs for an EIRP PwrC. Opt. network. This is an expected behaviour when looking at scenario II where, with only one UABS available, the percentage of covered users decreases for these larger populations.

Figure 19 shows that the electromagnetic radiation and power consumption increase for larger populations which is

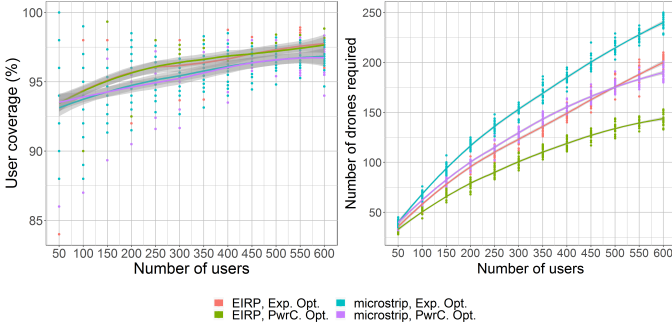


Fig. 17: This graph shows how much UAVs are required for different flying heights while trying to achieve a 100% coverage.

normal since more drones will be available. When the population increases from 50 to 600 users, the electromagnetic radiation increases between 80 and 130  $mV/m$  depending on the configuration. The power consumption with 50 users is for all configurations around 20 W. Once the population is increased to 600 users, a microstrip Exp. Opt. network will require 130 W, a microstrip PwrC. Opt. network requires 117 W, EIRP Exp. Opt. networks require 107 W and EIRP PwrC. Opt. network requires 92 W.

The correct behaviour of the decision algorithm became already clear in the previous subsection ?? but is also confirmed here. When comparing both optimization strategies, a power consumption optimized network requires around 5 W less but exposes its users between 27  $mV/m$  and 30  $mV/m$  more than exposure optimized networks. Further, it is also noticed that equivalent isotropic radiators cause more electromagnetic radiation for less energy compared to microstrip patch antennae. When comparing the two types of antennae for a default number of 224 users, an equivalent isotropic radiator will expose the average user between 25  $mV/m$  and 27  $mV/m$  more while requiring around 12 W less than when the network would be using a microstrip patch antennae.

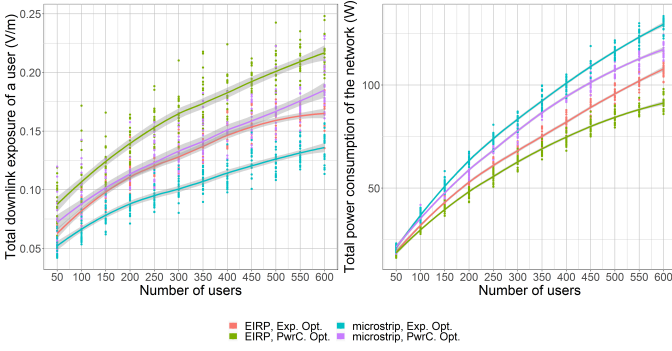


Fig. 18: The influence of the population size on the downlink electromagnetic radiation (a) and power consumption (b).

Figure 20 represents the SAR from the weighted average user and shows how the SAR coming from the user's

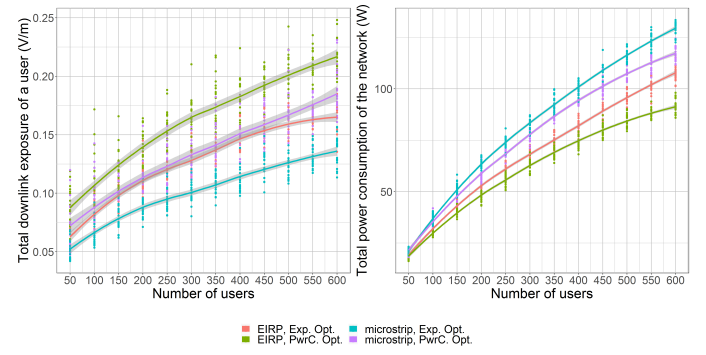


Fig. 19: These two figures show how the number of users influences the downlink electromagnetic radiation of the average user (left) and power consumption of the entire network (right) for an unlimited number of drones.

own device remains almost constant. The flying altitude is always the same so also the required energy to cover that distance will remain the same. For both optimization strategies, the  $SAR^{myUE}$  for networks with equivalent isotropic radiators vary around  $1.1 \mu W/kg$  and around  $0.7 \mu W/kg$  for networks using microstrip patch antennae. The  $SAR^{myUABS}$  barely increases in an exposure optimized network and is situated around  $0.5 \mu W/kg$  for both antennae. The power consumption optimized network also starts around  $0.5 \mu W/kg$  but increases when more users become online. A normal behaviour when considering that these UABSs try to cover much more users. Therefore, the  $SAR^{myUABS}$  with 600 users increases up to  $1 \mu W/kg$  for an equivalent isotropic radiator and almost  $2 \mu W/kg$  for a microstrip patch antenna. The SAR value that increases the most is  $SAR^{otherUABS}$  which starts really low with less than  $0.1 \mu W/kg$  for 50 users for all configurations. The SAR increases however very fast. The biggest increase is noticed in an EIRP PwrC. Opt. network where  $3 \mu W/kg$  is measured for 600 users. The  $SAR^{otherUE}$  increases the least for microstrip Exp. Opt. with only  $1 \mu W/kg$  for 600 users.

## VI. Conclusion

Literature showed that a network can be optimized towards either the power consumption of the entire network or the electromagnetic exposure of the average user using a fitness function [8]. However, the fitness function should be used with care considering that UABSs can be placed anywhere as opposed to the transmission towers from [8] who have a predetermined position. In an Exp. Opt. network, this causes a lot of users to get a UABS all by themselves because this is the best approach to minimize exposure. A PwrC. Opt. network on the other hand will try to limit the number of drones in order to save energy. So as a rule of thumb: an Exp. Opt. network will result in a lot of low powered devices (increasing the overall power consumption) while a PwrC. Opt. network results in a few high powered devices (increasing the exposure of the average user). If the goal is to remain in the air for a longer

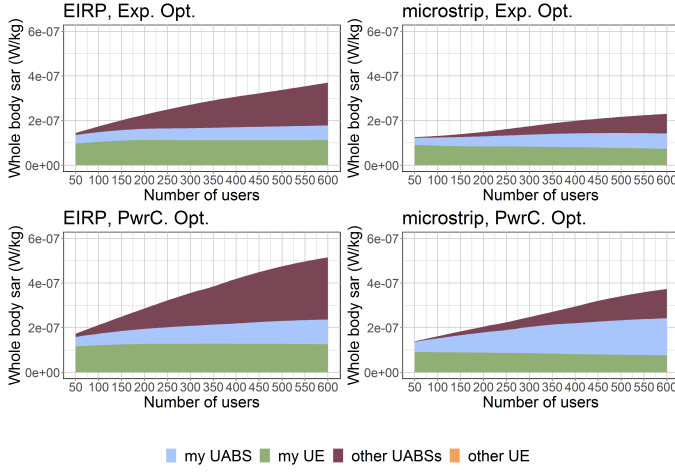


Fig. 20: Each figure corresponds with a certain configuration and shows how the SAR from different sources are influenced by an increasing population density. An unlimited number of UABSSs is available.

period of time, an Exp. Opt. network is recommended because the power consumption of an individual UABS is lower. On the other hand, a PwrC. Opt. network is cheaper because less drones are involved. Moreover, the results show that the electromagnetic radiation in a PwrC. Opt. network (with high powered UABSSs) is far below the thresholds enforced by the Flemish government.

The user's main sources of exposure are the user's own device and the UABSS who is serving him, followed by all other UABSSs in the network. When the population increases, there is not only more radiation from UE but also from more UABSSs that are serving the other users. The exposure from other people's UE is so low that it can be neglected. An Exp. Opt. network will limit the total exposure mainly by trying to reduce the exposure from other UABSSs.

A directional microstrip patch antenna is introduced because it gives several advantages compared to omnidirectional antennae. Directional antennae are able to focus their energy there where it is needed, namely towards the ground. Microstrip patch antennae further benefit from their thin and lightweight design. The performance of this directional microstrip patch antenna has been compared to a fictional equivalent isotropic radiator. This equivalent isotropic radiator has higher exposure and coverage for less power, compared to realistic antennae like microstrip patch antennae because of the absence of attenuation, and can hypothetically be compared with an antenna with a very big aperture angle. This type of antenna can achieve the same coverage with less resources like power and number of drones. A microstrip patch antenna with a more limited aperture angle of 90° requires more resources but causes less sideways radiation. So the exposure from other UABSSs will be way less.

Remarkable is that an EIRP Exp. Opt. network behaves very similar to a microstrip PwrC. Opt. network as shown

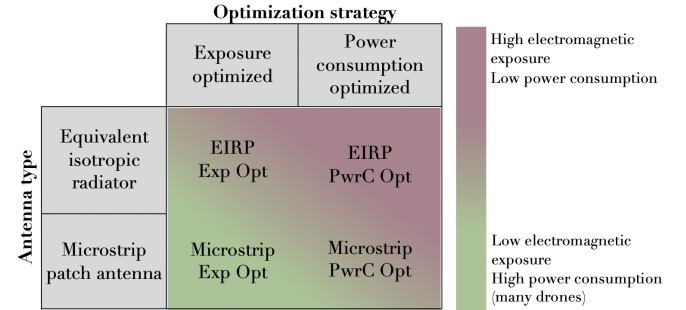


Fig. 21: Matrix with the four possible configurations, colour-coded based on the results.

in figure 21. This results in the best of both worlds. The microstrip patch antenna will generate less electromagnetic radiation by design and the power consumption optimization reduces the number of required drones and power. A microstrip patch antenna with an aperture angle of 90° is considered as a good solution but if budget is limited, an antenna with a larger aperture angle would further reduce cost without interfering with the Flemish legislation regarding electromagnetic exposure.

The electromagnetic radiation of an Exp. Opt. network increases with higher flying altitudes. Around 80 metres, the exposure from the user's device surpasses the exposure from the serving UABS. On the other hand, a PwrC. Opt. network shows that the lowest exposure is measured around 70 to 80 metres. Further, the results also show that the number of required drones decreases when the flying height becomes larger; a conclusion that was also made in [16]. When also considering the results from [17] where a flying altitude from 80 metres is suggested for an optimal access and backhaul connectivity, a flying height of 80 metres is also here proposed for the city centre of Ghent.

In short, a PwrC. Opt. network is proposed with a fixed flying height of 80 metres. A microstrip patch antenna with a sufficiently large aperture angle is a good starting point. However, different antenna configurations should be investigated.

### Acknowledgement

Special thanks to the WAVES research group at Ghent University for providing access to their capacity based deployment tool and therefore making this research possible.

### References

- [1] “Base overschreed stralingsnormen na aanslagen,” De standaard, 2019.
- [2] L. Hardell and C. Sage, “Biological effects from electromagnetic field exposure and public exposure standards,” *Biomedicine and Pharmacotherapy*, vol. 62, no. 2, pp. 104 – 109, 2008.
- [3] “What are electromagnetic fields.” <https://www.who.int/peh-emf/about/WhatisEMF/en/index1.html>. Accessed: 15-10-2019.
- [4] “Elektromagnetische velden en gezondheid: Uw wegwijzer in het elektromagnetische landschap,” Federale overheidsdienst: volksgezondheid, veiligheid van de voedselketen en leefmilieu, vol. 5, 2014.
- [5] “Normen zendantennes.” <https://omgeving.vlaanderen.be/normen-zendantennes>. Accessed: 19-03-2020.

- [6] E. Commission, "Council recommendation of 12 july 1999 on the limitation of exposure of the general public to electromagnetic fields (0 hz to 300 ghz)," *Official Journal of the European Communities*, vol. 59, 1999.
- [7] D. Plets, W. Joseph, K. Vanhecke, and L. Martens, "Exposure optimization in indoor wireless networks by heuristic network planning," *Progress In Electromagnetics Research*, vol. 139, pp. 445–478, 01 2013.
- [8] M. Deruyck, E. Tanghe, D. Plets, L. Martens, and W. Joseph, "Optimizing lte wireless access networks towards power consumption and electromagnetic exposure of human beings," *Computer Networks*, vol. 94, 12 2015.
- [9] D. Plets, W. Joseph, S. Aerts, K. Vanhecke, G. Vermeeren, and L. Martens, "Prediction and comparison of downlink electric-field and uplink localised sar values for realistic indoor wireless planning," *Radiation Protection Dosimetry*, vol. 162, no. 4, pp. 487–498, 2014.
- [10] D. Plets, W. Joseph, K. Vanhecke, and L. Martens, "Downlink electric-field and uplink sar prediction algorithm in indoor wireless network planner," in *The 8th European Conference on Antennas and Propagation (EuCAP 2014)*, pp. 2457–2461, IEEE, 2014.
- [11] S. Kuehn, S. Pfeifer, B. Kochali, and N. Kuster, "Modelling of total exposure in hypothetical 5g mobile networks for varied topologies and user scenarios," Final Report of Project CRR-816, Available on line at: <https://tinyurl.com/r6z2gqn>, 2019.
- [12] D. Plets, W. Joseph, K. Vanhecke, G. Vermeeren, J. Wiart, S. Aerts, N. Varsier, and L. Martens, "Joint minimization of uplink and downlink whole-body exposure dose in indoor wireless networks," *BioMed research international*, vol. 2015, 2015.
- [13] Y. Zeng, Q. Wu, and R. Zhang, "Accessing from the sky: A tutorial on uav communications for 5g and beyond," *Proceedings of the IEEE*, vol. 107, no. 12, pp. 2327–2375, 2019.
- [14] Y. Kawamoto, H. Nishiyama, N. Kato, F. Ono, and R. Miura, "Toward future unmanned aerial vehicle networks: Architecture, resource allocation and field experiments," *IEEE Wireless Communications*, vol. 26, no. 1, pp. 94–99, 2018.
- [15] R. Gangula, O. Esrafilian, D. Gesbert, C. Roux, F. Kaltenberger, and R. Knopp, "Flying robots: First results on an autonomous uav-based lte relay using open airinterface," in *2018 IEEE 19th International Workshop on Signal Processing Advances in Wireless Communications (SPAWC)*, pp. 1–5, IEEE, 2018.
- [16] M. Deruyck, J. Wyckmans, W. Joseph, and L. Martens, "Designing uav-aided emergency networks for large-scale disaster scenarios," *EURASIP Journal on Wireless Communications and Networking*, vol. 2018, 12 2018.
- [17] G. Castellanos, M. Deruyck, L. Martens, and W. Joseph, "Performance evaluation of direct-link backhaul for uav-aided emergency networks," *Sensors*, vol. 19, no. 15, p. 3342, 2019.
- [18] M. Mozaffari, W. Saad, M. Bennis, Y.-H. Nam, and M. Debbah, "A tutorial on uavs for wireless networks: Applications, challenges, and open problems," *IEEE communications surveys & tutorials*, vol. 21, no. 3, pp. 2334–2360, 2019.
- [19] Q. Wu, L. Liu, and R. Zhang, "Fundamental trade-offs in communication and trajectory design for uav-enabled wireless network," *IEEE Wireless Communications*, vol. 26, no. 1, pp. 36–44, 2019.
- [20] M. Deruyck, A. Marri, S. Mignardi, L. Martens, W. Joseph, and R. Verdone, "Performance evaluation of the dynamic trajectory design for an unmanned aerial base station in a single frequency network," in *2017 IEEE 28th Annual International Symposium on Personal, Indoor, and Mobile Radio Communications (PIMRC)*, pp. 1–7, IEEE, 2017.
- [21] A. V. Savkin and H. Huang, "Deployment of unmanned aerial vehicle base stations for optimal quality of coverage," *IEEE Wireless Communications Letters*, vol. 8, no. 1, pp. 321–324, 2018.
- [22] H. Huang and A. V. Savkin, "A method for optimized deployment of unmanned aerial vehicles for maximum coverage and minimum interference in cellular networks," *IEEE Transactions on Industrial Informatics*, vol. 15, no. 5, pp. 2638–2647, 2018.
- [23] C. T. Cicek, H. Gultekin, B. Tavli, and H. Yanikomeroglu, "Uav base station location optimization for next generation wireless networks: Overview and future research directions," in *2019 1st International Conference on Unmanned Vehicle Systems-Oman (UVS)*, pp. 1–6, IEEE, 2019.
- [24] A. Rizwan, D. Biswas, and V. Ramachandra, "Impact of uav structure on antenna radiation patterns at different frequencies," in *2017 IEEE International Conference on Antenna Innovations & Modern Technologies for Ground, Aircraft and Satellite Applications (iAIM)*, pp. 1–5, IEEE, 2017.
- [25] M. Nosrati, A. Jafargholi, and N. Tavassolian, "A broadband blade dipole antenna for uav applications," in *2016 IEEE International Symposium on Antennas and Propagation (APSURSI)*, pp. 1777–1778, IEEE, 2016.
- [26] M. Nosrati, A. Jafargholi, R. Pazoki, and N. Tavassolian, "Broadband slotted blade dipole antenna for airborne uav applications," *IEEE Transactions on Antennas and Propagation*, vol. 66, no. 8, pp. 3857–3864, 2018.
- [27] B. A. Arand, R. Shamsaei, and B. Yektakhah, "Design and fabrication of a broadband blade monopole antenna operating in 30 mhz–600 mhz frequency band," in *2013 21st Iranian Conference on Electrical Engineering (ICEE)*, pp. 1–3, IEEE, 2013.
- [28] L. Akhoondzadeh-Asl, J. Hill, J.-J. Laurin, and M. Riel, "Novel low profile wideband monopole antenna for avionics applications," *IEEE transactions on antennas and propagation*, vol. 61, no. 11, pp. 5766–5770, 2013.
- [29] S. S. Siddiq, G. Karthikeya, T. Tanjavur, and N. Agnihotri, "Microstrip dual band millimeter-wave antenna array for uav applications," in *2016 21st International Conference on Microwave, Radar and Wireless Communications (MIKON)*, pp. 1–4, IEEE, 2016.
- [30] Y. Zheng, J. Zhou, W. Wang, and M. Chen, "A low-profile broadband circularly polarized antenna array for uav ground-to-air communication," in *2018 IEEE Asia-Pacific Conference on Antennas and Propagation (APCAP)*, pp. 219–220, IEEE, 2018.
- [31] X. Sun, R. Blázquez-García, A. García-Tejero, J. M. Fernández-González, M. Burgos-García, and M. Sierra-Castañer, "Circular array antenna tor uav-uav communications," in *2017 11th European Conference on Antennas and Propagation (EUCAP)*, pp. 2025–2028, IEEE, 2017.
- [32] I. Singh and V. Tripathi, "Micro strip patch antenna and its applications: a survey," *Int. J. Comp. Tech. Appl.*, vol. 2, no. 5, pp. 1595–1599, 2011.
- [33] K. Kashwan, V. Rajeshkumar, T. Gunasekaran, and K. S. Kumar, "Design and characterization of pin fed microstrip patch antennae," in *2011 Eighth International Conference on Fuzzy Systems and Knowledge Discovery (FSKD)*, vol. 4, pp. 2258–2262, IEEE, 2011.
- [34] A. Sudarsan and A. Prabhu, "Design and development of microstrip patch antenna," *International Journal of Antennas (JANT)* Vol. 3, 2017.

# Evaluatie van de elektromagnetische blootstelling van de mens in een netwerk van drones

Thomas Detemmerman

Supervisor(s): Wout Joseph, Luc Martens, Luc Martens, German Dario Castellanos Tache

**Abstract**— De hedendaagse samenleving vertrouwt meer dan ooit op de aanwezigheid van draadloze netwerken. Tevens groeit ook de bezorgdheid bij de menigte over de elektromagnetische straling die hierbij gebruikt wordt. De overheid hanteert dan ook strenge richtlijnen waaraan mobiele toestellen en zendmasten moeten voldoen.

Dit onderzoek tracht de specifieke absorptie snelheid van elektromagnetische straling in kaart te brengen door rekening te houden met alle mobiele toestellen en zendmasten. Om dit te verwelijken wordt gebruik gemaakt van een tool ontwikkeld door de onderzoeksgrond WAVES aan de UGent. Deze tool simuleert een volledig netwerk waarbij zendmasten bevestigd worden aan drones. Dit onderzoek observeert verder hoe deze drones kunnen worden aangestuurd zodoende dat bepaalde doelstellingen zoals het minimaliseren van energieverbruik of elektromagnetische straling bereikt kunnen worden.

Uit de resultaten blijkt dat...

**Keywords**— LTE, elektromagnetische blootstelling, energieverbruik, drone, femtocell, microstrip patch antenne, stralingspatroon, specifieke absorptietempo (SAT)

## I. Introductie

**D**E samenleving is meer dan ooit afhankelijk van draadloze communicatie. Een elektronisch apparaat kan op elk gegeven moment in elke willekeurige plaats beroep doen op het draadloze netwerk, gaande van kleine Internet of Things (IoT) apparatuur tot volwaardige zelf-rijdende auto's.

Ook in uitzonderlijke en mogelijks levensbedreigende situaties verwacht de samenleving de aanwezigheid van het mobiele netwerk. Desondanks het feit dat dit netwerk zelf mogelijks beschadigd is door de situatie. Een mogelijk tijdelijke oplossing om een beschadigd netwerk bij te staan is met behulp van onbemande vliegtuigen zoals drones. Een base station kan geplaatst worden op een drone en zo efficiënt verplaatst worden naar de nodige locatie.

Deze aanpak is niet alleen handig als het bestaande netwerk beschadigd is maar ook voor onverwachte toename aan gebruikers. Bijvoorbeeld tijdens de aanslagen op de Brusselse Luchthaven zagen alle mobiele operatoren een toename in data verkeer. Sommige operatoren raakten zodoende verzadigd dat ze als enige oplossing zagen om de wetgeving te negeren en de elektromagnetische straling te laten toenemen zodoende dat toch iedereen behandeld kon worden [1].

De elektromagnetische straling die vrijkomt bij netwerken kunnen echter niet met onachtaamheid behandeld worden. Onderzoek toont aan dat buitensporige elektromagnetische straling verscheidende biologische neveneffecten kunnen veroorzaken [2], [3]. Het wordt dus duidelijk dat elektromagnetische straling een sleutelrol speelt bij het ontwikkelen van een met drones beholpen netwerk waarbij de wetgeving nauwkeurig nageleefd dient te worden.

Drone-gestuurde netwerken kunnen dankzij hun mobiliteit eenvoudig verplaatst worden. Verschillende onderzoeken tonen aan hoe deze netwerken geoptimaliseerd kunnen worden zodoende dat bepaalde doelstellingen zoals minimaal energieverbruik bereikt kunnen worden.

Desondanks is er zeer beperkt onderzoek gedaan waarbij een drone-gestuurd netwerk wordt geoptimaliseerd naar elektromagnetische straling. Verscheidene publicaties bespreken hoe elektromagnetische straling berekend kunnen worden maar overwegen zelden alle verschillende bronnen van straling.

Dit onderzoek stelt een methode voor waarbij rekening gehouden wordt met elektromagnetische straling en energieverbruik voor alle bronnen in een mobiel netwerk, zijnde: de gebruiker zijn eigen mobiel apparaat, de base station dat deze gebruiker aan het behandelen is, alle andere mobiele apparaten en alle andere base stations die andere gebruikers behandelen. Op deze manier kan duidelijk de bijdrage van elektromagnetische straling van elke bron duidelijk geïdentificeerd worden.

Het gedrag van de elektromagnetische straling en het energieverbruik zullen geanalyseerd worden door de tool toe te passen op verschillende scenario's door gebruik te maken van verschillende soorten antennes, vlieghoogtes en bevolkingsdichthes. Waarden zoals Specific Absorptietempo (SAT), elektromagnetische straling en energieverbruik zullen inzicht geven in hoe het netwerk reageert op deze veranderde scenario's en hoe het netwerk ernaar te optimaliseren.

Om dit onderzoek mogelijk te maken zal een bestaande deployment tool, ontwikkeld door de onderzoeksgrond WAVES van de universiteit van Gent, uitgebreid worden. Deze tool beschrijft een volledig geconfigureerd drone netwerk wat een geschikt startpunt is voor dit onderzoek.

## II. State of the Art

### A. Elektromagnetische Straling

Personen in een mobiel network worden blootgesteld aan verscheidene bronnen van elektromagnetische straling, uitgedrukt in  $V/m$ . Eenmaal deze elektromagnetische straling geabsorbeerd wordt door het menselijk lichaam spreken we van het specifieke absorptietempo (SAT). wat uitgedrukt wordt in  $W/kg$ . Al deze waarden zijn onderworpen aan limieten opgelegd door de overheid. Dit onderzoek vindt plaats in Gent, een Vlaamse stad in België, waarbij voor het 2.6 GHz spectrum een individuele zendmast is gelimiteerd tot 4.5  $V/m$  en de totale elektrische veld-

sterkte voor elk punt niet meer dan 31 V/m mag bedragen. [4], [5]. De maximale SAT voor het volledige lichaam komende van een mobiel apparaat verspreid over een 10 g tissue ( $SAR_{10g}$ ) is beperkt tot  $2W/kg$  [6].

Verschillende onderzoeken berekenen de elektromagnetische veldsterkte van verschillende bronnen [7], [8], [9], [10] waarbij sommigen de uplink (UL) elektromagnetische veldsterkte geconverteerd wordt naar lokale SAT [9], [10]. Met de naderende 5G technologie werd [11] gepubliceerd waarbij beschreven wordt hoe deze lokale SAT-waarden van alle verschillende bronnen berekend kunnen worden en bij elkaar opgeteld worden. Uiteindelijk beschrijft [12] hoe de elektromagnetische veldsterkte omgezet kan worden naar SAT-waarden voor het volledige lichaam.

In een realistisch netwerk kunnen sommige gebruikers telefoneren terwijl anderen andere vormen van telecommunicatie gebruiken zoals surfen op het internet. Aangezien de positie van het mobiel apparaat t.o.v. zijn gebruiker niet gekend is, is het belangrijk dat de SAT-waarden berekend worden in functie van het volledige lichaam.

### B. Geoptimaliseerde drone-gestuurde netwerken

Drones kennen verschillende toepassingen. Ze werden oorspronkelijk voornamelijk gebruikt door het leger waarbij ze dienst doen als camera bewaking of aanvallen zonder piloten in gevaar te brengen [13]. Deze drones zijn de laatste jaren in prijs gedaald waardoor ze beter toegankelijk worden voor het algemene publiek. Hierdoor is het onderzoek naar nieuwe toepassingen ervan sterk toegenomen.

Een drone uitgerust met een femtocell base station wordt een Unmanned Arial Base Station (UABS) genoemd en geniet verschillende voordelen zoals mobiliteit en snelle inzetbaarheid. Desondanks zijn er ook verschillende nadelen zoals het beperkte gewicht dat een drone kan dragen en de schaarse energievoorziening.

Kawamoto et al. introduceert in [14] een WiFi netwerk met behulp van drones waarbij rekening gehouden wordt met de richting van de geplaatste antennes op de drone. Gangula et al. illustreert in [15] hoe drones gebruikt kunnen worden voor Long-Term Evolution (LTE) en Zeng et al. presenteert in [13] een handleiding waarbij uitdagingen zoals energieverbruik, mobiliteit en de richting van de antenne voor een 5G netwerk besproken worden. In [16], Deruyck et al. ontwikkeld een deployment tool voor een drone gestuurd netwerk voor rampsituaties waarbij een ideale vlieghoogte van 100 meter aangeraden wordt. Dit wordt verder uitgebreid in [17] waarbij ook rekening gehouden wordt met direct-link backhaul connecties waarbij een ietwat lagere vlieghoogte van 80 meter bekomen wordt.

Mozaffari et al. voorziet in [18] richtlijnen hoe een drone-gestuurd netwerk geoptimaliseerd en geanalyseerd kan worden. Eén onderzoeksgebied dat uitgebreid onderzocht wordt is het optimaliseren van de locaties waar drones zich moeten bevinden. Deze algoritmen trachten bepaalde doelstellingen zoals minimaal energieverbruik of kortste vlieg afstand te bereiken [19], [20], [21], [22]. Deze optimalisatie kan gebeuren door verschillende implementaties waaronder exacte algoritmen of machinaal leren [18],

[23].

Onderzoek waarbij de elektromagnetische straling geïmiteerd wordt is echter beperkt. Deruyck et al. bespreekt in [8] hoe een conventioneel mobiel netwerk geoptimaliseerd kan worden zodoende dat het energieverbruik van het volledige netwerk minimaal wordt of de elektromagnetische bloodstelling van een individu. Echter onderzoek waarbij een drone-gestuurd netwerk geoptimaliseerd wordt naar elektromagnetische straling is door de auteur niet gekend.

### C. Technologies

Voor het ontwikkelen van het netwerk zullen de meer robuuste drones van [16] gebruikt worden (details in tabel II). De gekoppelde antennes zullen opereren in het 2.6 GHz spectrum. Aangezien het aangenomen wordt dat de gebruikers een voortdurende bloodstelling van elektromagnetische straling ondervinden zonder onderbrekingen, wordt frequency division duplexing gebruikt.

De antenne op de drone zullen dienst doen als gateway tussen de mobiele apparaten op de grond en het backbone netwerk. Bepalen welke antenne gebruikt moet worden en hoe deze vervolgens het beste gepositioneerd kan worden brengt verschillende uitdagingen met zich mee. Het stralingspatroon van de antenne kan beïnvloed worden door de drone [24]. Maar ook het feit dat deze drones boven de gebruikers zullen vliegen zorgt er voor dat 2D modelleren onvoldoende is. Een 3D model waarbij rekening gehouden wordt met zowel horizontale als verticale richting zal een veresite vormen [13].

Het eenvoudigste stralingspatroon is een hypothetische isotrope antenne dewelke straalt met gelijke hoeveelheid in elke richting. Een antenne die gelijkwaardig straalt over een specifiek vlak wordt een omnidirectionele antenne genoemd [13]. Hiervan bestaan verschillende soorten zoals monopoolantennes, dipoolantennes en vleugel antennes [25], [26], [27], [28]. Een andere vorm van antennes zijn directionele antennes dewelke energie besparen door de elektromagnetische straling daar te focussen waar het nodig is. Eén soort hiervan dat uitgebreid onderzocht zijn in verscheidene antenne-arrays zijn de microstrip-antennes [29], [30], [31]. Deze voorzien verschillende voordelen ten opzichte van meer traditionele antennes [32], [33] zoals het beperkte gewicht, lage productiekosten en aerodynamica.

Een microstrip-antennes is opgebouwd uit een grondplaat en een stralingsplaat met daartussen een diëlectrisch substraat. Verscheidene variates bestaan zoals microstrip patch antennes, microstrip slot antennes and geprinte dipool antennes. dewelke allemaal gelijkende karakteristieken hebben [32], [33]. Ze zijn allemaal dun, ondersteunen dubbele frequenties and hebben allemaal het nadeel dat ze interferentie kunnen veroorzaken op frequenties buiten het bedoelde spectrum. De microstrip patch en slot antenne ondersteunen beide circulaire en lineaire polarisatie terwijl de geprinte dipool antenne enkel lineare polarisatie ondersteund. Verder is de microstrip patch antenne het eenvoudigste te produceren ten opzichte van de andere overwogen antennes [32].

Figuur 1 toont een microstrip patch antenne dweelke bestaat uit aluminium die bevestigd is op een substraat van teflon. De microstrip patch antenna wijst naar de grond aangezien de drone boven de mensen zal vliegen.

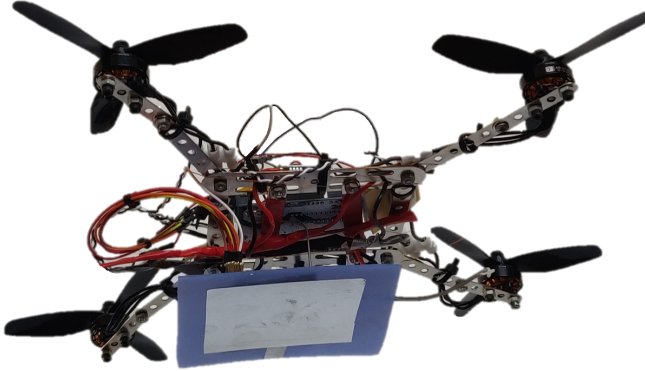


Fig. 1

Image of a microstrip patch antenna attached to the bottom of a Unmanned Aerial Vehicle (UAV).

### III. Methodologie

#### A. Elektromagnetische Straling

##### A.1 Totale Electromagnetische Straling

De totale SAT voor het volledige lichaam ( $SAT_{10g}^{wb,total}$ ) van een individu kan berekend worden als een eenvoudige som van de SAT-waarden van de verschillende bronnen. Dit is gebaseerd op de formule in [11] dweelke aanneemt dat het mobiele apparaat tegen het oor van zijn gebruiker gehouden wordt. Hierdoor worden alle waarden in lokale SAT-waarden voor het hoofd uitgedrukt. In dit netwerk is de plaats van het mobiele apparaat echter niet gekend wat zou leiden tot incorrecte conclusies. Bijgevolg zal alles uitgedrukt worden in functie van het volledige lichaam.

$$SAT_{10g}^{wb,total} = SAT_{10g}^{wb,myUE} + SAT_{10g}^{wb,myUABS} + SAT_{10g}^{wb,otherUE} + SAT_{10g}^{wb,otherUABSS} \quad (1)$$

In bovenstaande formule staat *wb* voor whole body oftewel het volledige lichaam en *UE* voor User Equipment oftewel het mobiele apparaat op de grond. De eerste parameter,  $SAT_{10g}^{wb,myUE}$ , duidt de geabsorbeerde elektromagnetische straling aan komende van de gebruik zijn eigen apparaat. Ondanks het feit dat de UL straling bedoeld is voor het UABS die deze gebruiker behandeld, een deel van deze straling wordt ook geabsorbeerd door zijn gebruiker. Dit komt vanwege het omnidirectionele gedrag van de gsm zijn antenne. Een tweede parameter is  $SAT_{10g}^{wb,myUABSS}$  dweelke de straling aanduid veroorzaakt door downlink (DL) dataverkeer, komende van de UABS die deze gebruiker behandeld. Als derde parameter hebben we  $SAT_{10g}^{wb,otherUE}$  dweelke de straling aanduidt veroorzaakt door andere gebruikers hun mobiel apparaat. Als laatste stelt  $SAT_{10g}^{wb,otherUABSS}$  de DL straling voor komende

van alle UABSen die andere gebruikers behandelen. Een illustratie is te vinden in 2 waarbij de groene pijl straling in het nabije veld voorstellen en alle andere pijlen straling in het verre veld voorstellen.

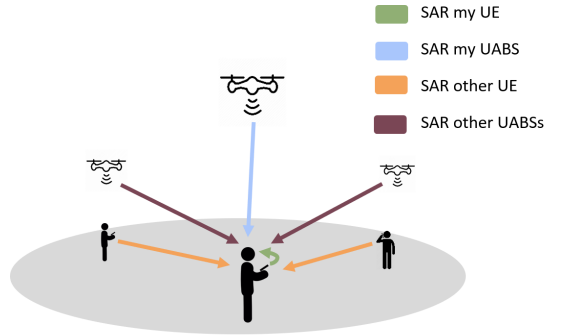


Fig. 2

Deze illustratie toont hoe de gemiddelde gebruiker (hier getoond in het midden) beïnvloed worden door verschillende bronnen van elektromagnetische straling.

#### A.2 Electromagnetische straling van een individuele bron

De elektromagnetische veldsterkte berekenen in een bepaald punt in het verre veld wordt gedaan worden voor alle UABS'en en alle mobiele apparaten behalve het apparaat in dat punt. Dit zal namelijk straling in het nabije veld zijn en dient anders berekend te worden. De elektromagnetische veldsterkte  $E$  voor het individu  $u$  komende van een brom  $i$  wordt als volgt berekend.

$$E_i(u)[V/m] = 10^{\frac{ES(u)[dBm] - 43.15 + 20 * log(f[MHz]) - PL(u)[dB]}{20}} \quad (2)$$

Het berekenen van de effectieve straling (ES) voor een gebruiker  $u$  vereist eerst om de equivalent isotropic radiation power (EIRP)-waarde te hebben berekend [7], [8]. Dit kan bekomen worden door de zendvermogen  $P_t$  op te tellen met de zendversterking  $G_t$  en het aftrekken van het kabelverlies  $L_t$ . Deze formule dient echter uitgebreid te worden zodoende dat er rekening gehouden wordt met signaalverzwakking die komt met verschillende stralingspatronen. Deze waarde hangt af van de hoek tussen de gebruiken en de richting waarnaar de antenne wijst. De signaalverzwakking bij een isotrope antenne is altijd nul ongeacht de hoek. Dit leidt tot de volgende formule.

$$RRP[dBm] = P_t[dBm] + G_t[dBi] - L_t[dB] - attenuation(u)[dB] \quad (3)$$

De gebruikte frequentie  $f$  in formule 2 is uitgedrukt in MHz. Aangezien LTE gebruikt wordt zal deze waarde 2600 MHz bevatten.

Als laatste dient formule 2 ook het padverlies  $PL$  te kennen. Een geschikt propagatie model dient gekozen te worden. Hier wordt geopteerd voor het Walfish-Ikegami model aangezien deze goed presteert voor femtocell netwerken in stedelijke gebieden [16].

### A.3 Samenvoegen van meerdere bronnen

De totale elektromagnetische straling  $E_{tot}$  in een bepaald punt, komende van alle verschillende bronnen kan berekend worden m.b.v. formule 4. Hierin staat  $E_i$  voor de elektromagnetische veldsterkte voor dat punt komende van bron  $i$  en  $n$  staat voor alle bronnen in het verre veld van een bepaalde categorie wat hier ofwel UABS's of mobiele apparaten van andere personen.  $E_{tot}$  zal berekend worden in elk punt waar er zich een gebruiker bevindt.

$$E_{tot}[V/m] = \sqrt{\sum_{i=1}^n (E_i[V/m])^2} \quad (4)$$

### A.4 Omzetten van elektromagnetische veldsterkte naar SAT

Formule 1 verwacht dat de SAT waarden in functie van het volledige lichaam uitgedrukt zijn. Om de elektromagnetische veldsterkte te kunnen omzetten naar deze SAT-waarden dient er een onderscheid gemaakt te worden tussen bronnen in het nabije veld ( $SAR^{wb,nf}$ ) en het verre veld ( $SAR^{wb,ff}$ ).  $SAR_{10g}^{wb,myUABS}$  is een bron waarbij de gebruiker zich in het nabije veld bevindt terwijl de gebruiker zich voor alle andere bronnen in het verre veld bevindt.

Het omzetten van deze waarden gebeurd door middel van een conversie constante dewelke gebaseerd is op Duke van de Virtual Family. Duke is een 34 jarige man met een gewicht van 72 kg, een hoogte van 1.74 en een bmi van 23.1 kg/m [12]. Onderzoek toont aan dat conversie constante voor WiFi in het verre veld  $0.0028 \frac{W/kg}{W/m^2}$  bedraagt en  $0.0070 \frac{W/kg}{W}$  in het nabije veld [12]. WiFi maakt gebruik van het 2400 MHz spectrum wat heel dichtbij LTE valt (2600 MHz). Daarom wordt in [12] aangenomen dat de conversie constante ook van toepassing is voor LTE.

Het berekenen van SAT in het verre veld word bijgevolg als volgt gedaan.

$$S[W/m^2] = \frac{(E_{tot}[V/m])^2}{337} \quad (5)$$

$$SAR_{10g}^{wb,ff}[W/kg] = S[W/m^2] * 0.0028 \left[ \frac{W/kg}{W/m^2} \right] \quad (6)$$

De constante is vergelijking 6 zet de vermogensdichtheid  $S$  om naar de verwachte  $SAR_{10g}^{ff,wb}$ . Om dit mogelijk te maken moet de uitkomst van formule 4 eerst nog omgezet worden naar vermogensdichtheid met behulp van formule 5.

De SAT die veroorzaakt wordt door het mobiel apparaat in het nabije veld kan gevonden worden door het zendvermogen  $P_{tx}$  van het apparaat te vermenigvuldigen met de conversie constante voor het nabije veld.

$$SAR_{10g}^{wb,nf} \left[ \frac{W}{kg} \right] = 0.0070 \left[ \frac{W/kg}{W} \right] * P_{tx}[W] \quad (7)$$

De energie die door het mobiele apparaat wordt gebruikt

kan berekend worden met formule 8 [12].

$$\begin{aligned} P_{tx}^{UE} &= \min\{P_{max}[dBm], \\ &P_{pusch}[dBm] + \alpha * PL[dB] + 10\log(M) + \sigma\} \end{aligned} \quad (8)$$

### B. Microstrip Patch Antenne

Een microstrip patch antenne is gekozen vanwege zijn eenvoudige productieproces maar voornamelijk vanwege het lage gewicht en aerodynamica wat heel voordelig is wanneer het aan een drone gekoppeld wordt [32].

De dimensies van de antenne hangen af van de gebruikte frequentie en de eigenschappen van het diëlectrisch substraat. De antenne zal opereren met een frequentie  $f_0$  van 2.6 GHz. Elk substraat heeft een diëlectrische constante  $\epsilon_r$  dat de doorlaatbaarheid van het substraat aanduid en hangt af van het gebruikte materiaal. Substraten met een hoge diëlectrische constante en kleine hoogte zullen de dimensies van de antenne reduceren terwijl een lager diëlectrische constante met een hogere hoogte de performantie van de antenne zullen bevorderen [33], [34]. Voor dit onderzoek is glas het gekozen substraat vanwege zijn hogere diëlectrische constante van  $\epsilon_r = 4.4$  ten opzichte van andere materialen zoals Teflon met een diëlectrische constante van  $\epsilon_r = 2.2$  [33]. Glass met een hoogte van 2.87 mm zal de dimensies van het volledige antenne oppervlakte verminderen wat voordelig is bij de beperkte ruimte die beschikbaar is op een drone.

beschrijving	symbool	waarde
middenfrequentie	$f_0$	2600 Hz
diëlectrische constante	$\epsilon_r$	4.4
Hoogte van het substraat	$h$	0.00287 m

TABLE I  
Overzicht van de configuratie parameters

De dimensies van de stralingsplaat kunnen berekend worden met de formules uit [33], [34]. Dit leidt tot een stralingsplaat van 35.09 mm bij 26.55 mm en een grondplaat van minstens 52.40 mm bij 43.80 mm. De resulterende microstrip patch antenne is geïllustreerd in figuur 3 en zal resulteren in het stralingspatroon getekend in figuur 4.

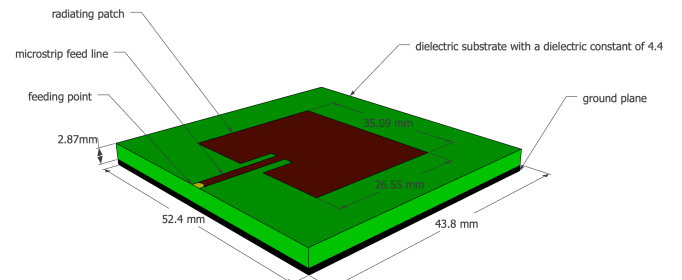


Fig. 3  
Design van een microstrip patch antenne.

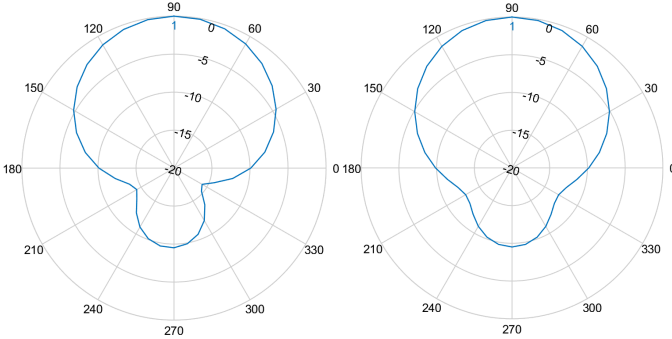


Fig. 4

Links is het stralingspatroon voor het E-vlak en rechts voor het H-vlak.

### C. Optimaliseren van het netwerk

Deruyck et al. bespreekt in [8] hoe een traditioneel mobiel netwerk geoptimaliseerd kan worden naar Hoewel een toenemend zendvermogen wel degelijk resulteert in een toenemend elektromagnetische veldsterkte is deze regel niet van toepassing indien we het energieverbruik bekijken over het hele netwerk heen. De auteurs van [8] tonen een omgekeerd equivalente relatie aan. De reden hierachter is dat het vaak goedkoper is op gebied van energie om de elektromagnetische straling van een al actieve base station verder te laten toenemen i.p.v. een nieuwe base station te activeren. Dit leidt tot de volgende fitness functie dewelke gebaseerd is op [8].

$$f = w * \left(1 - \frac{E_m}{E_{max}}\right) + (1 - w) * \left(1 - \frac{P}{P_{max}}\right) * 100 \quad (9)$$

Formule 9 geeft een gewicht terug dat aanduid hoe goed het netwerk presteert.  $w$  is de belangrijkheidsfactor die loopt van 0 tot 1, grenzen inbegrepen. Een  $w$  gelijk aan 0 betekent dat elektromagnetische straling niet belangrijk is. Een dergelijk netwerk wordt een power consumption optimized (PwrC. Opt.) netwerk genoemd. Aan de andere kant, een  $w$  gelijk aan 1 impliceert dat het minimaliseren van elektromagnetische bloedstelling top prioriteit is en zal bijgevolg resulteren in een exposure optimized (Exp. Opt.) netwerk.  $P_{max}$  is het energieverbruik van alle UABS's op maximaal zendvermogen, ongeacht of ze op non-actief staan of niet.  $P$  representeert de effectieve verbruikte energie van het huidig ontwikkelde netwerk.  $E_m$  is de gewogen elektromagnetische straling van de gemiddelde gebruiken van het huidig ontwikkelde netwerk en  $E_{max}$  is dezelfde waarde maar met alle UABS's op maximaal zendvermogen.

Bij het optimaliseren van het netwerk is het niet enkel belangrijk om de gemiddelde gebruiker te overwegen maar ook het limiteren van extrema [8]. Daarom wordt er gebruik gemaakt van het gewogen gemiddelde waarbij niet enkel rekening gehouden wordt met de mediaan maar ook met het 95<sup>ste</sup> percentiel. Dit leidt tot formule 10 waarbij  $w_1$  en  $w_2$  de gewichten zijn van respectievelijk de mediaan

en 95<sup>ste</sup> percentiel. Aangezien verondersteld wordt dat beiden waarden een gelijkwaardige rol spelen zullen beiden een gewicht van 0.5 krijgen.

$$E_m = \frac{w_1 * E_{50} + w_2 * E_{95}}{w_1 + w_2} \quad (10)$$

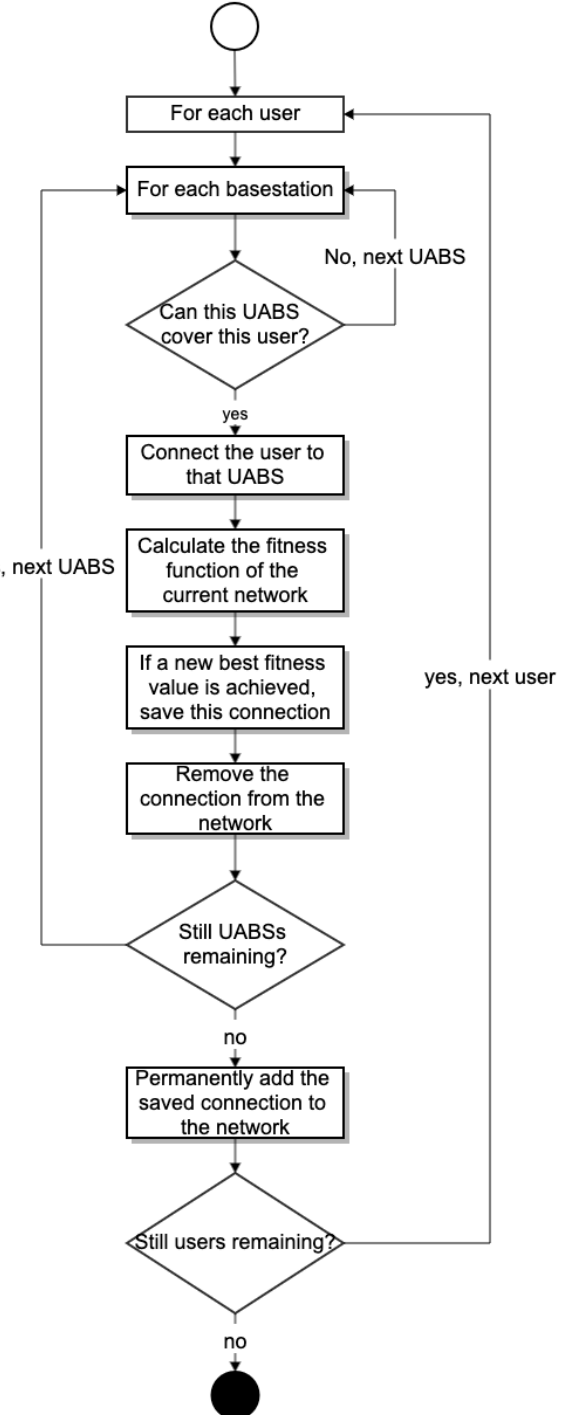


Fig. 5  
Flowchart of the decision algorithm.

## D. Simulatie Tool

### D.1 Hoofdalgoritme

In eerste instantie dient een beschrijving van het gebied voorzien te worden. Dit wordt verwezenlijkt met behulp van zogenaamde shape-bestanden. Deze bestanden bevatten een volledige beschrijving van de vorm van elk gebouw. Vervolgens worden gebruikers uniform verdeeld over het gebied en zal er een tijdelijke UABS geplaatst worden boven elke gebruiker? Nu is het aan het beslissingsalgoritme om te bepalen welke UABSs effectief zal blijven en hoe hoog het zendvermogen van elke UABS zal zijn. Eens het beslissingsalgoritme voltooid is zal de tool controleren of het aantal van online drones niet meer is dan de capaciteit van de stockageruimte toelaat. Indien dit wel het geval is zullen drones offline gehaald worden, beginnend bij drones die het minste personen behandelen.

### D.2 Beslissingsalgoritme

Het oplossen van het netwerk wordt gedaan door het beslissingsalgoritme en start met het berekenen van het padverlies tussen alle gebruikers en tussen gebruikers en drones. Hierna doorloopt het algoritme elke gebruiker waarbij getracht wordt deze te verbinden met elke mogelijke drone. Deze verbinding is niet altijd mogelijk omdat een drone al reeds verzadigd kan zijn met andere gebruikers of de drone is zo ver verwijderd van deze gebruiker dat het de maximale toegestane zendvermogen zou overschreiden. Indien een verbinding toch mogelijk is zal de gebruiker met deze drone verbonden worden en zal een score toegekend worden met behulp van de fitness functie 9. Dit proces wordt herhaald voor elke drone. Uitsluitend de verbinding dat resulteert in de beste score voor het volledige netwerk zal gebruikt worden. Wanneer de laatste gebruiker behandeld is geweest, bekomen we een volledig netwerk voor een ongelimiteerd aantal drones. Het netwerk wordt vervolgens terug aan het hoofdalgoritme gegeven voor eventueel verdere afhandeling. Een stroomdiagram van dit algoritme is gegeven in figuur 5.

## IV. Scenario's

De standaard configuratie is gegeven in tabel II en is altijd van toepassing tenzij anders vermeld.

Drie scenario's zullen onderzocht worden. Het eerste zal één enkele gebruiker en drone overwegen voor het gehele netwerk. SAT, elektromagnetische straling, energieverbruik en het nodige zendvermogen van de antenne zullen onderzocht worden voor verschillende vlieghoogtes.

In a second scenario, the network is expanded for multiple users while still considering only one UABS. The scenario is divided into two cases. One with a variable flying height but with a fixed number of 224 users as is average on an usual day at 5 p.m. in Ghent [16]. In the other case, the number of users varies but the flying height is set to 100 metres [16]. The power consumption, electromagnetic exposure and specific absorption rate are investigated for each case.

Mobiel netwerk	
technologie	LTE
frequentie	2.6 GHz
Power offset ( $P_{pusch}$ )	-120 dBm
Compenstatie voor padverlies ( $\alpha$ )	1
Correctie waarde	0 dBm
Aantal resource blokken	100
Drone	
energie drone	13.0 A
gemiddelde snelheid	12.0 m/s
gemiddeld energieverbruik	17.33 Ah
voltage batterij	22.2 V
Femtocell antenna	
maximum $P_{tx}$	33 dBm
richting van de antenne	neerwaarts (horizontaal: 0°; verticaal:
zendversterking	4 dBm
kabelverlies	2 dBm
implementation loss	0 dBm
stralingspatroon	EIRP or microstrip patch
vlieghoogte	100m
UE Antenna	
hoogte	1.5m vanaf de vloer
zendversterking	0 dBm
kabelverlies	0 dBm
stralingspatroon	EIRP
aantal aanwezig in het netwerk	224

TABLE II  
Overzicht van de waarden voor een standaard configuratie.

The third scenario is quite similar to the previous scenario. The same two cases are investigated, but now an unlimited number of UABSs is available.

Each case from each scenario consists out of four possible configurations. There are two possible antennae, namely EIRP and microstrip patch antenna, which can both be applied in a PwrC. Opt. network or an Exp. Opt. network.

It is important to note that all measured values are strictly limited to the sources mentioned in the previous section and thus only cover data traffic between User Equipment (UE) and UABSs. Any other potential sources like backhaul links will not be covered.

An overview of the simulation configuration scenarios is presented in figure 6

## V. Results

### A. One User and One UAV

The results show that for a varying flying height, a logarithmic relationship exists between the  $P_{tx}$  and the flying height. This is mainly caused by the logarithmic scale in which the decibels of the  $P_{tx}$  are expressed. So while 10 dBm equals 10 mW, 20 dBm equals 100 mW. Each time the flying height becomes too large to cover, the  $P_{tx}$  increases with one dBm. When using the default configuration, with

Antenna type	Optimization strategy	
	Exposure optimized	Power consumption optimized
Equivalent isotropic radiator	EIRP Exp Opt	EIRP PwrC Opt
Microstrip patch antenna	Microstrip Exp Opt	Microstrip PwrC Opt

Fig. 6

Matrix with the four possible configurations

a maximum  $P_{tx}$  of 33 dBm, a UABS can fly up to 387 m before losing connection in a free line of sight (LOS) scenario.

This scenario is investigated with a microstrip patch antenna using power consumption optimization. However, the chosen optimization strategy does not really matter because the decision algorithm decides which user needs to be connected to which UABS. Since only one UABS is available, both optimization strategies will behave identical. Further, also the used antenna will not make any difference. The user is namely positioned in the perfect centre of the main beam where there is no attenuation experienced for both antennae.

When investigating this scenario at different flying heights, we notice that the UL radiation increases exponentially while the DL radiation remains constant during the entire time. The reason that the DL radiation remains constant is because of power control which makes sure that no more power is used than strictly necessary. So at lower flying altitudes, there is less path loss and the UABS will therefore reduce the  $P_{tx}$ . We can therefore confirm that the electromagnetic exposure is a constant fraction of power and distance. The UL radiation starts very low but surpasses the DL radiation around 80 metres.

## B. Increased Population with one UABS

### B.1 Variable Flying Height

A PwrC. Opt. network has higher exposure compared to an Exp. Opt. network; a behaviour that was already proven by [8]. However, for this scenario, a PwrC. Opt. network will also result in a higher power consumption. To understand this, the behaviour of the deployment tool needs to be understood first. A PwrC. Opt. network will result in a few high powered UABSs because increasing the input power of an antenna costs less than activating a new UAV. Likewise, an Exp. Opt. network generates a lot of low powered UABSs because the lower the power of the antenna, the lower the exposure. This has the consequence that the cover radius is less and therefore more UAVs, which cost more energy, are required. When only a limited amount of UABSs are available, like only one in

this scenario, the tool will only keep UABSs which cover the most users. Therefore, the power consumption in a PwrC. Opt. network is much more higher.

Further, the results also show that the exposure increases with higher flying altitudes because there is a lower probability of having non line of sight (NLOS) links by obstructing buildings. This has as consequence that more users become covered. The increasing electromagnetic radiation is however not unlimited. At even higher flying altitudes, the distance between a given UABS and some users further away becomes too large causing the coverage to decrease again. When this decrease occurs depends on the configuration. A PwrC. Opt. network tends to decline earlier than an Exp. Opt. network.

When replacing the fictional EIRP antenna by a microstrip patch antenna, the percentage of covered users drops for both optimization strategies. This is because users, who have a higher horizontal distance between themselves and the UABS, experience a higher attenuation.

The results further show that the radiation from the UABS is the main factor followed by the near-field radiation from the user's own device. The far-field radiation from other UE barely contributes anything.

### B.2 Variable Number of Users

Also the results from this case show how EIRP antennae designs are able to cover more users than microstrip patch antennae just like PwrC. Opt. networks will reach more users than Exp. Opt. networks. The contribution to the total SAT from each individual source is identical to the previous scenario.

There is still only one UABS available. When population grows, more users become uncovered and therefore the average electromagnetic exposure decreases. For example, an EIRP PwrC. Opt. network will have the highest exposure and therefore covers the most users as opposed to a microstrip patch antenna in an Exp. Opt. network which will radiate the least and thus has the lowest number of covered users.

While the population grows, more and more users become uncovered causing the average SAR to drop. However, this does not conclude that by increasing the population, the SAR of a user who is directly beneath a UABS would be less. To investigate this, a user is positioned in the middle of the city centre of Ghent and a UAV is positioned above him. Initially, only 49 people are active around him. The SAT of our central user is monitored while the population around him is growing. Figure 7 shows with the black lines which users are connected. The left map is for only 50 users and shows that only one user is connected besides our central user. The map on the right considers 600 users and shows much more connected users. The results show that the UL SAT of the central user remains constant; a normal behaviour since the flying altitude does not change. The SAT from the UABS experiences a slight increase. When the population grows, more users become available and some will spawn near the central user. The UABS will likely decide to cover these users as well as vis-

ible in figure 7. These users might have a slightly worse path loss because of obstructing buildings or a somewhat bigger distance. The UABS reacts to this by increasing its power consumption causing an increase in the DL SAT for the central user. The results further also show that the SAT from other UE increases when the population increases. But as mentioned before, it is much less compared to the other sources.

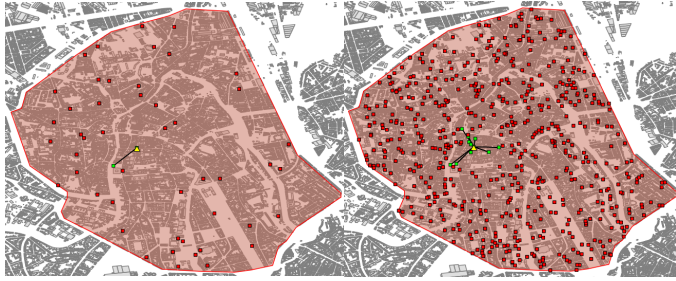


Fig. 7

Overview of which users are connected to the UABS. The map on the left is for 50 active users while the map on the right considers 600 active users.

### C. Unlimited Number of UABSs

#### C.1 Variable Flying Height

The same cases as in the previous scenario are investigated. Only now, an unlimited number of UABSs is available. The results prove that the different optimization strategies work as intended. PwrC. Opt. networks have indeed a lower power consumption but therefore result in higher electromagnetic radiation. On the other hand, an Exp. Opt. network will reduce the electromagnetic exposure by using more UAVs and thence also increase the network's power consumption. This conclusion was already made in [8] and is supported by these results.

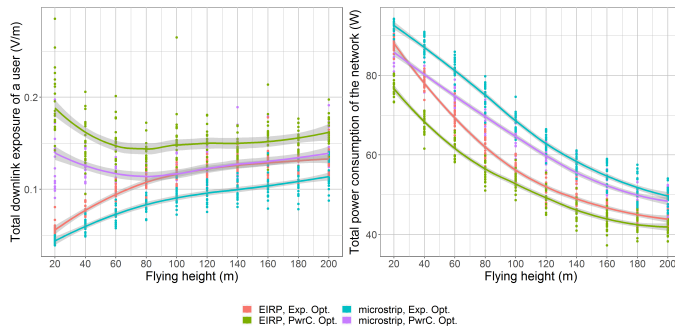


Fig. 8

These two figures show how the flying height influences the downlink electromagnetic radiation of the average user (left) and power consumption of the entire network (right) for an unlimited number of drones.

The exposure in figure 8 shows that an Exp. Opt. network increases logarithmically while the PwrC. Opt. net-

work rather has a concave relationship with the flying height, and has its lowest point at around 70 metres.

At a flying height of 20 m, the Exp. Opt. network has on average 220 to 224 UABSs. That is (almost) one UABS for each user so it is logical that the electromagnetic exposure is very low. The number of UAVs in a PwrC. Opt. network is much less in order to save energy but it is still able to achieve the same percentage of coverage. This is done by increasing the radiation so the cover radius would become larger. The results further show that the network profits from increasing the flying altitude. Not only less UAVs are needed but also the power consumption is lower. Both can be explained by the lower path loss when UABSs fly higher.

Figure 9 shows how each source contributes to the total SAT. A first consequence of higher flying altitudes is the increase in electromagnetic radiation from the user's own device; a behaviour also explained in the first scenario. A second consequence is that also the exposure from 'other UABSs' increases, caused by lower path loss from less obstructing buildings. The figures from 9 further also clearly show that this increase in electromagnetic radiation will be less for a microstrip patch antenna. The reason behind this is that energy will be more focussed towards the ground and there is less sideways radiation because of attenuation.

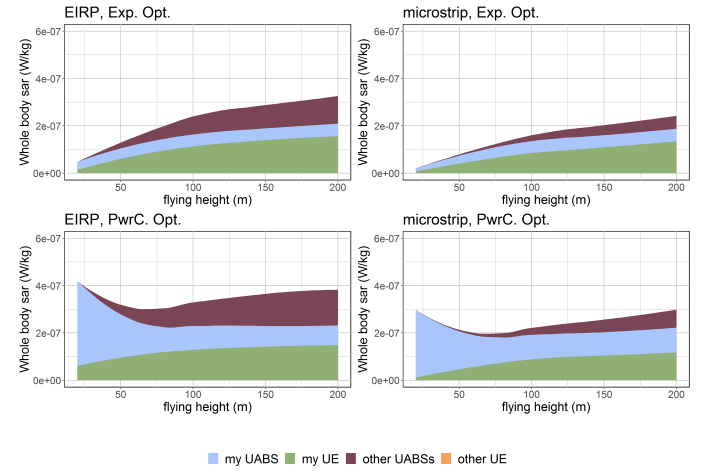


Fig. 9

Each chart corresponds with one of the four possible configurations. The contribution of each source towards the total SAT for a varying flying height is shown.

#### C.2 Variable Number of Users

When the flying height of the UABSs is fixed to 100 metres and the density of the population increases, also the number of required UAVs increases in order to reach a 100 % coverage. Figure 10 shows that when the number of UABSs and users increases, also the electromagnetic exposure and power consumption increases. Once again, the EIRP antenna in a power consumption network has the highest exposure for the lowest power consumption and a microstrip patch antenna in an Exp. Opt. network the

lowest exposure for the highest power consumption. The two other combinations are in the middle and behave very similar.

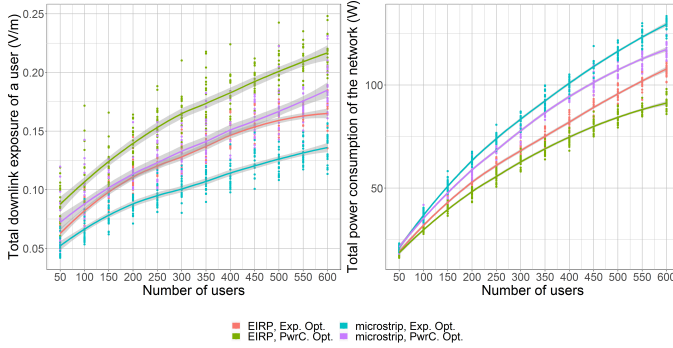


Fig. 10

These two figures show how the number of users influences the downlink electromagnetic radiation of the average user (left) and power consumption of the entire network (right) for an unlimited number of drones.

When looking at the different contributions to the total SAT in figure 11, we see that the weighted average SAT from the users' own device and from the serving UABS remains constant. The flying altitude is always the same so also the required energy to cover that distance will remain the same. The only SAT values that increase are the DL SAT from other UABSs and the UL SAT from other UE. When more users come online, also more UAVs will be radiating. The electromagnetic radiation will thus increase for both types of sources. Moreover, there is very little path loss at this flying altitude since it is higher than the average building.

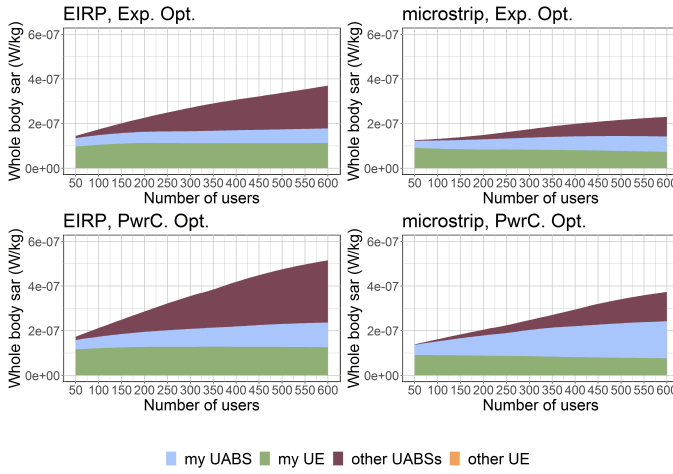


Fig. 11

Each chart corresponds with one of the four possible configurations. The contribution of each source towards the total SAT for a varying number of users shown.

## VI. Conclusion

Literature showed that a network can be optimized towards either the power consumption of the entire network or the electromagnetic exposure of the average user using a fitness function [8]. However, the fitness function should be used with care considering that UABSs can be placed anywhere as opposed to the transmission towers from [8] who have a predetermined position. In an Exp. Opt. network, this causes a lot of users to get a UABS all by themselves because this is the best approach to minimize exposure. A PwrC. Opt. network on the other hand will try to limit the number of drones in order to save energy. So as a rule of thumb: an Exp. Opt. network will result in a lot of low powered devices (increasing the overall power consumption) while a PwrC. Opt. network results in a few high powered devices (increasing the exposure of the average user). If the goal is to remain in the air for a longer period of time, an Exp. Opt. network is recommended because the power consumption of an individual UABS is lower. On the other hand, a PwrC. Opt. network is cheaper because less drones are involved. Moreover, the results show that the electromagnetic radiation in a PwrC. Opt. network (with high powered UABSs) is far below the thresholds enforced by the Flemish government.

The user's main sources of exposure are the user's own device and the UABS who is serving him, followed by all other UABSs in the network. When the population increases, there is not only more radiation from UE but also from more UABSs that are serving the other users. The exposure from other people's UE is so low that it can be neglected. An Exp. Opt. network will limit the total exposure mainly by trying to reduce the exposure from other UABSs.

A directional microstrip patch antenna is introduced because it gives several advantages compared to omnidirectional antennae. Directional antennae are able to focus their energy there where it is needed, namely towards the ground. Microstrip patch antennae further benefit from their thin and lightweight design. The performance of this directional microstrip patch antenna has been compared to a fictional isotropic antenne. This isotropic antenne has higher exposure and coverage for less power, compared to realistic antennae like microstrip patch antennae because of the absence of attenuation, and can hypothetically be compared with an antenna with a very big aperture angle. This type of antenna can achieve the same coverage with less resources like power and number of drones. A microstrip patch antenna with a more limited aperture angle of 90° requires more resources but causes less sideways radiation. So the exposure from other UABSs will be way less.

Remarkable is that an EIRP Exp. Opt. network behaves very similar to a microstrip PwrC. Opt. network as shown in figure 12. This results in the best of both worlds. The microstrip patch antenna will generate less electromagnetic radiation by design and the power consumption optimization reduces the number of required drones and power. A microstrip patch antenna with an aperture angle of 90°

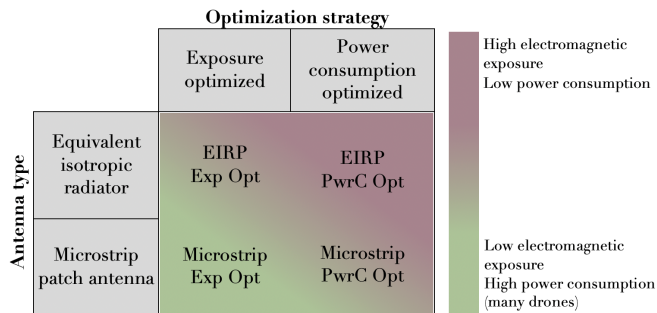


Fig. 12

Matrix with the four possible configurations, colour-coded based on the results.

is considered as a good solution but if budget is limited, an antenna with a larger aperture angle would further reduce cost without interfering with the Flemish legislation regarding electromagnetic exposure.

The electromagnetic radiation of an Exp. Opt. network increases with higher flying altitudes. Around 80 metres, the exposure from the user's device surpasses the exposure from the serving UABS. On the other hand, a PwrC. Opt. network shows that the lowest exposure is measured around 70 to 80 metres. Further, the results also show that the number of required drones decreases when the flying height becomes larger; a conclusion that was also made in [16]. When also considering the results from [17] where a flying altitude from 80 metres is suggested for an optimal access and backhaul connectivity, a flying height of 80 metres is also here proposed for the city centre of Ghent.

In short, a PwrC. Opt. network is proposed with a fixed flying height of 80 metres. A microstrip patch antenna with a sufficiently large aperture angle is a good starting point. However, different antenna configurations should be investigated.

### Acknowledgement

Special thanks to the WAVES research group at Ghent University for providing access to their capacity based deployment tool and therefore making this research possible.

### References

- [1] "Base overschreed stralingsnormen na aanslagen," De standaard, 2019.
- [2] L. Hardell and C. Sage, "Biological effects from electromagnetic field exposure and public exposure standards," *Biomedicine and Pharmacotherapy*, vol. 62, no. 2, pp. 104 – 109, 2008.
- [3] "What are electromagnetic fields." <https://www.who.int/peh-emf/about/WhatisEMF/en/index1.html>. Accessed: 15-10-2019.
- [4] "Elektromagnetische velden en gezondheid: Uw wegwijzer in het elektromagnetische landschap," Federale overheidsdienst: volksgezondheid, veiligheid van de voedselketen en leefmilieu, vol. 5, 2014.
- [5] "Normen zendantennes." <https://omgeving.vlaanderen.be/normen-zendantennes>. Accessed: 19-03-2020.
- [6] E. Commission, "Council recommendation of 12 july 1999 on the limitation of exposure of the general public to electromagnetic fields (0 hz to 300 ghz)," *Official Journal of the European Communities*, vol. 59, 1999.
- [7] D. Plets, W. Joseph, K. Vanhecke, and L. Martens, "Exposure optimization in indoor wireless networks by heuristic network planning," *Progress In Electromagnetics Research*, vol. 139, pp. 445–478, 01 2013.
- [8] M. Deruyck, E. Tanghe, D. Plets, L. Martens, and W. Joseph, "Optimizing lte wireless access networks towards power consumption and electromagnetic exposure of human beings," *Computer Networks*, vol. 94, 12 2015.
- [9] D. Plets, W. Joseph, S. Aerts, K. Vanhecke, G. Vermeeren, and L. Martens, "Prediction and comparison of downlink electric-field and uplink localised sar values for realistic indoor wireless planning," *Radiation Protection Dosimetry*, vol. 162, no. 4, pp. 487–498, 2014.
- [10] D. Plets, W. Joseph, K. Vanhecke, and L. Martens, "Downlink electric-field and uplink sar prediction algorithm in indoor wireless network planner," in *The 8th European Conference on Antennas and Propagation (EuCAP 2014)*, pp. 2457–2461, IEEE, 2014.
- [11] S. Kuehn, S. Pfeifer, B. Kochali, and N. Kuster, "Modelling of total exposure in hypothetical 5g mobile networks for varied topologies and user scenarios," Final Report of Project CRR-816, Available on line at: <https://tinyurl.com/r6z2gqn>, 2019.
- [12] D. Plets, W. Joseph, K. Vanhecke, G. Vermeeren, J. Wiart, S. Aerts, N. Varsier, and L. Martens, "Joint minimization of uplink and downlink whole-body exposure dose in indoor wireless networks," *BioMed research international*, vol. 2015, 2015.
- [13] Y. Zeng, Q. Wu, and R. Zhang, "Accessing from the sky: A tutorial on uav communications for 5g and beyond," *Proceedings of the IEEE*, vol. 107, no. 12, pp. 2327–2375, 2019.
- [14] Y. Kawamoto, H. Nishiyama, N. Kato, F. Ono, and R. Miura, "Toward future unmanned aerial vehicle networks: Architecture, resource allocation and field experiments," *IEEE Wireless Communications*, vol. 26, no. 1, pp. 94–99, 2018.
- [15] R. Gangula, O. Esrafilian, D. Gesbert, C. Roux, F. Kaltenberger, and R. Knopp, "Flying rebots: First results on an autonomous uav-based lte relay using open airinterface," in *2018 IEEE 19th International Workshop on Signal Processing Advances in Wireless Communications (SPAWC)*, pp. 1–5, IEEE, 2018.
- [16] M. Deruyck, J. Wyckmans, W. Joseph, and L. Martens, "Designing uav-aided emergency networks for large-scale disaster scenarios," *EURASIP Journal on Wireless Communications and Networking*, vol. 2018, 12 2018.
- [17] G. Castellanos, M. Deruyck, L. Martens, and W. Joseph, "Performance evaluation of direct-link backhaul for uav-aided emergency networks," *Sensors*, vol. 19, no. 15, p. 3342, 2019.
- [18] M. Mozaffari, W. Saad, M. Bennis, Y.-H. Nam, and M. Debbah, "A tutorial on uavs for wireless networks: Applications, challenges, and open problems," *IEEE communications surveys & tutorials*, vol. 21, no. 3, pp. 2334–2360, 2019.
- [19] Q. Wu, L. Liu, and R. Zhang, "Fundamental trade-offs in communication and trajectory design for uav-enabled wireless network," *IEEE Wireless Communications*, vol. 26, no. 1, pp. 36–44, 2019.
- [20] M. Deruyck, A. Marri, S. Mignardi, L. Martens, W. Joseph, and R. Verdone, "Performance evaluation of the dynamic trajectory design for an unmanned aerial base station in a single frequency network," in *2017 IEEE 28th Annual International Symposium on Personal, Indoor, and Mobile Radio Communications (PIMRC)*, pp. 1–7, IEEE, 2017.
- [21] A. V. Savkin and H. Huang, "Deployment of unmanned aerial vehicle base stations for optimal quality of coverage," *IEEE Wireless Communications Letters*, vol. 8, no. 1, pp. 321–324, 2018.
- [22] H. Huang and A. V. Savkin, "A method for optimized deployment of unmanned aerial vehicles for maximum coverage and minimum interference in cellular networks," *IEEE Transactions on Industrial Informatics*, vol. 15, no. 5, pp. 2638–2647, 2018.
- [23] C. T. Cicek, H. Gultekin, B. Tavli, and H. Yanikomeroglu, "Uav base station location optimization for next generation wireless networks: Overview and future research directions," in *2019 1st International Conference on Unmanned Vehicle Systems-Oman (UVS)*, pp. 1–6, IEEE, 2019.
- [24] A. Rizwan, D. Biswas, and V. Ramachandra, "Impact of uav structure on antenna radiation patterns at different frequencies," in *2017 IEEE International Conference on Antenna Innovations & Modern Technologies for Ground, Aircraft and Satellite Applications (iAIM)*, pp. 1–5, IEEE, 2017.
- [25] M. Nosrati, A. Jafargholi, and N. Tavassolian, "A broadband blade dipole antenna for uav applications," in *2016 IEEE Inter-*

- national Symposium on Antennas and Propagation (APSURSI), pp. 1777–1778, IEEE, 2016.
- [26] M. Nosrati, A. Jafargholi, R. Pazoki, and N. Tavassolian, “Broadband slotted blade dipole antenna for airborne uav applications,” *IEEE Transactions on Antennas and Propagation*, vol. 66, no. 8, pp. 3857–3864, 2018.
- [27] B. A. Arand, R. Shamsaei, and B. Yektakhah, “Design and fabrication of a broadband blade monopole antenna operating in 30 mhz–600 mhz frequency band,” in 2013 21st Iranian Conference on Electrical Engineering (ICEE), pp. 1–3, IEEE, 2013.
- [28] L. Akhoondzadeh-Asl, J. Hill, J.-J. Laurin, and M. Riel, “Novel low profile wideband monopole antenna for avionics applications,” *IEEE transactions on antennas and propagation*, vol. 61, no. 11, pp. 5766–5770, 2013.
- [29] S. S. Siddiq, G. Karthikeya, T. Tanjavur, and N. Agnihotri, “Microstrip dual band millimeter-wave antenna array for uav applications,” in 2016 21st International Conference on Microwave, Radar and Wireless Communications (MIKON), pp. 1–4, IEEE, 2016.
- [30] Y. Zheng, J. Zhou, W. Wang, and M. Chen, “A low-profile broadband circularly polarized antenna array for uav ground-to-air communication,” in 2018 IEEE Asia-Pacific Conference on Antennas and Propagation (APCAP), pp. 219–220, IEEE, 2018.
- [31] X. Sun, R. Blázquez-García, A. García-Tejero, J. M. Fernández-González, M. Burgos-García, and M. Sierra-Castañer, “Circular array antenna for uav-uav communications,” in 2017 11th European Conference on Antennas and Propagation (EUCAP), pp. 2025–2028, IEEE, 2017.
- [32] I. Singh and V. Tripathi, “Micro strip patch antenna and its applications: a survey,” *Int. J. Comp. Tech. Appl.*, vol. 2, no. 5, pp. 1595–1599, 2011.
- [33] K. Kashwan, V. Rajeshkumar, T. Gunasekaran, and K. S. Kumar, “Design and characterization of pin fed microstrip patch antennae,” in 2011 Eighth International Conference on Fuzzy Systems and Knowledge Discovery (FSKD), vol. 4, pp. 2258–2262, IEEE, 2011.
- [34] A. Sudarsan and A. Prabhu, “Design and development of microstrip patch antenna,” *International Journal of Antennas (JANT)* Vol, vol. 3, 2017.

# Contents

<b>List of Figures</b>	<b>vii</b>
<b>List of Tables</b>	<b>viii</b>
<b>List of Listings</b>	<b>ix</b>
<b>Glossary</b>	<b>x</b>
<b>Acronyms</b>	<b>xi</b>
<b>1 Introduction</b>	<b>1</b>
1.1 Outline of the Issue . . . . .	1
1.2 Objective . . . . .	2
1.3 Outline . . . . .	4
<b>2 State of the Art</b>	<b>5</b>
2.1 Electromagnetic Exposure . . . . .	5
2.1.1 Electromagnetic Field Radiation . . . . .	5
2.1.2 Specific Absorption Rate . . . . .	6
2.1.3 Related Work . . . . .	7
2.2 Optimized UAV-aided networks . . . . .	8

2.3	Technologies . . . . .	10
2.3.1	Type of Drone . . . . .	10
2.3.2	Long Term Evolution . . . . .	10
2.3.3	Type of Antennae . . . . .	11
2.4	Summary . . . . .	14
<b>3</b>	<b>Methodology</b>	<b>15</b>
3.1	Electromagnetic Exposure . . . . .	15
3.1.1	Calculation of the Total Specific Absorption Rate . . . . .	15
3.1.2	Electromagnetic Exposure Caused by Far-Field Radiation . . . . .	17
3.1.3	Electromagnetic Exposure Caused by Near-Field Radiation . . . . .	20
3.2	Microstrip Patch Antenna . . . . .	22
3.2.1	Design of a Microstrip Patch Antenna . . . . .	22
3.2.2	Radiation Pattern . . . . .	24
3.3	Optimizing the Network . . . . .	26
3.4	Simulation Tool . . . . .	28
3.4.1	Implementation of the Deployment Tool . . . . .	28
3.4.2	Implementation of the Radiation Pattern . . . . .	31
3.4.3	Performance Improvement . . . . .	33
3.5	Summary . . . . .	35
<b>4</b>	<b>Scenarios</b>	<b>36</b>
4.1	Scenario I: A Single User . . . . .	38
4.2	Scenario II: Increasing Traffic with only one Drone available . . . . .	40
4.3	Scenario III: Increasing Traffic with an Undefined Amount of Drones . . . . .	42

4.4	Overview of Configurations . . . . .	43
<b>5</b>	<b>Results and Discussion</b>	<b>44</b>
5.1	Scenario I: One User and One Unmanned Aerial Vehicle (UAV) . . . . .	45
5.1.1	The Influence of the Maximum Transmission Power . . . . .	45
5.1.2	Influence of the Flying Height . . . . .	46
5.2	Scenario II: Increased Population . . . . .	48
5.2.1	Influence of the Flying Altitude . . . . .	48
5.2.2	Influence of the Number of Users . . . . .	54
5.3	Scenario III: Unlimited UAVs . . . . .	60
5.3.1	Influence of the Flying Altitude . . . . .	60
5.3.2	Influence of the Number of Users . . . . .	63
5.4	Summary . . . . .	66
<b>6</b>	<b>Conclusions</b>	<b>68</b>
6.1	Conclusion . . . . .	68
6.2	Summary . . . . .	72
6.3	Future work . . . . .	72
<b>Appendices</b>		<b>79</b>
<b>A</b>	<b>Radiation Patterns: Datasheet</b>	<b>80</b>
<b>B</b>	<b>Radiation patterns: Example Configuration</b>	<b>82</b>

## List of Figures

1.1	This illustration shows how a UAV-aided network is able to either assist or replace existing transmission towers. . . . .	2
2.1	Resource allocation scheme for FDD. . . . .	11
2.2	Resource allocation scheme for TDD. . . . .	11
2.3	General design of a microstrip antenna. . . . .	12
2.4	Image of a microstrip patch antenna attached to the bottom of a UAV. . . . .	13
3.1	Illustration of the radiation affecting the average user (here shown in the center) by different types of sources. . . . .	16
3.2	Distribution of how many phones belong to a certain SAR interval. Upper boundary not included. . . . .	21
3.3	Design of the microstrip patch antenna. . . . .	24
3.4	Radiation pattern 1 (in dBi) with the configuration as described above. . . . .	26
3.5	Radiation pattern 2 (in dBi) which is generated with a groundplane of 0.06m by 0.06m. . . . .	26
3.6	Example of how users are randomly distributed over the city centre of Ghent. . . . .	28
3.7	Flowchart of the main algorithm. . . . .	29
3.8	Flowchart of the decision algorithm. . . . .	30
3.9	Illustration of the two possible movements. The UAV in fig. (a) is a top view while the UAV in fig. (b) is a side view. . . . .	31

3.10	Schematic example of slices in a radiation pattern. . . . .	32
3.11	Schematic example of how bilinear interpolation works. . . . .	33
3.12	Example of a KD-tree in two dimensions. . . . .	34
3.13	Distribution of how many connections belong to a certain interval of distance. Upper boundaries are not included. . . . .	35
4.1	The red area covers the city centre of Ghent, Belgium. . . . .	37
4.2	Location of ‘Koningin Maria Hendrikaplein’ on the town planning map of Ghent	39
4.3	Illustration of an example network that satisfies the restrictions of scenario I. . .	40
4.4	Illustration of an example network that satisfies the restrictions of scenario II. .	41
4.5	Illustration of an example network according to the description of scenario III. .	42
5.1	Minimal required transmission power by the antenna to reach the ground just below it. The red line shows the default maximum transmission power. . . . .	46
5.2	This figure shows how SAR values from different sources are influenced by different flying altitudes. . . . .	47
5.3	This figure shows the behaviour of the power consumption over the entire network at different flying heights. For this scenario, the power is used by only one UABS.	48
5.4	Example of an EIRP power consuption optimized network (PwrC Opt) network with only one UABS (yellow triangle). Only a very few users (green) are con- nected. All other users (red) remain uncovered. . . . .	49
5.5	Fig. (a) show how the flying height influences the downlink electromagnetic radiation of the average user and fig. (b) the power consumption of the entire network for the only UABS available in the network. . . . .	50
5.6	Schematic overview of scenario II with only 2 users. . . . .	50
5.7	scenario II with only 2 users. The coloured areas are only applicable for the red user. The blue user is connected during the entire time. . . . .	52
5.8	This graph shows the percentage of covered users for only one UABS at different flying heights. . . . .	52

5.9	Each figure corresponds with a certain configuration and shows how the SAR from different sources are influenced by an increasing flying height. . . . .	53
5.10	The influence of increasing traffic on the user coverage. . . . .	54
5.11	These two figures show how various sizes of population influence the downlink electromagnetic radiation of the average user (left) and power consumption of the entire network (rights) for one UABS available in the network. . . . .	56
5.12	This figure shows how different sources are influenced by an increasing number of users. . . . .	57
5.13	Overview of which users are connected to the UABS. . . . .	58
5.14	SAR-values for the user who is directly beneath the only UABS available. . . . .	59
5.15	Example of two networks with users distributed over the area. Yellow triangles represent UABSs and are connected with black lines to users in green. Uncovered users are coloured in red. . . . .	60
5.16	These two figures show how the flying height influences the downlink electromagnetic radiation of the average user (left) and power consumption of the entire network (right) for an unlimited number of drones. . . . .	61
5.17	This graph shows how much UAVs are required at different flying heights while trying to achieve a 100% coverage. . . . .	62
5.18	Each figure corresponds with a certain configuration and shows how the SAR from different sources are influenced by an increasing flying height. . . . .	63
5.19	This graph shows how much UAVs are required for different flying heights while trying to achieve a 100% coverage. . . . .	64
5.20	The influence of the population size on the downlink electromagnetic radiation (a) and power consumption (b). . . . .	65
5.21	Each figure corresponds with a certain configuration and shows how the SAR from different sources are influenced by an increasing population density. An unlimited number of UABSs is available. . . . .	66
6.1	Matrix with the four possible configurations, colour-coded based on the results. .	70

6.2 Contribution from each source towards the total SAR that is experienced by the weighted average user. The percentages are averaged over the four considered configurations. . . . .	71
---	----

## List of Tables

2.1	Overview of the different SAR limitations.	6
2.2	Specifications of the used drone.	10
3.1	Overview of the configuration parameters.	23
4.1	Overview of default configuration values.	38
4.2	Evaluated parameters	39
4.3	Restrictions	40
4.4	Evaluated parameters	41
4.5	Restrictions	41
4.6	Evaluated parameters	42
4.7	Matrix with the four possible configurations	43
A.1	Overview of attenuation in dBm.	81

## List of Listings

1	Matlab code to generate the radiation patterns for the microstrip patch antenna.	25
2	Example configuration of a radiation pattern.	83

# Glossary

<b>dielectric constant</b>	The dielectric constant is the ratio of permittivity of the substance to permittivity of free space.. , 13, 22–24
<b>equivalent isotropic radiator</b>	A theoretical source of electromagnetic waves which radiates the same intensity for all directions. , 11, 17, 31, 34, 36, 37, 39, 41, 46, 51, 54, 56, 60, 64, 68–70
<b>exact algorithm</b>	An exact algorithm solves an optimization problem optimally. , 9, 72
<b>power flux density</b>	Magnitude of power ( $W$ ) that travels through a curtain area ( $m^2$ ). , 20
<b>RRP</b>	RRP is an abbreviation used in this paper to indicate an extension on EIRP and stands for Real Radiation Pattern. An RRP value indicates the power (in dBm) for a certain location unlike an EIRP where the power (in dBm) is independent of the location. , 17
<b>spurious radiation</b>	According to the thefreedictionary.com: Any emission from a radio transmitter at frequencies outside its frequency band. Also known as spurious emission. , 12, 13
<b>thermoregulatory capacity</b>	The capacity of an organism to regulate body temperature. , 6



## Acronyms

<b>DL</b>	downlink. , 7, 10, 16, 46, 47, 49, 50, 52, 57, 61
<b>EIRP</b>	equivalent isotropic radiation power. , 17, 36, 38, 49, 51, 53, 55, 61–65, 70, 71
<b>EU</b>	European Union. , 5, 6
<b>Exp Opt</b>	exposure optimized network. , 27, 60–65
<b>FCC</b>	Federal Communications Commission. , 6, 20
<b>FDD</b>	Frequency Division Duplex. , 10, 11
<b>GSM</b>	Global System for Mobile Communications. , 8, 70
<b>ICNIRP</b>	International Commission on Non-Ionizing Radiation Protection. , 5, 6, 8
<b>IEC</b>	International Electrotechnical Commission. , 20
<b>IEEE</b>	Institute of Electrical and Electronics Engineers. , 6
<b>IoT</b>	Internet of Things. , 1
<b>LOS</b>	line of sight. , 17, 18, 45, 46, 51, 71
<b>LTE</b>	Long-Term Evolution. , 8–10, 20, 21, 39, 45
<b>NLOS</b>	non line of sight. , 9, 18, 50, 62
<b>PUSCH</b>	Physical Uplink Shared Channel. , 22, 71, 72
<b>PwrC Opt</b>	power consuption optimized network. , 27, 49, 53, 55, 56, 60–65
<b>SAR</b>	Specific Absorption Rate. , 6–8, 14–16, 20, 35, 44, 46, 47, 52, 53, 56, 57, 61, 63, 65, 66, 69–71

<b>SNR</b>	Signal to Noise Ratio. , 45, 47
<b>TDD</b>	Time Division Duplex. , 10, 11
<b>UABS</b>	Unmanned Arial Base Station. , 3, 8, 9, 16, 19, 20, 22, 27–34, 36, 38–53, 55–72
<b>UAV</b>	Unmanned Aerial Vehicle. , 2, 8–14, 26, 31, 36, 37, 40, 45–49, 51, 57, 60–65, 68
<b>UE</b>	User Equipment. , 5, 6, 8, 9, 11, 14, 16, 19, 20, 22, 28, 36–39, 42, 46, 47, 53, 56, 57, 61, 67
<b>UL</b>	uplink. , 7, 10, 16, 20, 22, 46, 47, 51, 57, 61, 71
<b>UMTS</b>	Universal Mobile Telecommunications System. , 7, 8, 70
<b>USA</b>	United States of America. , 6
<b>WHIPP</b>	WiCa Heuristic Indoor Propagation Prediction.
<b>WHO</b>	World Health Organization. , 2



# 1

## Introduction

This chapter gives a general introduction to the subject. First, the problem with classic terrestrial networks is explained and illustrated with some examples. Thereafter, the research questions that are believed to give a solution to this problem are discussed. Finally, an overview of the entire document is given.

### 1.1 Outline of the Issue

Society is constantly getting more and more dependent on wireless communication. On any given moment, in any given location, an electronic device can request to connect to the bigger network. Devices need more than ever to be connected, starting from small Internet of Things (IoT) up to self-driving cars which all need to be supported by the existing infrastructure. It is not surprising that the city centre of Ghent has an average coverage of 97% of 4G over all telecom operators [1]. Once again it becomes clear why we're on the eve of a new generation of cellular communication named 5G.

Also in exceptional and possibly life-threatening situations, the public relies on the cellular network. In 2011, Pukkelpop, a yearly festival in Belgium, got struck by a severe storm. However the storm was quite short, the damage was done, including the mobile network which remained

defective for the rest of the evening [2]. One solution for a fast temporarily deployable network is with the usage of UAVs. Base stations can be attached to these flying UAVs to support the damaged network over a limited area. This approach does not only come in handy for damaged networks but also in case of an unexpected increase of traffic. For example during the terrorist attacks at Brussels Airport, mobile network operators saw all telecommunications drastically increasing causing moments of contention. Some operators even decided to temporarily exceed the exposure limits in order to handle all connections [3]. This is illustrated in figure 1.1. Electromagnetic exposure can however not be neglected. Research shows how excessive electromagnetic radiation can cause diverse biological side effects [4]. Because of increasing public concern [4], the World Health Organization (WHO) had launched a large multidisciplinary research effort which eventually concluded that there was no sufficient evidence that confirmed that exposure to low level electromagnetic fields is harmful [5]. A large part of the population remains nevertheless very concerned about potential health risks. It becomes clear that electromagnetic exposure is a key value when designing a UAV-aided network and should definitely not surpass the predefined limits.

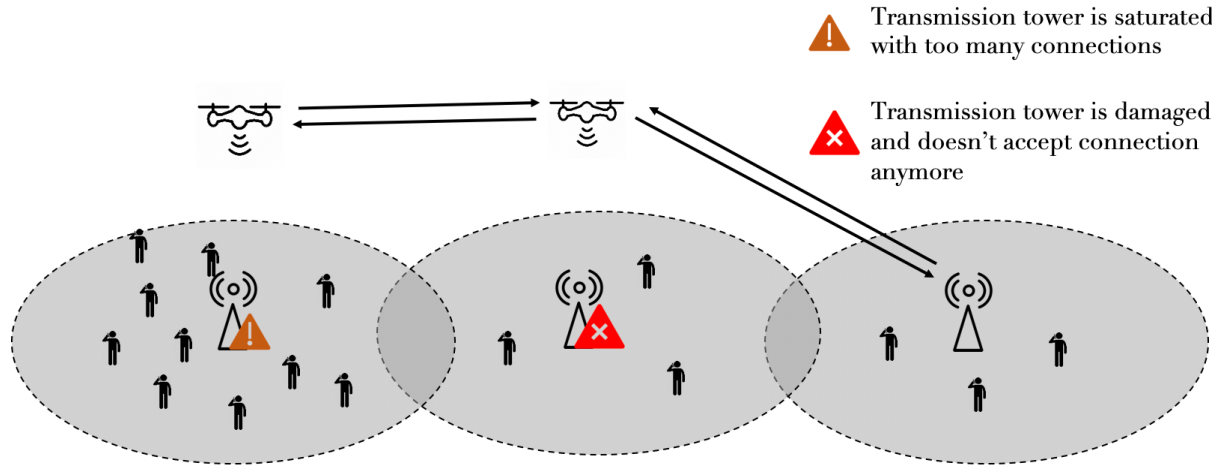


Figure 1.1: This illustration shows how a UAV-aided network is able to either assist or replace existing transmission towers.

## 1.2 Objective

UAV-aided networks can, thanks to their mobility, easily be repositioned towards a certain goal. Several papers in literature exist, explaining how a network can be optimized towards different goals like power consumption. However, very limited research has been done where a UAV-aided network is optimized towards electromagnetic exposure. While several publications exist, discussing how the electromagnetic exposure can be calculated, most of them only consider a

limited number of sources like only base stations or only mobile phones. Papers who cover electromagnetic exposure from all the different sources and convert it into a single value are rather limited.

This master dissertation proposes a method to optimize the network towards electromagnetic exposure and power consumption when considering all four sources of radiation in a telecommunications network, being: the user's own phone, the base station that is serving this user, all devices from other users in the network and all other active base stations that are not serving this user. In this way, the contribution of each source towards the total electromagnetic exposure can easily be identified.

The behaviour of the electromagnetic exposure and power consumption of the network will be analysed by applying the tool in different scenarios to give insight into which variables influence the exposure and how the network can be optimized accordingly. Further, also the difference between omnidirectional and directional antennae will be considered. This leads to the following research questions:

**Research question 1:** How a Unmanned Arial Base Station (UABS) based network could be optimized to minimize global exposure and overall power consumption? What are the effects on the network?

**Research question 2:** How does the network behave differently after the introduction of a realistic antenna?

**Research question 3:** How does the UABS flying height and number of users influence electromagnetic exposure and power consumption?

**Research question 4:** What is the contribution of each source towards the total electromagnetic exposure?

To make this research possible, an existing planning tool is extended which gives insight in user and base station distributions. The tool also calculates information about path loss between radiators, power usage of the different electrical devices and which base station serves which user. In other words, the tool describes a fully configured UABS based access network. In this way, all needed parameters will be known.

### **1.3 Outline**

This section briefly describes the structure of this document. Related research to the subject is discussed in chapter 2, where the State of the Art explains electromagnetic exposure and its absorption into the body. Also the used technology such as type of antennae, type of base station and which infrastructure will be examined. The chapter also discusses why this master dissertation differs from other research documents. Thereafter, chapter 4 talks about the different scenarios that will be investigated. Each scenario has different restrictions and consists of various configurations where different parameters will be evaluated. Eventually, the methodology is covered in chapter 3, where the calculations and implementation of the different aspects discussed in the State of the Art are presented. Chapter 5 shows the results of this implementation for the scenarios described in chapter 4. Finally, a conclusion and its results is formed in chapter 6 including future research trends.

# 2

## State of the Art

This chapter gives an overview of related research that has been done in the field of work and aims to familiarize the reader with the subject. First, an overview of the legislation related to electromagnetic exposure and specific absorption rate is given after which the related work about electromagnetic exposure is discussed. The second section describes how UAV-networks are designed and how they can be optimized. Finally, the used technologies are summed up including the type of drone, the characteristics of the cellular network and the type of antennae that are often used for this type of applications.

### 2.1 Electromagnetic Exposure

#### 2.1.1 Electromagnetic Field Radiation

People in wireless telecommunication networks are exposed to far-field electromagnetic radiation originating from base stations and other User Equipment (UE). Network planners need to make sure that the electromagnetic fields (expressed in V/m) do not exceed location dependent limitations enforced by the government. These limits are location dependent. The European Union (EU) recommends the guidelines as defined by the International Commission on Non-Ionizing Radiation Protection (ICNIRP) which limit electromagnetic exposure to 61 V/m. Each Euro-

pean country needs to decide for themselves which limitations to enforce. Belgium for example delegated this responsibility to Flanders, Brussels and Wallonia [6]. In order to have a comparable scenario, this study will be focused in the city center of Ghent. Therefore, the standards will be defined by the Flemish government, which state that in the 2.6 GHz frequency band, an individual antenna cannot exceed 4.5 V/m and the cumulative sum of all fixed sources has its maximum at 31 V/m [6, 7].

### 2.1.2 Specific Absorption Rate

The Specific Absorption Rate (Specific Absorption Rate (SAR)) represents the rate at which electromagnetic energy is absorbed by human tissue with the thermal effect as its most important health consequence. The volume of this tissue is typically 1 g ( $SAR_{1g}$ ) or 10 g ( $SAR_{10g}$ ).  $SAR$  values can be categorized based on the covered area, as an example, the whole body SAR ( $SAR^{wb}$ ) is defined as the average radiation over the entire body. Another example are localized SAR-values that only cover a certain part of the human body like the head. The ICNIRP has concluded that the threshold effect for  $SAR_{10g}^{wb}$  is at 4 W/kg meaning that any higher absorption rate would overwhelm the thermoregulatory capacity of the human body. Whole body SAR-values between 1 and 4 W/kg increase the temperature of the human body less than 1°C, which is proven not to be harmful for a healthy human being [8, 9]. Thereafter, a safety margin is introduced to tackle unknown variables like experimental errors, increased sensitivity for certain population groups and so on. The EU follows the recommendation from the ICNIRP [6] and suggests a whole body  $SAR_{10g}$  of 0.8 W/kg and 2 W/kg for localized  $SAR_{10g}$  at head and torso area [4, 10]. The first metric is applicable for UE and the second one for transmission towers [11]. Belgium follows this recommendation [6, 7]. The Federal Communications Commission (FCC) of the United States of America (USA) follows the recommendations of the Institute of Electrical and Electronics Engineers (IEEE) Std C95.1-1999 [12, 9] that defines regulations based on 1 g tissue. The  $SAR_{1g}^{wb}$  is therefore defined at 1.6 W/kg despite the fact that this value has been reviewed and changed by the IEEE to 8 W/kg in Std C95.1-2005 [9]. An overview is given in table 2.1.

Description	Value	Units
Max $SAR_{10g}^{wb}$ (defined by ICNIRP)	4	W/kg
Max $SAR_{10g}^{wb}$ for transmission towers (defined by the Belgian government)	0.8	W/kg
Max $SAR_{10g}$ for UE at head area (defined by the Belgian government)	2	W/kg
Max $SAR_{1g}$ for UE at head area (defined by the FCC)	1.6	W/kg

Table 2.1: Overview of the different SAR limitations.

The actual maximum SAR-value of a phone is usually much lower. As an illustration, the iPhone 11 pro has a maximum  $SAR_{10g}^{head}$  of 0.99 W/kg [13] and a Samsung Galaxy S20 (GT-I8530) a

$SAR_{10g}^{head}$  of  $0.516 \text{ W/Kg}$  [14, 15]. The phone with the highest recorded  $SAR_{10g}^{head}$  value according to [15] is the discontinued LG 510W with a maximum of  $1.94 \text{ W/kg}$ .

### 2.1.3 Related Work

The goal of this master dissertation is the investigation of electromagnetic exposure considering all sources. Four types of sources are considered: the user's own phone, the base station that is serving this user, all devices from other users in the network and all other active base stations that are not serving this user. This electromagnetic radiation is thereafter absorbed by the human body and will be expressed in SAR-values. Any other type or source of electromagnetic radiation like bluetooth, WiFi or backhaul connections will not be considered.

Several papers calculate exposure originating from certain sources, but very limited research has been done covering the whole picture. Plets et al. addresses in [16] the problem that electromagnetic exposure is often a neglected factor when designing a network. Therefore, they propose a heuristic indoor network planner aiming to optimize exposure and coverage in a WiFi network. They conclude that higher allowed exposure limits and more separation between the user and the access point have positive influence on the throughput. The authors of [17] used this knowledge to investigate electromagnetic exposure originating from base stations in a more outdoor environment and propose a capacity based deployment tool capable of optimizing towards electromagnetic exposure and power consumption in order to support future green networks. Plets et al. later extended their indoor network planner in [18] and [19] so that also uplink (UL) traffic from the user's device will be calculated. They did not only consider the electromagnetic radiation for Universal Mobile Telecommunications System (UMTS) and WiFi but also how much is absorbed by the body, which will be expressed as specific absorption rates. Since the authors only cover voice calls, uplink SAR is expressed in localized SAR values while the downlink traffic is expressed in whole body SAR. With the advent of 5G, paper [20] has been published, describing a guideline on how the total exposure of in a hypothetical 5G network has to be modelled and applies it to various scenarios. They discuss how localized SAR values are achieved from different sources including all mobile phones and all base stations. They conclude that the user's own device is the most important contributor to the total localized SAR. The exposure for unconnected users is mainly originating from bystanders instead of base stations. The exposure from these bystanders will be four times higher than from base stations. The authors also conclude that reducing the cell size has a positive influence on the exposure of active users by a factor 2 to 10. In short, they state that a network with a lower path loss, smaller cells and additional indoor coverage, helps to reduce total exposure. Finally, Plets et al. published in [21] how to minimize UL and downlink (DL) exposure dose for an indoor environment. They describe how both UL and DL traffic can be converted in whole body SAR values making it possible to achieve an overall picture. They conclude that a dose reduction of

75% can be achieved by increasing number of base stations and decreasing transmission power. Further, their optimization algorithm is able to reduce downlink doses for WiFi with more than 95%. The reduction for UMTS will vary between 73% and 83% and the dose reductions for Long-Term Evolution (LTE) will be at least 80%. Thanks to power control, UMTS and LTE require an almost continuous uplink usage in order to see a significant effect by the optimization algorithm.

Research about SAR-values have not only been done in function of an entire network. Also various papers exist considering other scenarios. In this way, Mahfouz et al. performs an analysis on the total SAR from a mobile phone considering the fact that the device contains multiple antennae. They concluded that the localized SAR for the different configurations never exceeds the limit defined by the ICNIRP [22]. The authors of [23] performed a research on the SAR-values for the head area when the mobile phone is positioned in the near-field and far-field and concluded that a difference in SAR-values was measured between both scenarios. In [24] are the standardization efforts discussed to predict localized and whole body SAR of users in and around the car when an antenna is attached to the outside of the car. Piuzzi et al. investigates in [25] the SAR of numeric models. The model of the children is achieved by anatomically downscaling the adult. The results show that the whole body SAR is higher for the children and therefore conclude that while the SAR measured for an adult might comply with restrictions enforced by the government, it is not necessarily the case for children. In [26] is the problem raised that developing a numeric model, often used for SAR analysis, is a timely and costly process. Therefore, an equation is proposed to estimate whole body SAR when using a half-wave dipole. Further, it is important to note that UE is not necessarily a mobile phone. For example, the authors of [27] investigated the exposure of a user to a nearby smart meter and concluded that SAR was well below the guideline restrictions. As last, the authors from [28] explained the duality between UE and base stations and concluded that the exposure from UE will decrease when the received signal improves. They also noticed that the exposure from UABSSs in a Global System for Mobile Communications (GSM) network is below than from UE. However, this is not always the case. An UMTS network will, thanks to power control, drastically reduce the exposure from UE and will therefore sometimes even be equal to radiation from the base station.

In a realistic network, some users are calling while others are using other types of telecommunication services like browsing the web. Therefore, all absorbed electromagnetic exposure should be expressed in whole body SAR while still covering all sources.

## 2.2 Optimized UAV-aided networks

A UAV knows several applications. It was originally mainly used to support the military for surveillance and remote attacks without endangering pilots [29]. However, UAVs have recently become more accessible by the general public due to decreasing costs. This allowed UAVs to be researched for various applications.

When attaching an antenna to a UAV, it can be used as a gateway for cellular communication for UE on the ground. Such a flying base station will be called a UABS. This has several advantages like mobility and rapid deployment which is ideal for emergency situations or temporary events. Thanks to this mobility, UABSs can easily be repositioned to satisfy certain requirements. A UAV-aided network also brings some challenges with it like the limited weight of the payload and sparse power supply.

Kawamoto et al. introduced in [30] a WiFi network with the support of UAVs while considering resource allocation and antenna directivity. Gangula et al. illustrates in [31] how UAVs can be used as a relay for LTE. If a terrestrial base station is in non line of sight (NLOS) with a user, a UABS can be used as a relay. Zeng et al. proposes in [29] a tutorial in 5G-and-beyond wireless systems where challenges like energy consumption, mobility and antenna direction are discussed. Deruyck et al. designed in [32] a capacity based deployment tool for UAV-aided emergency networks for large-scale disaster scenarios where an ideal flying height of 100 m is suggested. This was expanded in [33] with a performance evaluation of the direct-link backhaul of this tool where a slightly lower flying height of 80 metres is recommended.

These UAV-aided networks can be optimized towards certain goals. Mozaffari et al. provides in [34] guidelines on how to optimize and analyse UAVs equipped for wireless communication equipment. Issues like deployment, performance and power consumption are addressed. A research area that has been excessively studied is the location solutions optimization problem. For instance, [35] provides an algorithm that minimizes latency, [36, 37] minimizes interference between UABS and [38] minimizes the distance between UABS and UE. Other papers investigate trajectory optimization like in [36, 39]. Further, [34, 40] discuss several implementation approaches on how optimization algorithms should be tackled by discussing options like heuristic algorithms, exact algorithms and machine learning.

Optimizing the network towards electromagnetic exposure is rather limited. For a terrestrial network, using traditional base stations, Deruyck et al. discusses in [17] how the network can be optimized towards either a minimal exposure or minimal power consumption of the entire network. However, to the best of the author knowledge, no research has been done where a UABS-network has been optimized towards electromagnetic exposure.

## 2.3 Technologies

### 2.3.1 Type of Drone

The type of UAV will have a major impact on the network performance. Two types of drones are considered in [32]: an off-the-shelf drone affordable by the general public and a more robust one. The results in [32] show that the second type will require less drones to cover the same number of users and will last longer in the air. The research in this paper will therefore be done with the usage of the second type. A technical overview of this drone is given in table 2.2.

Parameter	Value	Units
Carrier power	13.0	A
Average carrier speed	12.0	m/s
Average carrier power usage	17.33	Ah
Carrier battery voltage	22.2	V

Table 2.2: Specifications of the used drone.

### 2.3.2 Long Term Evolution

The tool makes use of LTE, by the general public better known as 4G. LTE allows better UL and DL data speeds compared to its predecessors and is based on an all IP architecture. This technology can cover macrocells supporting cell sizes ranging from 5 km up to 100 km. Macrocell antennae are usually used by transmission towers along highways or on top of buildings. LTE supports however also smaller cells like femtocells covering only a few hundred meters. These femtocell antennae are therefore more portable, require less energy and will not require a telecommunication operator because of their simplicity [41]. Femtocell base stations are therefore used by the deployment tool. Further, LTE also supports both Frequency Division Duplex (FDD) and Time Division Duplex (TDD).

FDD makes simultaneous UL and DL traffic possible by assigning different frequencies within the same frequency range to both data streams. A small guard band is used between the UL and DL direction in order to prevent interference. An illustration is given in fig 2.1.

TDD allows UL and DL traffic by splitting the time domain. Meaning that both traffic directions use the same frequency and therefore alternately (in time) use the same frequency. A small time interval is used to prevent interference in case of a slightly bad timed synchronization as illustrated in fig. 2.2

Since it is assumed in this master dissertation that the user is continuously exposed without

interruption, FDD will be used throughout this document.

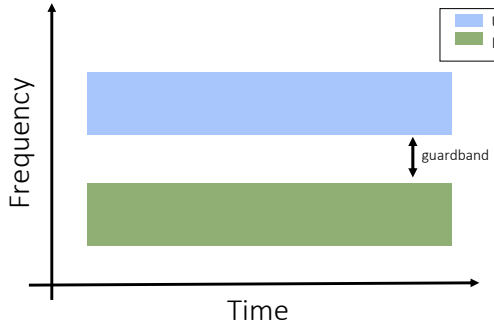


Figure 2.1: Resource allocation scheme for FDD.

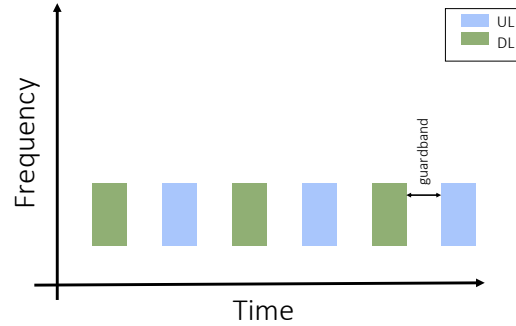


Figure 2.2: Resource allocation scheme for TDD.

### 2.3.3 Type of Antennae

The onboard antenna of the UAV will act as the gateway between the UE and the backhaul network. However, determining which antenna to use and how to position it, can be challenging.

Attaching an antenna to a UAV brings some additional challenges with it as explained by Rizwan et al. in [42]. Namely, the structure of the UAV can influence the radiation pattern. This can either have a constructive or destructive impact and depends on the relative position between the UAV and the antenna. When the antenna is too close to the UAV, the UAV can behave as a parasitic radiator, also emitting radiation. When using a directional antenna, the influence of the UAV will be much less but still existing, even when the UAV is not positioned in the direction of the mean beam. [42] suggest that this side-effect can be reduced by introducing a little offset between the antenna and the UAV. Another challenge that comes with attaching an antenna to a UAV is the need for 3D modelling of radiation patterns. In traditional terrestrial networks, the waves mainly propagated horizontally. When using UAVs, waves will have to travel rather downwards causing 2D antenna modelling to become insufficient. A 3D-model which accounts for both elevation and azimuth directivity will be required [29].

The easiest radiation pattern is a hypothetical equivalent isotropic radiator which radiates equally in all directions. Antennae that radiate equal quantities for a certain plane are called omnidirectional antennae [29] and several types exist. Attaching a conventional dipole antenna array might be low-cost, yet they are too high in profile and weight [43]. The authors of [44] and [45] both propose a broadband monopole blade antenna for UAV applications but this type suffers from a large surface which is a big disadvantage for the limited space available on the used UAVs in 2.3.1. [46, 47] propose a broadband blade dipole antenna which is much smaller.

Their wing-shaped design allows good aerodynamics when flying. [48] proposes an alternative to blade antennae by presenting a wideband low profile monopole. The radiation pattern behaves similar to a traditional monopole but has a reduced height.

Another type of antennae are directional antennae that take advantage of throughput, lower interference and battery life [49]. This is done by focussing the electromagnetic energy there where it is needed. One type of directional antennae that has been investigated excessively for UAV-usage are microstrip antennae since they provide several advantages compared to traditional antennae [50, 51]. Microstrip antennae are lightweight, low in cost and thin causing them to be more aerodynamic which is a useful feature since the antennae will be attached to UAVs. Zeng et al. proposes in [43] the use of such an antenna in a sunflower-shaped array configuration. Also the authors from [52] attach star-shaped millimetre wave antennae to the wings of a UAV and [53] uses circular patch antennae in a circular array configuration for communication between UAVs.

A basic microstrip antenna like the one presented in figure 2.3 consists of a ground plane and a radiating patch, both separated by a dielectric substrate. Several variations exist like microstrip patch antennae, microstrip slot antennae and printed dipole antennae which all have similar characteristics [50, 51]. They are all thin, support dual frequency operation and they all have the disadvantage that they will transmit at frequencies outside the aimed band. This is also known as spurious radiation. The microstrip patch and slot antenna support both linear and circular polarization while the printed dipole only supports linear polarization. Further, the fabrication of a microstrip patch antenna is considered to be the easiest of the considered patch antennae [50].

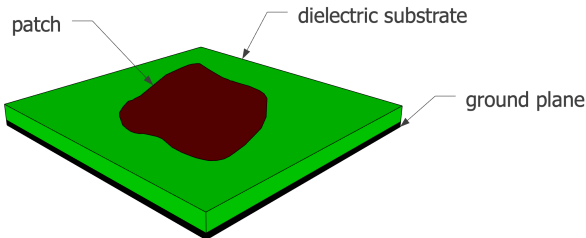


Figure 2.3: General design of a microstrip antenna.

The microstrip antenna requires besides the groundplane, dielectric substrate and the radiation patch also a feed line. Several feeding techniques exist of which the most popular are: coaxial probe feeding, microstrip line and aperture coupling.

A first feeding method is the usage of a coaxial cable where the outer conductor is attached to the ground plane and the inner conductor to the radiations patch. Modelling is however difficult, especially for thick substrates as will be used in this master dissertation. A second option is the

usage of a microstrip line. This type of feeding is much easier to model since the microstrip line can be seen as an extension of the radiating patch. A disadvantage is the increased spurious radiation which limits bandwidth. A third is proximity coupling which has the largest bandwidth and low spurious radiation. It consists however of two dielectric substrates causing the overall thickness of the antenna to increase as well as its fabrication difficulty [50].

The increasing usage of the microstrip patch antennae can be explained by its easy fabrication and lightness and therefore knows a widespread application in the military, global positioning systems, telemedicine, WiMAX applications and so on. The authors of [50] also state that some of the disadvantages like lower gain and power handling can be solved by using an array configuration.

The radiating patch is usually made of a thin layer of either gold or copper [51, 54] and can have any form. However, shapes other than circles or rectangles would require large numerical computation [51]. Thus, a simple rectangular shape will be used. Further, also the dielectric constant of the substrate is important. It typically varies between 2.2 and 12. Finding a good dielectric depends on how the antenna will be used. A lower dielectric constant with a thick substrate will result in better performance, better efficiency and larger bandwidths [54]. On the other hand, a larger dielectric constant reduces the dimensions of the antenna [51] which is also useful when attaching the antenna to a limited surface. Glass as a dielectric substrate with a constant of 4.4 will be used.

Figure 2.4 shows a microstrip patch antenna constructed out of an aluminium patch and a teflon substrate. The microstrip patch antenna is pointing towards the ground since the UAV will be flying above the user.

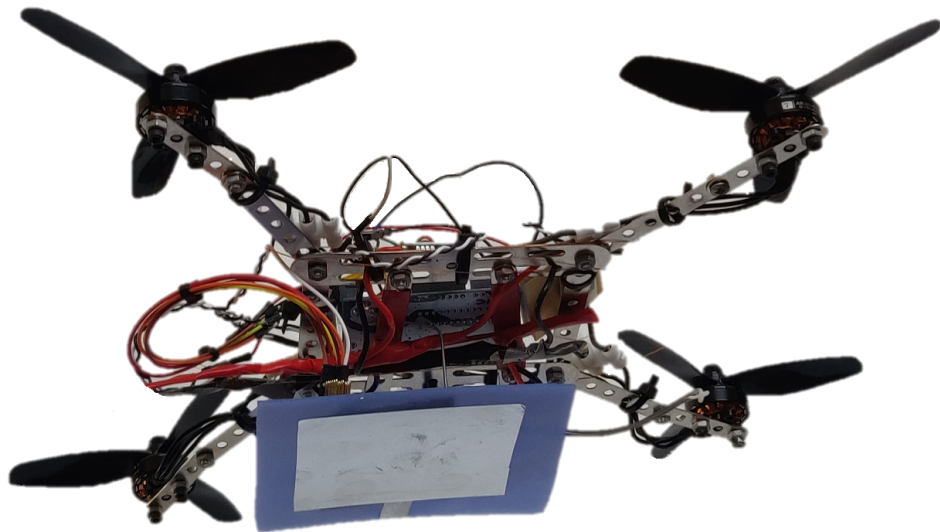


Figure 2.4: Image of a microstrip patch antenna attached to the bottom of a UAV.

## 2.4 Summary

In this chapter, related papers are discussed that perform research in the same field as well as the restrictions and guidelines by different organizations. First, legislations about electromagnetic exposure and specific absorption rates are discussed followed by giving an overview of related work. It turns out a lot of research has been performed about electromagnetic exposure but calculating whole body SAR considering all UE and all base stations is rather scarce. Secondly, related work about UAV-aided networks is presented. Various optimization strategies have been proposed in the past. Even optimizing towards electromagnetic radiation and power consumption has been investigated. However, this one was for terrestrial networks. To the best of the author's knowledge, exposure and power consumption optimized UAV-aided networks remain unknown.

# 3

## Methodology

The content of this chapter gives an answer to which steps that have to be taken to be able to answer the research questions. The first section explains how electromagnetic radiation is calculated for each source and how to convert these values to specific absorption rates. The second section gives a detailed overview of how a microstrip patch antenna can be designed and how its radiation pattern is achieved. The third section discusses how the network can be optimized towards either electromagnetic exposure or power consumption. The final section explains how these algorithms are implemented and how to further improve performance.

### 3.1 Electromagnetic Exposure

#### 3.1.1 Calculation of the Total Specific Absorption Rate

The total whole body SAR ( $SAR_{10g}^{wb,total}$ ) (expressed in  $W/kg$ ) of a user can be calculated by a simple sum of individual SAR values from the different sources. Formula 3.1 was originally described in [20]. This formula assumes that the users are holding their device next to their ear and therefore investigates localized SAR for head and torso area. However for this case, this would result into incorrect conclusions since the position of the device relative to the user is unknown. The position of the phone can be next to the head but also in front of the user. The

induced electromagnetic radiation will therefore be expressed in function of the entire body.

$$SAR_{10g}^{wb,total} = SAR_{10g}^{wb,myUE} + SAR_{10g}^{wb,myUABS} + SAR_{10g}^{wb,otherUE} + SAR_{10g}^{wb,otherUABSs} \quad (3.1)$$

The first parameter,  $SAR_{10g}^{wb,myUE}$ , indicates the absorbed electromagnetic radiation by the whole body originating from the user's own device. Despite that the UL radiation is destined for the serving UABS, a portion of that radiation is directly absorbed by its user, due to the omnidirectional nature of the mobile's antenna. The second parameter,  $SAR_{10g}^{wb,myUABS}$ , represents the DL radiation caused by the UABS that is serving the user. As the third parameter, we have the  $SAR_{10g}^{wb,otherUE}$  which is radiation caused by other people's devices. The radiation of these devices is once again destined for a specific UABS but again, a portion of that UL radiation will also be absorbed by our user. Finally,  $SAR_{10g}^{wb,otherUABSs}$  represents the DL radiation by the other UABSs to which our user is exposed to but not served by. An illustration is given in figure 3.1. We can only speak in terms of SAR when the electromagnetic radiation is absorbed by the user. This last step is however not shown in the illustration.

The electromagnetic exposure to which people are exposed can be categorized in two groups. One of them is near-field radiation which is caused by the user's own device which is indicated with the green arrow in figure 3.1 and will be discussed in 3.1.3. The other arrows are a form of far-field radiation and will be explained in section 3.1.2. Examples of these types of radiators are UE which belong to other people and UABSs.

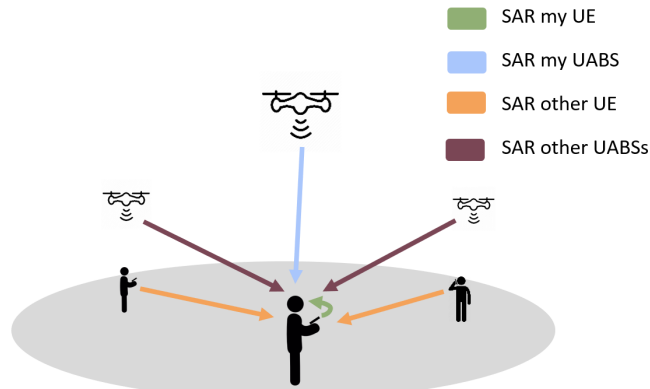


Figure 3.1: Illustration of the radiation affecting the average user (here shown in the center) by different types of sources.

### 3.1.2 Electromagnetic Exposure Caused by Far-Field Radiation

#### Electromagnetic Radiation from a Single Source

To determine the total exposure of a single human being or even of the entire network, the electric-field  $\vec{E}$  from a single radiator  $i$  should be calculated. The formula to determine this electromagnetic value  $E$  (expressed in V/m) for a specific location  $u$  is given in equation 3.2.

$$E_i(u)[V/m] = 10^{\frac{RRP(u)[dBm] - 43.15 + 20 \cdot \log(f[MHz]) - PL(u)[dB]}{20}} \quad (3.2)$$

**Real radiation power and EIRP.** In formula 3.2, as it was described in [16, 17], RRP was defined as equivalent isotropic radiation power (EIRP). EIRP is the radiation generated by an equivalent isotropic radiator which is a theoretical source of electromagnetic waves that radiate with the same intensity in all directions. The formula to find this EIRP value (in dBm) is described in 3.3 where  $P_{tx}$  stands for the input power of the antenna,  $G_t$  for the gain of the transmitter and  $L_t$  being its feeder loss.

$$EIRP[dBm] = P_{tx}[dBm] + G_t[dBi] - L_t[dB] \quad (3.3)$$

This formula, which is constructed out of different gains and losses, misses a factor when accounting for real life radiation patterns. Formula 3.2 solves this by using RRP instead of EIRP and can be defined as follows:

$$RRP(u)[dBm] = EIRP[dBm] - \text{attenuation}(u)[dB] \quad (3.4)$$

The attenuation for a user  $u$  is given based on the angle between the main beam and the user. More details on how this can be implemented are described where the radiation patters of antennae are explained. When assuming that  $\text{attenuation}(u)$  returns positive values, the attenuation can simply be subtracted from the EIRP-value.

**frequency** The used frequency in the formula above is denoted as  $f$  and is expressed in MHz. Since LTE is used, this value will be 2600 MHz.

**path loss** At last, formula 3.2 requires the path loss  $PL$ . In order to calculate this, an appropriate propagation model —of which several exist— is required . The Walfish-Ikegami model is used since it performs well for femtocell networks in urban areas [32]. The model makes a distinction between whether a free line of sight (LOS) between the user and the base station exists or not. The mathematical representation is given in the formulas below and is based on [41, 55].

The formula for LOS situation is rather simple.

$$L_p = 42.6 + 20 \cdot \log(f[\text{MHz}]) + 26 \cdot \log(d[\text{km}]) \quad (3.5)$$

where  $f$  is the used frequency and  $d$  the distance between the two radiators. The formula for NLOS is more complex and translates as follows:

$$L_p = \begin{cases} L_0[\text{dB}] + L_{rts}[\text{dB}] + L_{msd}[\text{dB}] & \text{if } L_{rts}[\text{dB}] + L_{msd}[\text{dB}] > 0[\text{dB}] \\ L_0[\text{dB}] & \text{if } L_{rts}[\text{dB}] + L_{msd}[\text{dB}] \leq 0[\text{dB}] \end{cases} \quad (3.6)$$

with  $L_0$  the path loss in free space,  $L_{rts}$  the roof-top-to-street diffraction and scatter loss. Further,  $L_{msd}$  stands for he multi-screen diffraction loss. The free space loss  $L_0$  can be calculated as follows:

$$L_0 = 32.4 + 20 \cdot \log(f[\text{MHz}]) + 20 \cdot \log(d[\text{km}]) \quad (3.7)$$

where  $f$  is the used frequency in MHz and  $d$  the radio-path length. The second term in equation 3.6 is the roof-top-to-street diffraction and scatter loss calculated with the following formulas.

$$L_{rts} = -16.9 - 10 \log(w) + 10 \cdot \log(f[\text{MHz}]) + 20 \cdot (h_{roof}[\text{m}] - h_{rx}[\text{m}]) + L_{orientation} \quad (3.8)$$

with  $w$  representing the width of the roads and  $h_{roof} - h_{rx}$  the difference in height between the receiver and the roof.  $L_{orientation}$  depends on the orientation of the road and can be calculated as follows:

$$L_{orientation} = \begin{cases} -10 + 0.354 \cdot \phi[\text{deg}] & \text{if } 0^\circ \leq \phi < 35^\circ \\ 2.5 + 0.075 \cdot (\phi[\text{deg}] - 35) & \text{if } 35^\circ \leq \phi < 55^\circ \\ 4.0 - 0.114 \cdot (\phi[\text{deg}] - 55) & \text{if } 55^\circ \leq \phi \leq 90^\circ \end{cases} \quad (3.9)$$

where  $\phi$  is the angle of incidence relative to the direction of the street. The final parameter required by equation 3.6 is the multi-screen diffraction loss and can be defined as follows:

$$L_{msd} = L_{bsh} + k_a + k_d \cdot \log(d) + k_f \cdot \log(f) - 9 \cdot \log(b) \quad (3.10)$$

$L_{bsh}$  and  $k_a$  quantify the increase of path loss caused by obstructing buildings. This is especially the case for lower positioned base stations.  $b$  is the distance between buildings along the path where the signal travels. The factors  $k_f$  and  $k_d$  control the dependence of  $L_{msd}$  as a function

of radio frequency and distance, respectively.  $L_{bsh}$  and  $k_a$  can be calculated with respectively equations 3.11 and 3.12 and  $k_f$  and  $k_d$  respectively with equations 3.13 and 3.14.

$$L_{bsh} = \begin{cases} -18 \log(1 + \Delta h_{Base}) & \text{if } h_{Base} > h_{Roof} \\ 0 & \text{if } h_{Base} \leq h_{Roof} \end{cases} \quad (3.11)$$

$$K_a = \begin{cases} 54 & \text{if } h_{Base} > h_{Roof} \\ 54 - 0.8 \cdot (h_{tx}[m] - h_{rooF}[m]) & \text{if } d \geq 0.5 \text{ km and } h_{Base} \leq h_{Roof} \\ 54 - 0.8 \cdot \frac{(h_{tx}[m] - h_{rooF}[m])}{0.5} & \text{if } d < 0.5 \text{ km and } h_{Base} \leq h_{Roof} \end{cases} \quad (3.12)$$

$$k_d = \begin{cases} 18 & \text{if } h_{Base} > h_{Roof} \\ 18 - 15 * \left( \frac{(h_{tx}[m] - h_{rooF}[m])}{h_{rooF}[m] - h_{rx}} \right) & \text{if } h_{Base} > h_{Roof} \end{cases} \quad (3.13)$$

$$K_f = -4 + \begin{cases} 0.7 \left( \frac{f[MHz]}{925} - 1 \right) & \text{for medium sized and suburban areas} \\ 1.5 \left( \frac{f[MHz]}{925} - 1 \right) & \text{for metropolitan centres} \end{cases} \quad (3.14)$$

### Combining Exposure

The total electromagnetic exposure  $E_{tot}$  for a given location originating from different sources can be calculated with formula 3.15 (in V/m).  $E_i$  stands for the electromagnetic exposure from source  $i$  and  $n$  stands for all far-field radiators of a certain category; they can either be UABSs or UE from other people.  $E_{tot}$  will be calculated for each location where a user is positioned.

$$E_{tot}[\text{V}/\text{m}] = \sqrt{\sum_{i=1}^n (E_i[\text{V}/\text{m}])^2} \quad (3.15)$$

### Converting Far-Field Electromagnetic Exposure to $SAR_{10g}^{wb}$

Formula 3.1 expects that the radiation from each far-field source is expressed in  $SAR_{10g}^{wb,myUABS}$ ,  $SAR_{10g}^{wb,otherUE}$  and  $SAR_{10g}^{wb,otherUABSs}$ . The calculation for all these values is in fact identical since the only difference is the source. Physically seen, they all are whole body SAR values induced by far-field radiation ( $SAR_{10g}^{ff,wb}$ ).

The electromagnetic radiation needs to be converted into  $SAR_{10g}^{ff,wb}$ . The conversion factor is based on Duke from the Virtual Family. Duke is a 34-year old male with a weight of 72 kg, a height of 1.74 m and body mass index of 23.1 kg/m [21]. Research shows that the conversion

factor for WiFi is  $0.0028 \frac{W/kg}{W/m^2}$ . Since WiFi works at a frequency of 2400 MHz which is very close to LTE, at 2600 MHz, it is assumed in [21] that this value is also applicable for LTE. The constant in equation 3.17 converts the power flux density  $S$  (in units  $\frac{W}{m^2}$ ) to the required  $SAR_{10g}^{ff,wb}$ . To make this possible, the electromagnetic radiation from formula 3.15 (expressed in  $V/m$ ) should first be converted to the power flux density with formula 3.16 before formula 3.17 can be applied.

$$S[W/m^2] = \frac{(E_{tot}[V/m])^2}{337} \quad (3.16)$$

$$SAR_{10g}^{wb,ff}[W/kg] = S[W/m^2] * 0.0028 \left[ \frac{W/kg}{W/m^2} \right] \quad (3.17)$$

### 3.1.3 Electromagnetic Exposure Caused by Near-Field Radiation

Up till now, only sources that cause far-field radiation have been considered. However, when a user is operating his device, a part of the UL radiation will enter his body despite the fact that the data traffic is destined for the serving UABS. This device is very close to the user and the emitted radiation is therefore considered to be near-field radiation.

#### Localized Specific Absorption Rate

When assuming that all users hold their device next to their ear, a localized SAR-value for the head  $SAR_{10g}^{head}$  can be calculated. Various governments have defined different legislations. The European Union uses the directions of the IEC who define in IEC:62209-2 a maximum for a 10g tissue  $SAR_{10g}^{head}$  at 2 W/kg [6]. The FCC limits the maximum in the United States for a 1g tissue  $SAR_{1g}^{head}$  at 1.6 W/kg [56]. Most countries, including Belgium, enforce the 10g model and this will, therefore, be the point of reference for this master dissertation. The  $SAR_{10g}^{head}$  values are phone dependent. The values reported by mobile manufacturers are worst-case scenarios meaning that the values are measured when the phone is transmitting at maximum power. This is an understandable decision but will not result in a realistic scenario since modern cellular networks use power control mechanisms to prevent unnecessary high radiation of a nearby device. UE will therefore never use more energy than required to maintain a connection. To compensate for this overestimation, the actual  $SAR_{10g}^{head}$  of each user will be predicted. These will, however, remain an estimation since the position of the phone relative to the head differs from user to user. For example, by holding the phone differently, a hand can absorb more or less electromagnetic radiation. The SAR values will also depend on the age of the user, especially children who experience on average higher exposure in the brain regions because of different

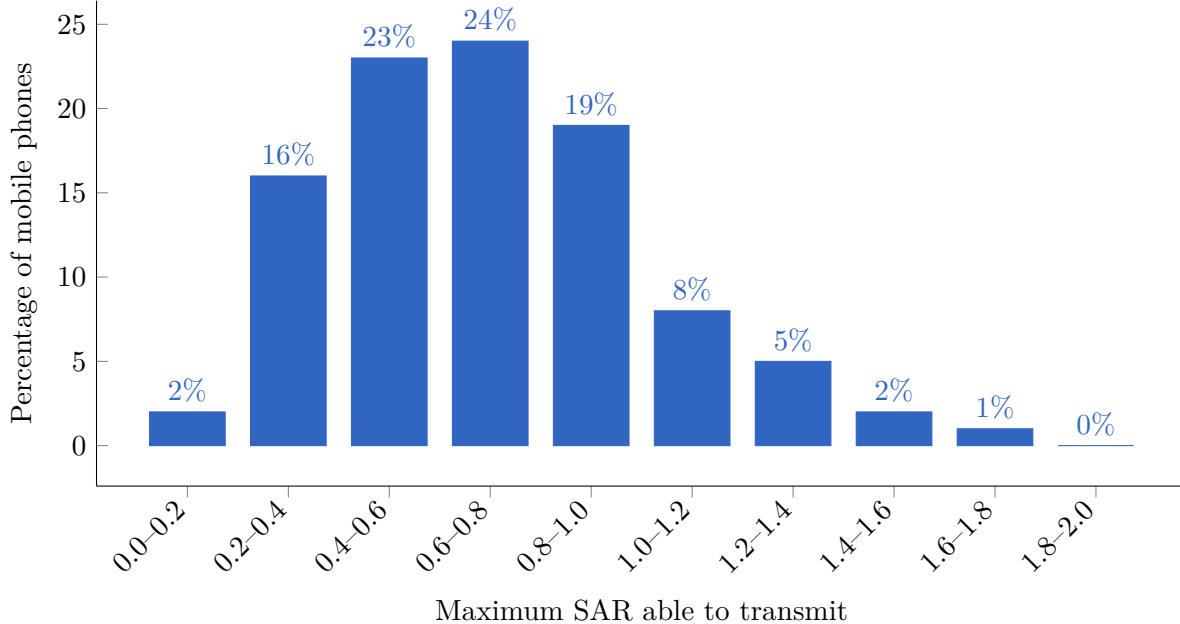


Figure 3.2: Distribution of how many phones belong to a certain SAR interval. Upper boundary not included.

anatomical proportions [57, 18].

$$SAR_{10g}[W/kg] = \frac{P_{tx}[W]}{P_{tx}^{max}[W]} * SAR_{10g}^{max}[W/kg] \quad (3.18)$$

Equation 3.18 will be used to predict the actual  $SAR_{10g}^{head}$  of a certain user with  $P_{Tx}^{max}$  being the maximum transmission power for a phone which is in LTE and UMTS 23 dBm [58, 18]. The actual transmitted power ( $P_{tx}$ ) is calculated with equation 3.19 where  $P_{sens}$  stands for the receiver sensitivity and  $PL$  the path loss between sender and receiver.

$$P_{tx} = P_{sens}[W] + PL[dB] \quad (3.19)$$

Despite the legal  $SAR_{10g}^{max}$  for Belgium is set to 2  $W/kg$ , the actual  $SAR_{10g}^{max}$  value is usually lower and different for each mobile device. An average is calculated based on 3516 different phones from various brands using a German database [15]. An overview can be found in fig. 3.2. When the phone is positioned at the ear, an average  $SAR_{10g}^{max}$  of 0.7  $W/kg$  is found with a standard deviation of 0.25  $W/kg$  which are very similar results as in ref. [?]. The median of 0.67  $W/kg$  is used as  $SAR_{10g}^{max}$  in formula 3.18.

### Whole Body Specific Absorption Rate

The position of the phone relative to the user's body is however unknown. Some users will be calling and therefore probably holding their phone next to their ear while others are using

other services like browsing the web. This would result in different types of localized values. To be able to give an average SAR based on all active users, the whole body SAR will be used. For this reason formula 3.1 expects that the specific absorption rate is expressed for the entire body instead of localized  $SAR_{10g}^{head}$ . The conversion factors for Duke from the Virtual Family will be used again as it was already the case in 3.1.2. The constant to convert UL exposure to  $SAR_{10g}^{wb,myUE}$  for WiFi is defined to be  $0.0070 \frac{W/kg}{W}$  [21] which leads to eq. 3.20.

$$SAR_{10g}^{wb,myUE} \left[ \frac{W}{kg} \right] = 0.0070 \left[ \frac{W/kg}{W} \right] * P_{tx}^{UE}[W] \quad (3.20)$$

The power of the UE can be calculated using equation 3.21 [21].

$$P_{tx}^{UE} = \min \{ P_{max}[dBm], P_{pusch}[dBm] + \alpha * PL[dB] + 10\log(M) + \sigma \} \quad (3.21)$$

$P_{max}$  is the maximum allowed transmission power by UE for LTE, defined at 23 dBm. However, this is the worst case and the actual used power is usually much lower thanks to power control.  $P_{pusch}$  is the required received power at the UABS and will be advertised by the base station over the Physical Uplink Shared Channel (PUSCH). This research will use a  $P_{pusch}$  of -120 dBm.  $\alpha$  is the path loss compensation factor where  $\alpha$  must equal {0,0.4,0.5,0.6,0.7,0.8,0.9,1}. An  $\alpha$  set to zero indicates there is no path loss compensation [59, 60]. For this document, full pathloss compensation will be used with an  $\alpha$  equal to one. For the 20-MHz channel used in this paper,  $M$  will be set to 100; indicating the number of used resource blocks by PUSCH [21]. Finally, we have  $\sigma$  as the correction factor and is set to zero. Other possible values are {-1, 0, 1, 3} [21, 59]. The presented values can be found in the overview given in table 4.1.

## 3.2 Microstrip Patch Antenna

### 3.2.1 Design of a Microstrip Patch Antenna

A microstrip patch antenna is chosen because it allows easy production but more important, it has a low weight and has a thin profile causing it to be very aerodynamic which is useful when attaching it to a drone [50].

The dimensions of the antenna depend on the frequency it is operating at and the characteristics of the used substrate. The antenna will be radiating at a center frequency  $f_0$  of 2.6 GHz. Each substrate has a dielectric constant  $\epsilon_r$  representing the permittivity of the substrate that depends on the used material. Substrates with a high dielectric constant and low height reduce the dimensions of the antenna while a lower dielectric constant with a high height improves antenna performance [51, 54]. In this document, a substrate like glass is chosen because of the higher

dielectric constant of  $\epsilon_r = 4.4$  compared to materials like Teflon with only a dielectric constant of  $\epsilon_r = 2.2$  [51]. Doing this in combination with an antenna height of 2.87 mm will decrease the dimensions of the entire antenna surface. This comes in handy since drones only have limited space available.

Description	Symbol	Value
Center frequency	$f_0$	2600 Hz
Dielectric constant	$\epsilon_r$	4.4
Height of the substrate	$h$	0.00287 m

Table 3.1: Overview of the configuration parameters.

The dimensions of the radiating patch can be calculated with the formulas from [51] and [54] using the defined values from table 3.1. In that way, the width of the patch  $W_p$  is calculated using formula 3.22.

$$W_p[m] = \frac{C[m/s]}{2 * f_0[Hz]} * \sqrt{\frac{\epsilon_r + 1}{2}} \quad (3.22)$$

With  $C$  being the speed of light,  $f_0$  the center frequency of 2600 MHz and a dielectric constant  $\epsilon_r$  of 4.4, the width of the patch becomes 35.09 mm.

In order to find the length of the radiating patch, some other values need to be determined first. Formula 3.23 will calculate the effective dielectric constant ( $\epsilon_{ref}$ ).

$$\epsilon_{ref} = \frac{\epsilon_r + 1}{2} + \frac{\epsilon_r - 1}{2} * \left(1 + 12 * \frac{h[m]}{W_p[m]}\right)^{-\frac{1}{2}} \quad (3.23)$$

This formula requires the width found in the previous formula along with the dielectric constant and substrate height from table 3.1. This will result in a  $\epsilon_{ref}$  of 3.91.

$$L_{eff}[m] = \frac{C[m/s]}{2 * f_0[Hz]} * \sqrt{\epsilon_{ref}} \quad (3.24)$$

Now formula 3.24 can be used to calculate the effective length ( $L_{eff}$ ), resulting in 29.16 mm.

$$\Delta L[m] = 0.412 * h * \frac{(\epsilon_{ref} + 0.3) \left( \frac{W_p[m]}{h[m]} + 0.264 \right)}{(\epsilon_{ref} - 0.258) \left( \frac{W_p[m]}{h[m]} + 0.8 \right)} \quad (3.25)$$

Eventually, the length extension is found with formula 3.25 by substituting the values from above. Doing so determines that the  $\Delta L$  equals 1.3071 mm.

Finally, the length of the patch can be calculated using the expression 3.26

$$L_p[m] = L_{eff}[m] - 2 * \Delta L[m] \quad (3.26)$$

The length  $L_p$  results in 26.55 mm.

The dimensions of the radiation patch are now known. The only remaining questions are the dimensions of the ground plane and dielectric substrate to which the radiation patch is attached. The transmission line model is in fact only applicable for an infinite ground plane but it has been proven that similar results can be achieved if the ground plane's dimensions are bigger than the patch by approximately 6 times the height of the dielectric substrate [51, 54].

$$L_g[m] = 6 * h[m] + L_p[m] \quad (3.27)$$

$$W_g[m] = 6 * h[m] + W_p[m] \quad (3.28)$$

Therefore, the length of the ground plane  $L_g$  should be at least 0.0438 m and the width  $W_g$  at least 0.0524 m. A schematic overview of how the antenna will look like is given in figure 3.3.

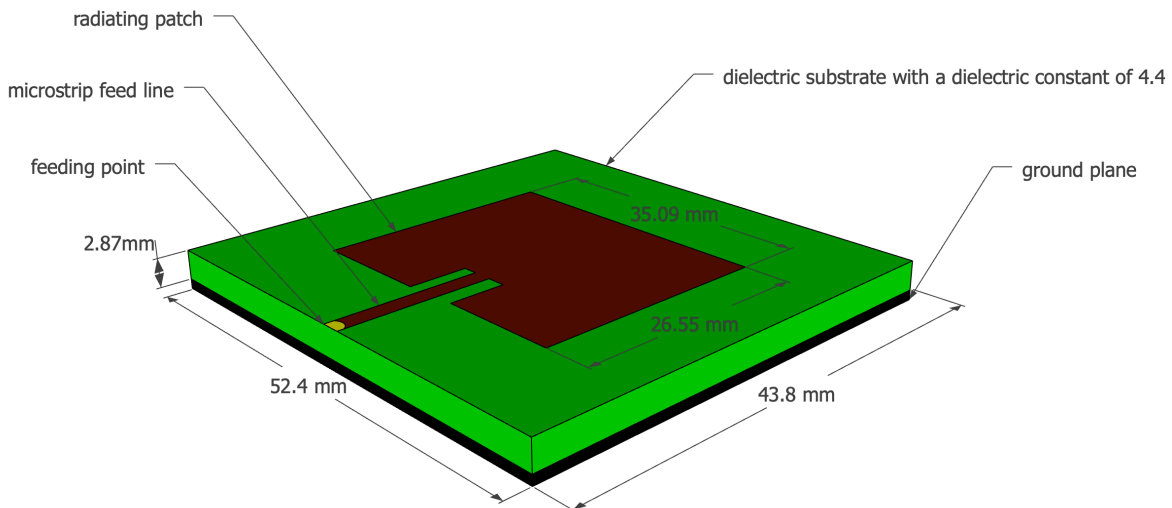


Figure 3.3: Design of the microstrip patch antenna.

### 3.2.2 Radiation Pattern

Matlab is able to generate the radiation pattern for this microstrip patch antenna. The code in listing 1 starts by defining the dielectric substrate which will be glass with a dielectric constant of 4.4 and a height of 0.00287 m. Thereafter, the microstrip patch antenna is generated with the `width` and `length` being the dimensions of the radiation patch and the `GroundPlaneLength` and `GroundPlaneWidth` the dimensions of the ground plane and dielectric substrate. The `FeedOffset` is the relative offset from the center where the radio frequency power is fed to

the radiating patch which will here be at the edge. This is in figure 3.3 indicated with a yellow dot. At last, the `dielectric`-object is substituted into the `patchMicrostripInsetfed`-object.

Generating the pattern is done with the `pattern`-command. The first value is the `patchMicrostripInsetfed`-object followed by the frequency at which the antenna will be operating. Optionally, an azimuth value can be parsed like in line 7 and 8 where 90 and 0 relatively stand for the H-plane and E-plane.

```

1 d = dielectric("Name",'glass',"Thickness",0.00287,"EpsilonR",4.4)
2 p = patchMicrostripInsetfed("Width",0.0351,"Length",0.02655,
3 "GroundPlaneLength",0.0438,"GroundPlaneWidth",0.0524,
4 "FeedOffset",[-0.021885 0],"Substrate",d)
5
6 pattern(p,2.6e9, "CoordinateSystem", 'polar', "Normalize",true)
7 pattern(p,2.6e9, 90, 0:10:360,
8 "CoordinateSystem", 'polar', "Normalize",true)
9 pattern(p,2.6e9, 0, 0:10:360,
10 "CoordinateSystem", 'polar', "Normalize",true)
```

Listing 1: Matlab code to generate the radiation patterns for the microstrip patch antenna.

Running the configuration from listing 1 will generate the radiation pattern from figure 5.15. When running the same configuration for a slightly bigger square ground plane with an edge of 0.060 m, the radiation pattern from 3.5 is achieved. Both radiation patterns show an aperture angle of approximately 90°. It becomes clear that the radiation pattern from figure 5.15 has a higher attenuation in the direction it is not facing compared to the radiation pattern of figure 3.5. If it is assumed that drones fly lower than some users are positioned in some buildings, the pattern of 3.5 would be a better approach. However, for the continuation of this master dissertation, the radiation pattern from figure 5.15 will be used since this antenna is the smallest and therefore most suitable to attach to the limited space available under a drone. A more extensive comparison between different radiation patterns is out of the scope of this master dissertation. A data sheet of the exact values from both radiation patterns can be found in appendix A.

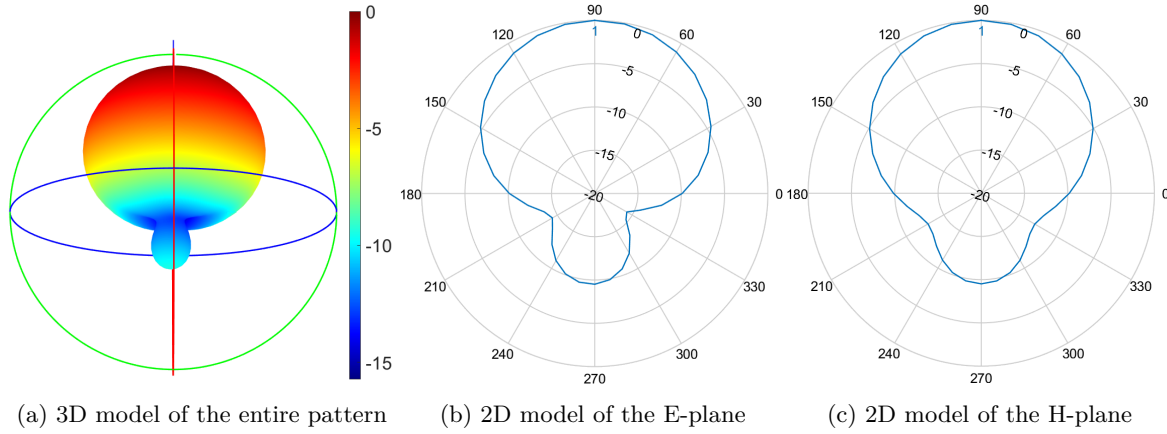


Figure 3.4: Radiation pattern 1 (in dBi) with the configuration as described above.

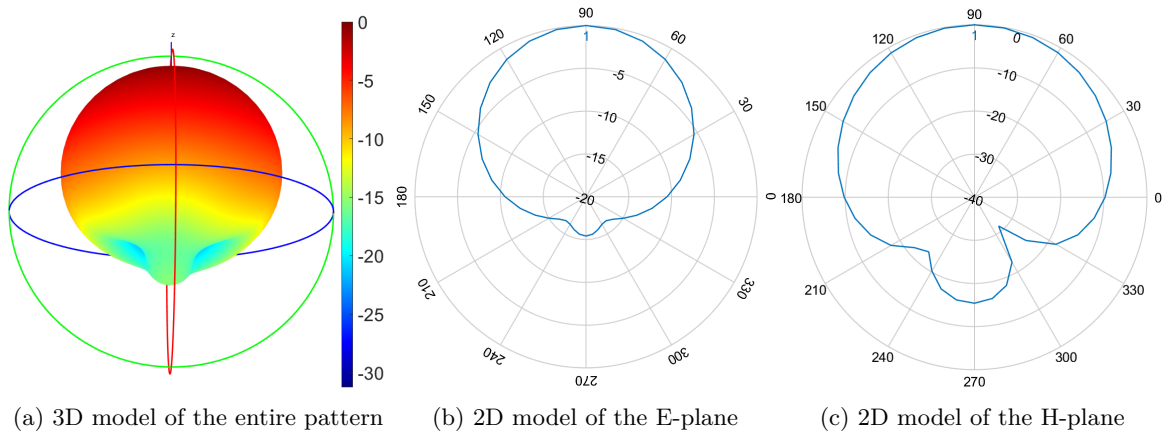


Figure 3.5: Radiation pattern 2 (in dBi) which is generated with a groundplane of 0.06m by 0.06m.

### 3.3 Optimizing the Network

UAVs can remain in the air for only a limited time, which is certainly the case when also an antenna needs to be connected to the battery of his carrier. It is therefore interesting to not only consider electromagnetic exposure of the user but also the power consumption that comes with it. However, an increasing transmission power of an antenna comes with an increasing electromagnetic exposure, this is not the case considering both values for an entire network. In fact, the authors from [17] prove that both become inversely equivalent.

The reason the network behaves like this is because it is often cheaper to increase the exposure of an already active base station than activating a new one. As an example, imagine there is a new user who can either be covered by activating a nearby base station or by an already

active base station a little further away. When this user is in a power consumption optimized network, the already active base station will increase its power level because that will be cheaper than activating a new base station. Users close by will thus experience a higher electromagnetic exposure. On the other hand, if the user would have been in an exposure optimized network, the nearby base station which was offline would be activated at a lower power level. So the electromagnetic exposure will also be lower but by activating a new base station, the overall power consumption increases.

This results in conflicting requirements. An optimization strategy that optimizes towards either electromagnetic exposure or total power consumption is given in 3.29 and is based on the fitness function described in [17].

$$f = w * \left(1 - \frac{E_m}{E_{max}}\right) + (1 - w) * \left(1 - \frac{P}{P_{max}}\right) * 100 \quad (3.29)$$

Formula 3.29 returns a fitness value which represents the performance of the entire network. Users are connected to different UABSs and each time a fitness value is calculated. The user will eventually be connected to the drone that results in the highest fitness value. This is repeated for each user. This process is explained in detail in section 3.4.1.  $w$  is the importance factor of electromagnetic exposure ranging from 0 to 1, boundaries included. A  $w$  set to zero means that electromagnetic exposure is not important. Such a network will therefore be called a PwrC Opt. Likewise, a  $w$  set to one means that minimizing exposure is top priority and will result in an exposure optimized network (Exp Opt).  $P_{max}$  is the power consumption of all UABSs, both active and inactive, when radiating at the highest possible level while  $P$  is the effective power used by the current designed network. This will be the power required for the flying drones themselves and their antenna.  $E_m$  will be the weighted exposure of the average user for the current designed network and  $E_{max}$  the weighted average of electromagnetic exposure when all antennae are at their highest power level.

When optimizing the network, it is not only important to consider the average exposure of all users, but also to limit high extremes [17]. In formula 3.30 a weighted average of exposure will be found by not only considering the median but also the 95 percentile of all users' DL exposure. Since both values are considered to have equal importance, the weight factors  $w_1$  and  $w_2$  will both have an equal importance of 50%.

$$E_m = \frac{w_1 * E_{50} + w_2 * E_{95}}{w_1 + w_2} \quad (3.30)$$

## 3.4 Simulation Tool

### 3.4.1 Implementation of the Deployment Tool

#### Main Algorithm

Calculating electromagnetic exposure requires knowledge about the area. For instance, the position of UABSs needs to be known but also other variables like the used transmission power and the distances between antennae.

The WAVES research group at Ghent University has developed a capacity based deployment tool for disaster scenarios with the aid of UAVs [32]. The idea of this UAV-aided emergency network is that in case of a disaster, the existing terrestrial network might be damaged and will not be able to handle all users who are trying to reconnect to the backbone network. The tool makes a fast deployable network possible by attaching femtocells to UAVs, so-called UABSs. The tool will orchestrate the UABSs over the disaster area by describing a fully configured network. This tool is thus a suitable starting point and works as follows:

The deployment tool will try to calculate the optimal placement for each UABS and requires therefore a description of the area where the UAV-aided network needs to be deployed. This is done with the use of so-called shape files. These files contain three dimensional descriptions of the buildings present in the area and are key values in approaching results as realistic as possible. Furthermore, the tool also requires a configuration file containing technical specifications of the type of UABS that is being used. The tool will thereafter randomly distribute users over the area and assigns a certain bitrate to them (figure 3.6). If a user is indoor, the height of the user will be estimated at half the height of the building. The height UE itself will be 1.5 metres above the floor.

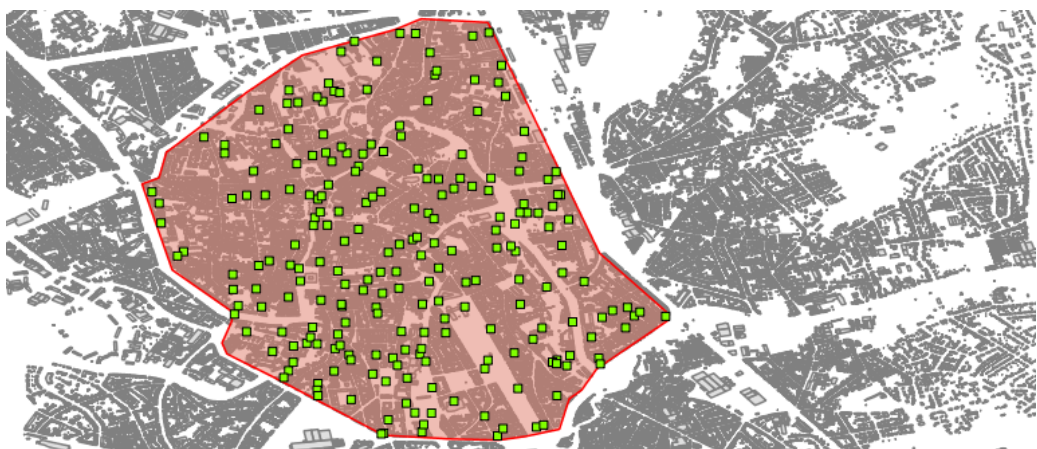


Figure 3.6: Example of how users are randomly distributed over the city centre of Ghent.

In a second phase, the optimal position for each UABS is calculated. This is done by trying to locate a UABS above each active user. Two options are possible. If a fixed flying height is defined, a UABS is placed above each user at the given height, unless a building is obstructing its location. Then, no base station will be located above that user. Alternatively to the fixed flying height, a flying margin can be defined which represents the distance between the outdoor user and the drone. If the user is inside, this margin will be measured between the drone and the rooftop of that building. The latter is only allowed if the suggested height remains below the given maximum allowed height.

Thereafter, the decision algorithm calculates which users should be connected to which UABSSs. These decisions are based on the specified optimization strategy. For this master dissertation, this will either be power consumption optimized or exposure optimized.

In the final state, unused UABSSs are removed and the capacity of the facility is checked. If the number of active drones would exceed this capacity, UABSSs will be sorted based on the number of users they cover. Thereafter, drones with too few users are removed so that all the active drones could be stored in the facility. The flowchart of the main algorithm is given in figure 3.7.

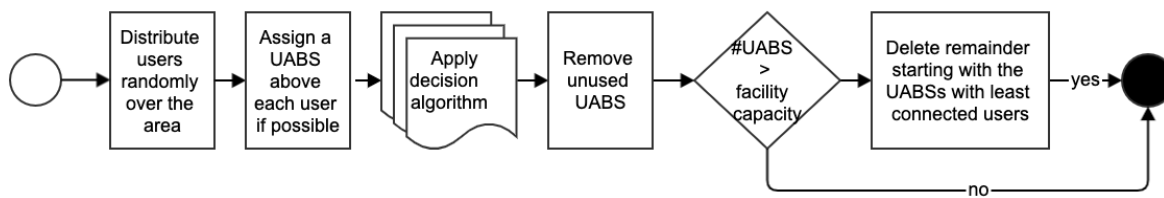
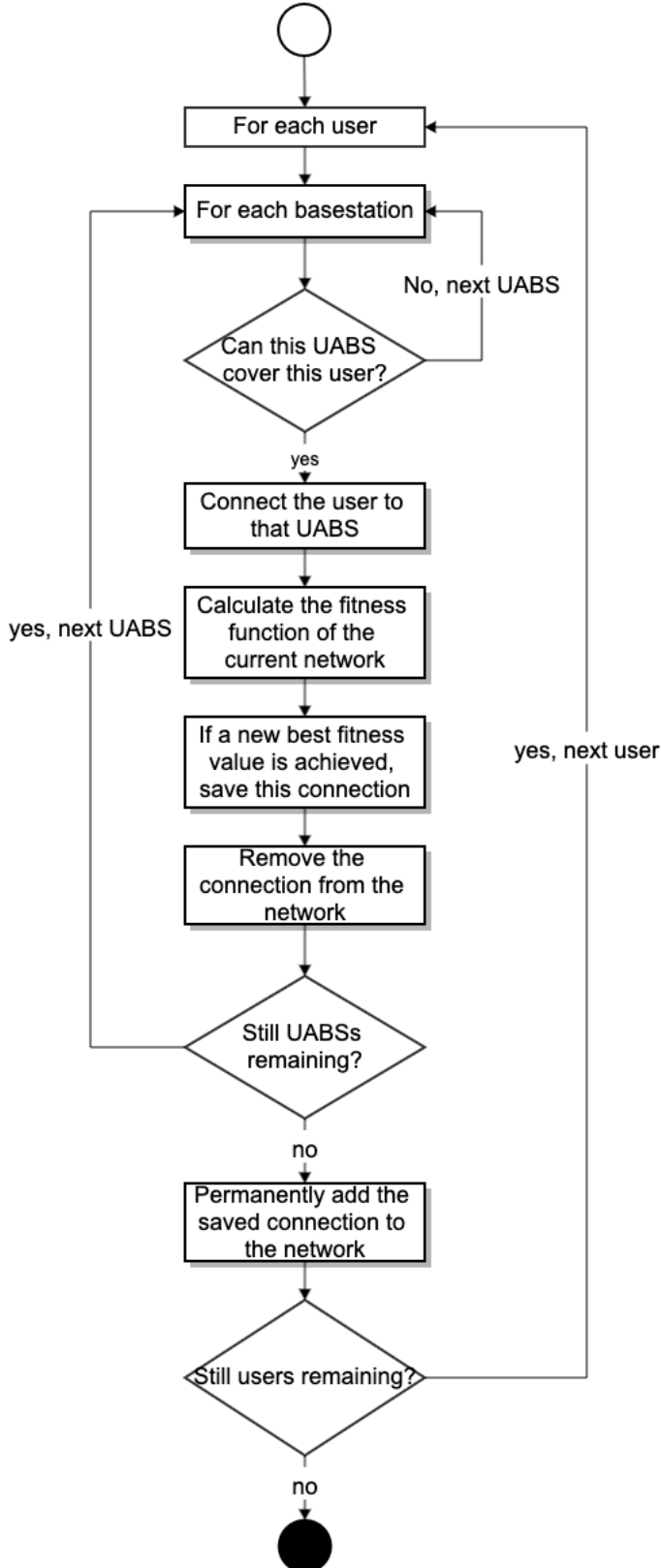


Figure 3.7: Flowchart of the main algorithm.

### Decision Algorithm



Solving the network is done by the decision algorithm and starts by calculating the path loss between the different users and thereafter between users and UABSs. Thereafter, the tool iterates over each user and tries to connect that user to each UABS. This connection is not always possible. A UABS might be saturated with users and will not be able to cover yet another one or maybe the user is so far away that in order to cover that user, the UABS would have to exceed its maximum allowed input power. However, if a connection is possible, the user will be connected to that UABS and the fitness function from section 3.3 is applied. This is repeated for each UABS. Only the connection which results in the best fitness value for the entire network will be used. Doing so will make sure that, given the currently designed network, the user is optimized. In other words, each user is optimized and not the entire network. It is however assumed that the average network will be optimized as well. Thereafter, the tool shifts to the next user. When the last user has been processed, the network is fully designed for an unlimited number of drones and the result is returned to the main algorithm for further processing. The flowchart of this algorithm is given in figure 3.8.

Figure 3.8: Flowchart of the decision algorithm.

### 3.4.2 Implementation of the Radiation Pattern

Originally, the deployment tool did not consider attenuation. Therefore, the radiation from the antenna attached to the UAV was equal in each direction. Such a fictional antenna is called an equivalent isotropic radiator. Thus the tool has been extended in order to support several types of antennae by introducing new parameters like attenuation and direction. Doing so allows any type of antennae which is fully configurable in any given orientation. This configuration is done with the usage of an XML-file which will apply to all UABSs in the network. An equivalent isotropic radiator is still supported by returning a zero value when the attenuation is requested.

The orientation is done using two values called ‘downtilt’ and ‘north offset’. The first value defines the downtilt angle under which the antenna is pointing. A downtilt angle of zero degrees is perfectly horizontal and an antenna with a downtilt angle of 90° will be pointing straight to the ground. This parameter only supports positive values ranging from 0° to 360° (upper boundary not included). An antenna pointing to the sky would therefore require a value of 270°. The second value, the north offset, defines the azimuth orientation of the drone. The value given to this parameter indicates the offset between the north and the horizontal direction to which the antenna should be pointing at. The value once again ranges from 0° to 360° with the upper boundary not included. The angle is calculated in counterclockwise orientation. For instance, a north offset of 270° will let the UABS point to the east. An example is given in figure 3.9 where fig. 3.9.a shows a UAV that performs a horizontal movement with a north offset of 90°. The antenna attached to the UAV in fig. 3.9.b performs a downtilt movement of 90°.

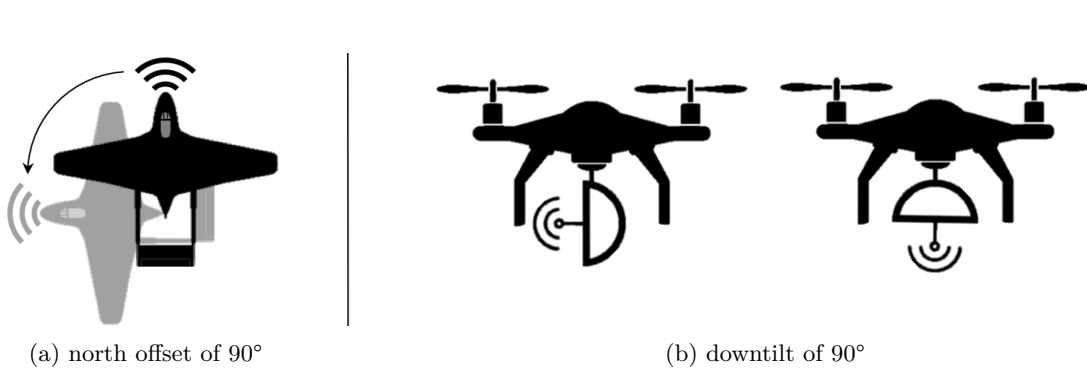


Figure 3.9: Illustration of the two possible movements. The UAV in fig. (a) is a top view while the UAV in fig. (b) is a side view.

Thereafter, the normalized radiation pattern is supplied to the tool, the actual pattern is three dimensional. To simplify this, slices perpendicular to the az-axis are extracted. These are indicated in figure 3.10 with azimuth cuts. With an angle of 90° four slices are achieved, each consisting out of elevation cuts. The intersection of an elevation and azimuth plane corresponds

with a certain attenuation which is fed to the tool. Figure 3.10 shows only 3 elevation planes. The radiation pattern used in the tool has an attenuation every  $10^\circ$ . In other words, a slice consists of 19 values ranging from  $0^\circ$  to  $180^\circ$  (boundaries included).

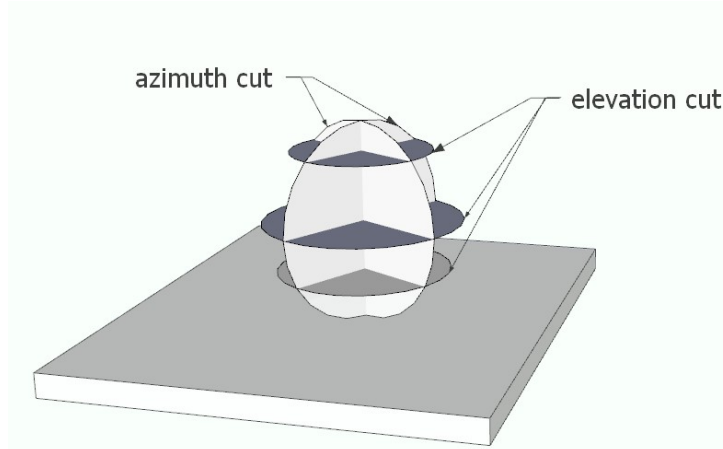


Figure 3.10: Schematic example of slices in a radiation pattern.

The number of required slices depends on the complexity of the radiation pattern. For symmetrical radiation patterns, like in figure 5.15 and 3.5, two azimuth cuts perpendicular to each other are definitely sufficient. This is also illustrated in figure 3.10 where two azimuth planes are shown and that, once cut, will result in four slices. However, this might not be the case for radiation patterns with a more complex structure containing several side lobes. To tackle this issue, more azimuth-slices can be defined for increased precision. Each slice should however contain an equal amount of elevation slices. A concrete example of a configuration file can be found in appendix B.

When the attenuation of a user from a certain UABS needs to be known, the elevation and azimuth angles between the user and the antenna's direction should be calculated. Figure 3.11 represents a radiation pattern with the black dot indicating the user whose attenuation needs to be calculated. The small black lines represent azimuth and elevation planes. The tool knows the exact attenuation only at the intersection of those lines. The chance that a user is positioned at such an intersection is very small. Therefore, the attenuation for the requested point has to be estimated using bilinear interpolation. First, the attenuation is estimated at the intersection of the red and orange line using linear interpolation on the horizontal axis with the known values at the end of the red line. The same is done for the orange-green intersection using the known values at the end of the green line. Finally, linear interpolation is applied to the y-axis for the black dot on the orange line using the estimated values at the end of the orange line.

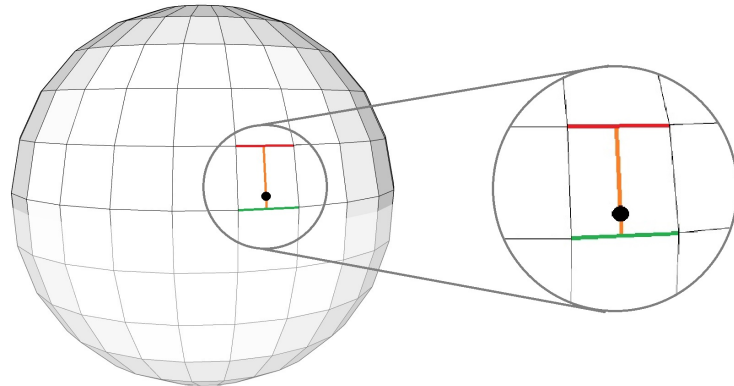


Figure 3.11: Schematic example of how bilinear interpolation works.

### 3.4.3 Performance Improvement

#### Calculating Path Loss

The path loss is required by several formulas. For instance, the formula that decides whether a UABS is feasible for a certain user makes use of this parameter but also the calculations for the downlink electromagnetic exposure require this value to be known. The formulas for the whole body  $SAR_{10g}$  require not only the path loss between the user and all UABSs but even the path loss between users themselves. These path loss calculations are based on the Walfish-Ikegami model that causes a high computational load. The calculation between two points is completely independent of any other calculation between any other points and is therefore a suitable candidate to multithread. The deployment tool creates two thread pools. The first pool creates a thread for each user where each thread calculates the path loss between the user assigned to him and all possible UABSs, causing a time complexity of  $n^2$ . Each user stores all path losses between himself and any other UABS. This results therefore in a total space complexity of  $n^2$ . When all users are finished, the thread pool is shut down and the second one is created for the same calculations but between users. The pool will, just like the previous, create threads for each user but there is an important difference. When a certain user calculates the path loss to another user, this path loss also applies for the other direction. The tool saves time by calculating the path loss only once and stores the path loss at both users. It is therefore sufficient that a given user only calculates path losses of users at his right side, since the other path losses will be calculated by the users on his left. This results in a time complexity of only  $n(\frac{n}{2})$ . When the last user finishes his thread, all users know the path loss of all other users causing a space complexity of  $n(n - 1)$ .

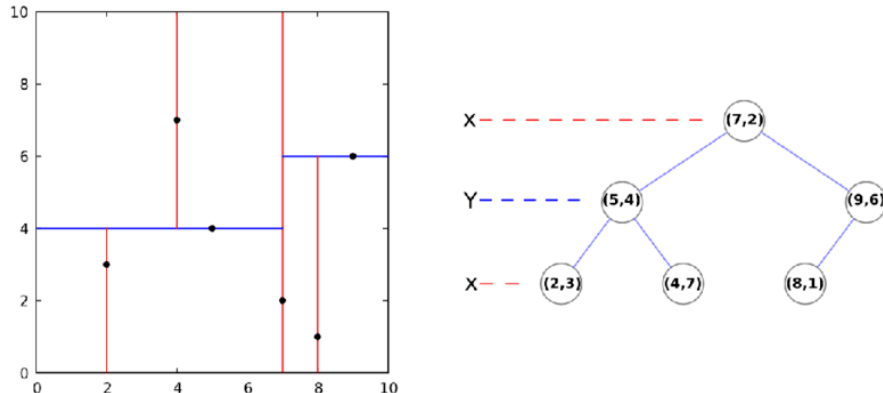


Figure 3.12: Example of a KD-tree in two dimensions.

### Limiting Antenna Searching

The user needs to be connected to the ‘best’ base station. To identify this best UABS, the user should be connected to each base station and the value of the fitness function presented in equation 3.29 has to be evaluated. The connection that resulted in the best fitness function will be added to the solution. This process is repeated for each user but can further be improved. A user will likely be connected to either the UABS directly above him or to a UABS in the direct neighbourhood. Time complexity can thus be improved by not considering drones outside a certain radius. An ideal data structure for neighbourhood-search with geographical coordinates is a KD-tree [61, 62]. This data structure is described by Bentley in [63] and is based on a binary tree, optimal for objects consisting out of multiple keys. Each node in this tree is associated with a certain dimension and will split the hyperplane over exact one dimension. In this case, the x and y coordinate will be used in a 2D-tree ( $k=2$ ) like in figure 3.12.

The length of the connections is investigated to define a proper cut-off radius. The investigated network is a power consumption optimized network with an equivalent isotropic radiator because this configuration will result in the biggest cell sizes due to the absence of attenuation in the antenna. Figure 3.13 shows that for small networks with 50 users, 78% of the connections are less than 100 metres. The other 22% are situated between 100 and 400 metres and decrease logarithmically. For bigger networks with 600 users, 57% of the connections is less than 100 metres. The remaining 43% of the connections are situated between 100 and 500 metres. No significant percentage of connections longer than 500 metre were recorded for either cases. The percentage of connections less than 100 metres will even be higher when using exposure optimized networks and/or microstrip patch antennae. In this case the choice was made to only consider UABSs within a radius of half a kilometre which is believed to have a sufficient safety margin. The rare connections that would have exceeded this radius would not contribute much to the average values.

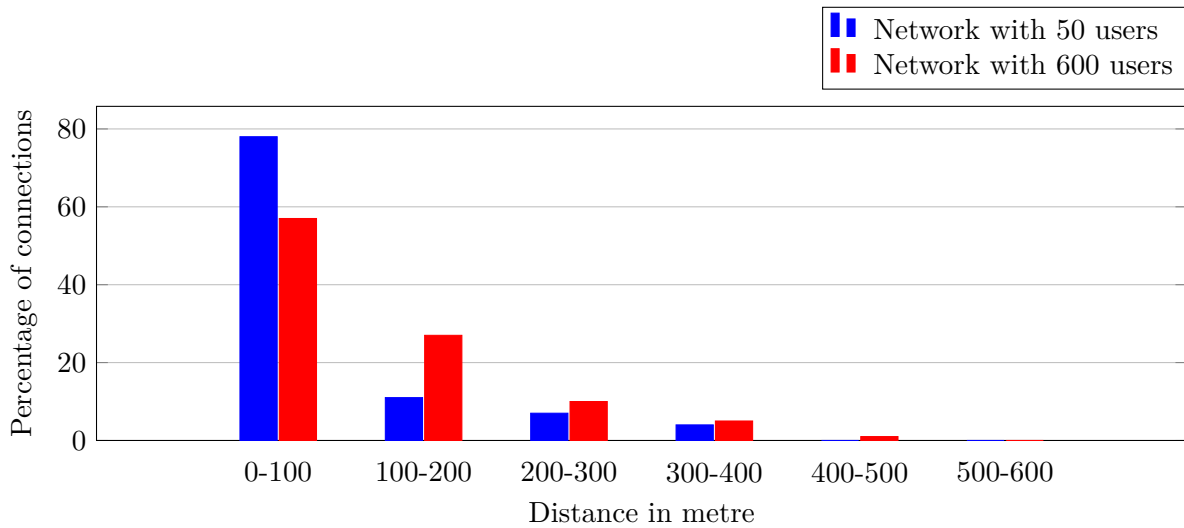


Figure 3.13: Distribution of how many connections belong to a certain interval of distance. Upper boundaries are not included.

### 3.5 Summary

This chapter discussed the different formulas that will be used by the tool and how to program or optimize some of the more complex problems like radiation patterns or path loss calculations.

First, the formulas about calculating the electromagnetic exposure from different sources and how they can be converted in SAR-values are presented. The electromagnetic field radiation in the far-field and near-field can be converted with the constants  $0.0028 \frac{W/kg}{W/m^2}$  and  $0.0070 \frac{W/kg}{W}$ , respectively. Secondly, a proper microstrip patch antenna has been defined, optimized for the 2.6 GHz frequency band. The dimensions of the groundplane and glass substrate resulted in 52.4 mm by 43.8 mm and a height of 2.87 mm. The radiating patch itself has a width of 35.09 mm and a length of 26.55 mm. Thereafter, the radiation pattern of this antenna is achieved with the use of Matlab. Thirdly, a fitness function for the optimization strategy is introduced, explaining how this function will be able to optimize the network towards either electromagnetic exposure or network power consumption. Eventually, the implementation itself is tackled by discussing the main algorithm of the deployment tool and its embedded optimization algorithm. This is followed by an explanation on how a program can provide support for any possible radiation pattern. Finally, some improvements towards the general performance are discussed in order to reduce time complexity. The path loss calculations can be multithreaded, a proper data structure for neighbourhood search is introduced and non-essential computations are avoided by limiting the neighbourhood search to half a kilometre.

Once all these values and formulas have been implemented, the tool is ready to be applied to different scenarios which will be discussed in chapter 4.

# 4

## Scenarios

The tool supports multiple configurations and the behaviour will be different for most of these configurations. Three main scenarios will be investigated, ordered, based on the network complexity. Within each scenario, different parameters are evaluated. First, only one user with one drone will be present in the network. The network will thereafter be expanded for multiple users but with still only one drone available. Finally, the last restriction will be dropped, meaning that a network with multiple users and an unlimited number of UABSs is examined. It is important to note that all considered values are strictly limited to the mentioned sources in chapter 3 and thus only cover data traffic between UE and UABSs. Any other potential sources like backhaul links will not be covered.

Table 4.1 shows the default values that are always applicable unless mentioned otherwise. Firstly, the table shows the specifications for LTE operating at a frequency of 2.6 Ghz. The mentioned values are used for calculating the transmission power of UE as discussed in chapter 3: equation 3.21. Secondly, the details of the antenna used by the femtocell base station are presented. The antenna is attached under the UABS and will be pointing downwards. The antenna has a maximum transmission power of 33 dBm and a gain of 4 dBm. Two types of antennae are considered, which is either an equivalent isotropic radiator generating an EIRP or a microstrip patch antenna with a slightly more complex radiation pattern. The design of this radiation pattern is shown in chapter 3: fig. 5.15. By default, the UABSs will fly at a fixed altitude of 100 metres. Thirdly, the specifications of the carrying UAVs are summed up. The authors

from [32] investigated two types of UAVs for their UAV-aided emergency network and concluded that the more robust UAV outperformed the off-the-shelf UAV. The specifications of the more advanced UAV will be used in this master dissertation. Finally, the characteristics of the antenna belonging to UE are listed. The antenna will be located one and a half metre from the floor. Note that the floor does not necessarily mean the ground. For example, a user can be indoor at the third floor. The antenna will be an equivalent isotropic radiator. By default, 224 users with each one device will be distributed over the city centre of Ghent. This city planning map is given in figure 4.1



Figure 4.1: The red area covers the city centre of Ghent, Belgium.

<b>Broadband cellular network</b>	
Technology	LTE
Frequency	2.6 GHz
Power offset ( $P_{pusch}$ )	-120 dBm
Path loss compensation ( $\alpha$ )	1
Correction value	0 dBm
Number of used resource blocks	100
<b>Femtocell antenna</b>	
Maximum $P_{tx}$	33 dBm
Antenna direction	downwards (az: 0°; el: 90°)
Gain	4 dBm
Feeder loss	2 dBm
Implementation loss	0 dBm
Radiation pattern	EIRP or microstrip patch antenna
Flying altitude	100 m
<b>UAV</b>	
UAV power	13.0 A
Average UAV speed	12.0 m/s
Average UAV power usage	17.33 Ah
UAV battery voltage	22.2 V
<b>UE Antenna</b>	
Height	1.5m from the floor
Gain	0 dBm
Feeder loss	0 dBm
Radiation pattern	EIRP
Quantity in network	224

Table 4.1: Overview of default configuration values.

## 4.1 Scenario I: A Single User

This first scenario will investigate how  $SAR_{10g}$  and power consumption behave in an isolated environment meaning there is no influence from other base stations or other UE. The tool will provision one single drone and position it directly above the user. These results will however depend on the position of the user. If the randomly generated location of the user is indoor, the flying height of the drone might be obstructed by the building where the user resides, causing the user to become uncovered. If this is not the case, the expected altitude of the user is half of the height of the building meaning that the user would be closer to the UABS as if he would

have been outdoors. For more consistent results, the user will be positioned outdoor while systematically increasing the flying height.

Another considered variable will be the transmission power of the antenna. LTE makes use of power control meaning that no more power will be used than strictly necessary. The actual transmission power therefore ranges between zero dBm and the maximum input power. This power is zero when either no user is present or the user is so far away that the actual transmitted power would exceed the maximum allowed transmission power. Increasing the maximum transmission power will not influence the actual power consumption or  $SAR_{10g}$  because of power control. However, the used transmission power of the UABS does influence power consumption and  $SAR_{10g}$  and its behaviour will be investigated at different flying heights.

This scenario investigates  $SAR_{10g}$ , power consumption and minimal transmission power for two different types of antennae: a fictional equivalent isotropic radiator and a realistic antenna as presented in figure 4.2. The used optimization strategy is not important for this scenario. This is because the decision algorithm decides which user needs to be connected to which drone. Since only one UABS is available, both optimization strategies will behave identical.

The user gets a fixed position. The exact location does not matter as long as it is outside. For this experiment is chosen for the ‘Koningin Maria Hendrikaplein’, a square just next to the train station of Ghent (fig. 4.2). Doing so will force the UE to always be at the same height of 1.5 meters. An overview of the simulation configuration scenarios is presented in figure 4.3.



Figure 4.2: Location of ‘Koningin Maria Hendrikaplein’ on the town planning map of Ghent

Input variables	Output variables
type of antenna {EIRP, microstrip} flying height [20m-200m]	$SAR_{10g}$ ( $W/kg$ ) power consumption ( $W$ ) minimal $P_{tx}$ ( $dBm$ ) electromagnetic field radiation ( $V/m$ )

Table 4.2: Evaluated parameters

Parameter	Value
x position user (longitude)	3.711198
y position user (latitude)	51.036747
shadow margin	-3.0398193
number of users	1

Table 4.3: Restrictions

Note that there is no explicit restriction on the number of UAVs in table 4.3. The deployment tool initially places UABSs above each user and it is the optimization strategy that decides which of these potential positions will remain in the end solution. Since there is only one user, there can also be only one UAV.

Figure 4.3 illustrates a possible network which satisfies the restrictions of scenario I. In the middle is the average user drawn with above him the only available UABS. It is clear that the user is only exposed to his own device and the UABS above him.

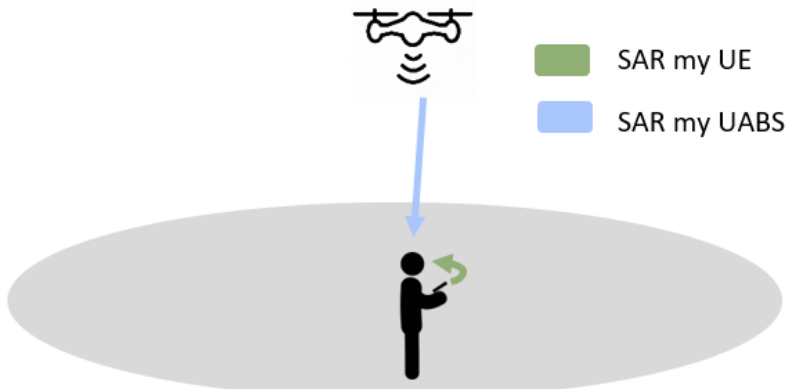


Figure 4.3: Illustration of an example network that satisfies the restrictions of scenario I.

## 4.2 Scenario II: Increasing Traffic with only one Drone available

This scenario investigates the same behaviour as the previous one. Still with only one drone but for a higher number of users. Two parameters will be investigated for this scenario. First, the flying height will be investigated for a fixed number of 224 users. This is the number of active users on an average day at 5 p.m. implying rush hour and therefore resulting in the highest number of simultaneous users for the day [32]. The other evaluated parameter is a variable number of users. When investigating this parameter, the flying height will be fixed to 100 m as recommended by [32]. An overview of the evaluated parameters is shown in table 4.4 To force

the tool to only use one drone, a facility capacity is set to one indicating that there is only one spot available in the facility where the UABSs are stored. The tool will still consider as much potential places as there are users in the network. But when the optimization algorithm is done, only one drone will remain. An overview of the restrictions is presented in figure 4.5.

For each parameter investigated, four configurations are possible because there are two antennae available (equivalent isotropic radiator and a microstrip antenna) which can both operate in a power consumption optimized network or an exposure optimized network. The  $SAR_{10g}$ , power consumption and user coverage will be investigated for all four configurations.

Input variables	Output variables
type of antenna {EIRP, microstrip}	$SAR_{10g}$ ( $W/kg$ )
flying height [20m-200m]	power consumption ( $W$ )
number of users [50-600]	user coverage
optimization strategy {Exp Opt, PwrC Opt}	electromagnetic field radiation ( $V/m$ )

Table 4.4: Evaluated parameters

Parameter	Value
capacity of the facility	1

Table 4.5: Restrictions

An illustration of a possible network is given in figure 4.4. The average user is drawn in the middle. The only available UABS covers him along with the person to the right. The two other users at the left side are uncovered and are therefore not emitting any radiation.

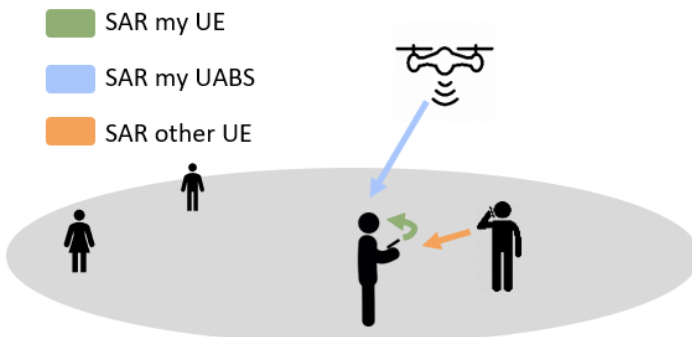


Figure 4.4: Illustration of an example network that satisfies the restrictions of scenario II.

### 4.3 Scenario III: Increasing Traffic with an Undefined Amount of Drones

The third scenario has no restrictions. The tool can use as much UABSs as desired while trying to maximize coverage. A UABS will be considered above each user as was also the case in scenario II. However, the last step where the capacity of the facility was checked and drones got eliminated, as discussed in chapter 3, is omitted here. It is expected that the optimization strategies will perform best for this scenario since the decision algorithm has been written with multiple drones in mind. Again, two parameters will be evaluated: one with a fixed flying height of 100 m and a variable number of users and a second one with a variable flying height and a fixed number of 224 users. The influence that these input parameters have on the network will be based on the electromagnetic exposure, power consumption, number of drones required and user coverage. An overview of these parameters is given in table 4.6.

Input variables	Output variables
type of antenna {EIRP, microstrip}	$SAR_{10g}$ ( $W/kg$ )
flying height [20-200]	power consumption ( $W$ )
number of users [50-600]	user coverage
optimization strategy {Exp Opt, PwrC Opt}	electromagnetic field radiation ( $V/m$ )

Table 4.6: Evaluated parameters

An illustration is presented in figure 4.5 with the average user drawn in the middle. Most users are covered by the many UABSs available. The average user will be exposed to all these UABSs and to all the UE that belong to covered users.

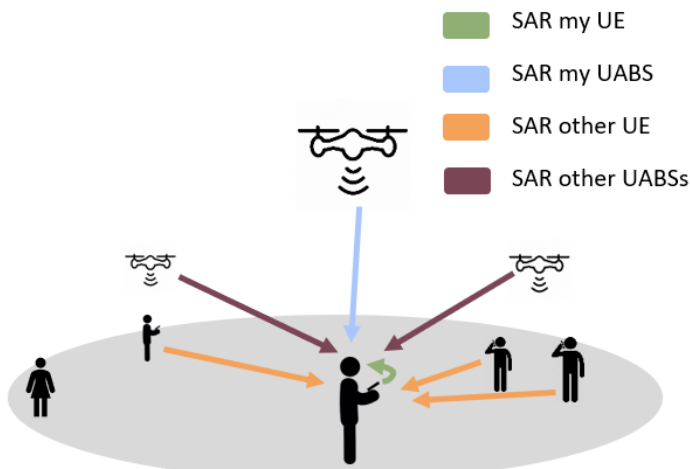


Figure 4.5: Illustration of an example network according to the description of scenario III.

## 4.4 Overview of Configurations

Three different scenarios are considered. The first one with one user and one UABS. The second one has still only one UABS available but has much more users. The third one has an unlimited number of UABSs available in order to cover as much users as possible. All three scenarios evaluate the influence of a varying flying height while only the second and third one investigate different population sizes. Four possible configurations exist for each evaluated parameter within each scenario. The matrix in table 4.7 shows that two types of antennae are investigated and how the optimization strategy can operate towards two goals: exposure optimized and power consumption optimized.

		<b>Optimization strategy</b>	
		Exposure optimized	Power consumption optimized
<b>Antenna type</b>	Equivalent isotropic radiator	EIRP Exp Opt	EIRP PwrC Opt
	Microstrip patch antenna	Microstrip Exp Opt	Microstrip PwrC Opt

Table 4.7: Matrix with the four possible configurations

# 5

## Results and Discussion

This chapter gives an overview of the achieved results from all considered scenarios. The two parameters, flying height and number of users, are evaluated by monitoring the power consumption, electromagnetic exposure and SAR-values. This is done for the two considered antennae who can both operate in two optimization strategies, making a total of four possible configurations. These configurations will be investigated in three different scenarios. The first section talks about scenario I which is a small network with only one user and one UABS. In the following section, scenario II is investigated where the network is expanded for a larger population but with still only one UABS available. The network in the last section investigates scenario III which serves a large population with an unlimited number of UABSs.

The electromagnetic radiation and SAR are measured for the weighted average user. This means that equation 3.30 is used with both  $w_1$  and  $w_2$  set to 50%. Doing so will not only optimize the network towards the average user but also limit higher electromagnetic radiation. Each simulation is repeated 20 times. Therefore, the values for the weighted average user will be averaged over these 20 simulations.

Some interesting values are presented to give the reader an idea on how long these computations take. For example, the variable flying height in each scenario ranges from 20 m to 200 m in steps of 20 m resulting in a total of 200 simulations for one scenario. This results in more than 15 million 52 thousand path loss calculations. The evaluated parameter ‘number of users’

ranges from 50 to 600 in steps of 50, resulting in 240 simulations. Such one scenario takes 48 million 750 thousand path loss calculations. Remember that path loss calculations are done in the preparation phase and the network has not even been optimized at this point.

## 5.1 Scenario I: One User and One UAV

The network contains only one user in this scenario. This means that there is only one location possible for the UAV, being just above the user. This section will investigate minimal required transmission power and SAR values from different sources. Finally, also the power consumption of the entire network is measured. The “entire network” refers to all UABSs. For this scenario, the entire network will be constructed out of a single UABS.

### 5.1.1 The Influence of the Maximum Transmission Power

LTE makes use of power control meaning that no more power will be used than strictly necessary. The actual transmission power  $P_{tx}$  therefore ranges between zero dBm and the maximum allowed input power.  $P_{tx}$  is zero dBm when the UABS does not cover anybody. For instance when the flying height is too high and therefore also the path loss that comes with it, the maximum allowed  $P_{tx}$  is not enough to cover the distance. In such case, the UABS is shut down since it cannot meet the requirements. Increasing the maximum transmission power will not influence the actual used  $P_{tx}$  because the UABS will not use more than strictly required. It is therefore more useful to match the actual transmission power against a variable flying height.

Figure 5.1 shows a logarithmic relationship between  $P_{tx}$  and flying height. As already discussed in 4.1, the user is outdoor and just below the UABS. There is thus a free LOS between both radiators. It is clear from figure 5.1 that a discontinue step function is achieved. This is because multiple flying heights correspond to the same transmission power. When the flying height increases, so does the path loss. This causes the Signal to Noise Ratio (SNR) to drop under the required boundary. LTE tries to counteract this by increasing the power level. Each time the path loss becomes too high, the power level of the antenna increases with one dBm. Doing so, increases the SNR allowing the user to properly receive and decode the signal again. After a jump in the step function, there is an overestimation meaning the  $P_{tx}$  increased more than necessary. So multiple flying heights correspond with the same  $P_{tx}$ . Further, dBm is also a logarithmic scale meaning that while 10 dBm equals 10 mW, 20 dBm equals 100 mW. This explains why the black lines become longer at higher flying altitudes. Each time the power level increases with one dBm, the overestimation becomes larger. If the tool would make use of a smaller step size, a more continuous logarithmic function would be achieved. This would however worsen the time complexity because it would take much more iterations before the

power level exceeds the path loss. The red line in figure 5.1 indicates the default maximum transmission power of 33 dBm used during simulations as defined in table 4.1. In a free LOS scenario with only one user, a UABS can fly up to 387 metres before losing connection.

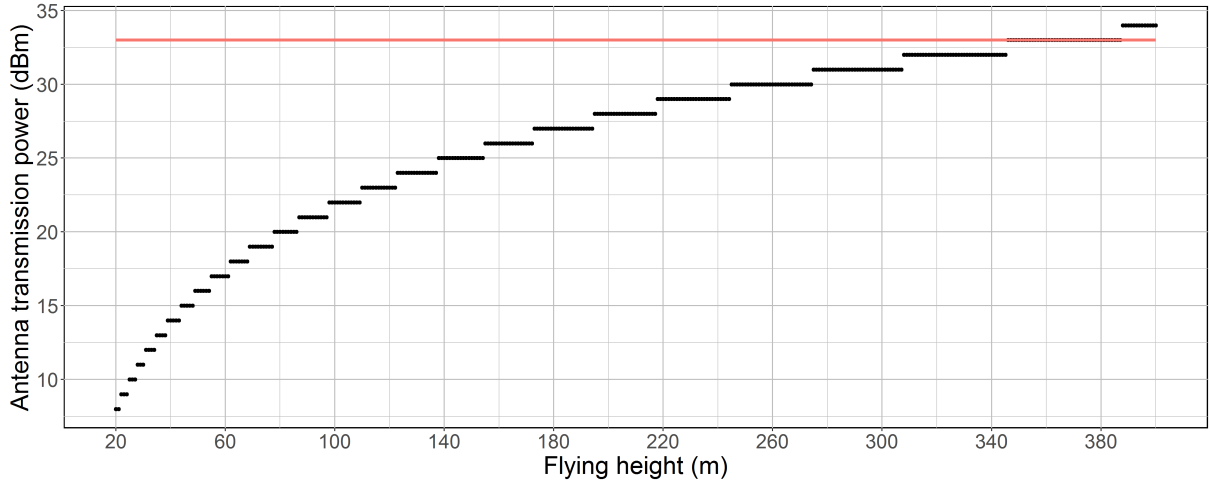


Figure 5.1: Minimal required transmission power by the antenna to reach the ground just below it. The red line shows the default maximum transmission power.

This scenario is investigated with a microstrip patch antenna using power consumption optimization. However, the chosen optimization strategy does not really matter as already explained in 4.1. This is because the decision algorithm decides which user needs to be connected to which UABS. Since only one UABS is available, both optimization strategies will behave identical. Further, also the used antenna will not make any difference despite the fact that a microstrip patch antenna has attenuation while an equivalent isotropic radiator does not. The user is namely positioned in the perfect center of the main beam where there is no attenuation experienced in either cases. So the results are applicable for the four possible cases from figure 4.7.

### 5.1.2 Influence of the Flying Height

This section investigates how the flying height of a UABS influences  $SAR_{10g}$  and power consumption. The  $SAR_{10g}$ , which is actually induced electromagnetic radiation into the user, is represented in figure 5.2 and shows that for a low flying UAV, DL radiation is the main source of electromagnetic exposure. This changes around an altitude of 80 metres where the UL radiation from the UE exceeds the DL radiation in order to still be able to reach the high flying UABSs.

SAR-values are caused by the transmitted power  $P_{tx}$  of the antenna. The  $P_{tx}$  in section 5.1.1 showed a discontinuous behaviour that sometimes radiates more than strictly necessary. This has thus a direct influence on the DL SAR; hence, the same discontinuous behaviour. The DL SAR can

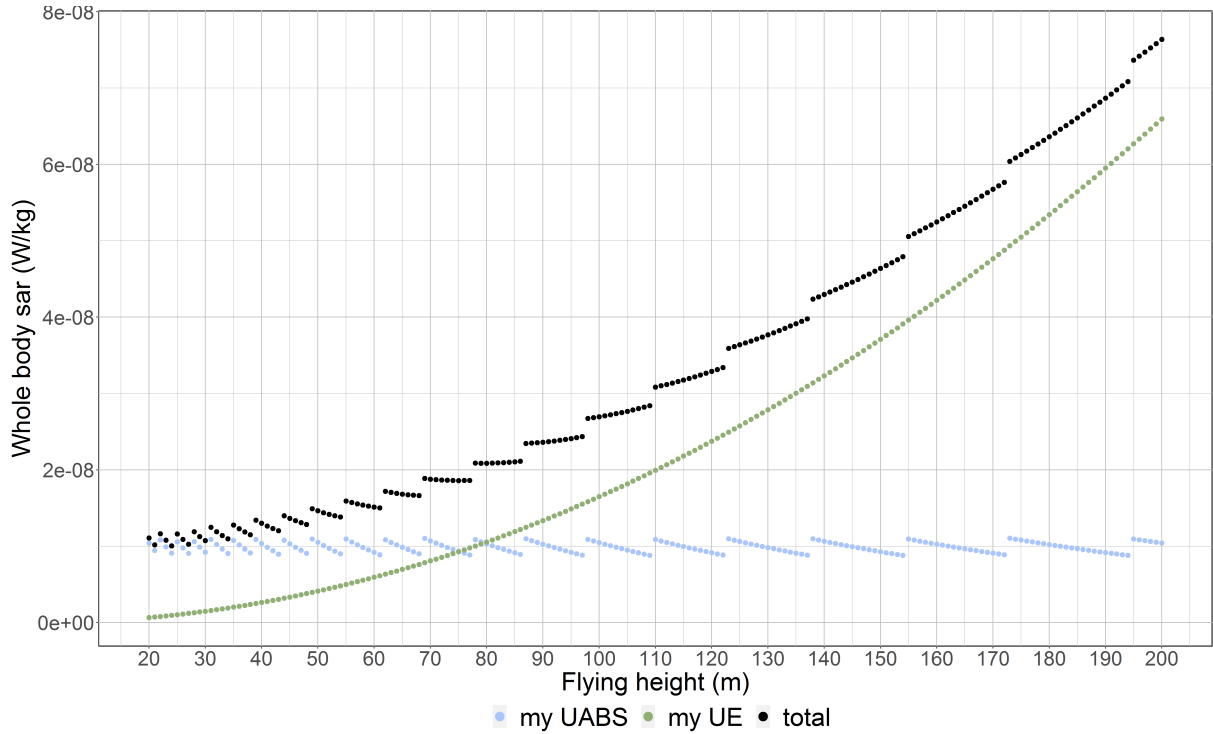


Figure 5.2: This figure shows how SAR values from different sources are influenced by different flying altitudes.

be simplified to a perfect constant line at  $10 \text{ nW/kg}$ . This constant behaviour can once again be explained with power control. When the UABS flies lower, there is less path loss and the UABS will therefore reduce the  $P_{tx}$ . We can therefore confirm that the electromagnetic exposure from the UABS is a constant fraction of power and distance. The electromagnetic radiation from the UE shows in figure 5.2 an exponential behaviour. The power used by the antenna is calculated with formula 3.21 and depends mainly on path loss. UE will, similar to UABSSs, radiate just enough so the SNR is high enough to be decoded by the receiver. The only difference with DL radiation is that the distance between the radiator and the user remains unchanged. Therefore, the UL electromagnetic radiation experienced by the user will increase when the flying altitude of the UABS increases. Figure 5.2 does not show radiation from neighbours, because there are none present in this scenario. Finally, all these values are added up as explained in formula 3.1 resulting in the total SAR to which our user is exposed, represented by the black line in 5.2.

The power consumption of the entire network presented in figure 5.3 is here of course for the only UABS available. The energy is based on the transmission power of the antenna and the used battery by the UAV. Section 5.1.1 already explained the reason behind the stepped function. The transmission power is an important parameter when calculating the used power and is the cause that we see the same stepped behaviour in figure 5.3. All individual results (indicated with dots) can once again be simplified with a connected line that clearly shows an exponentially

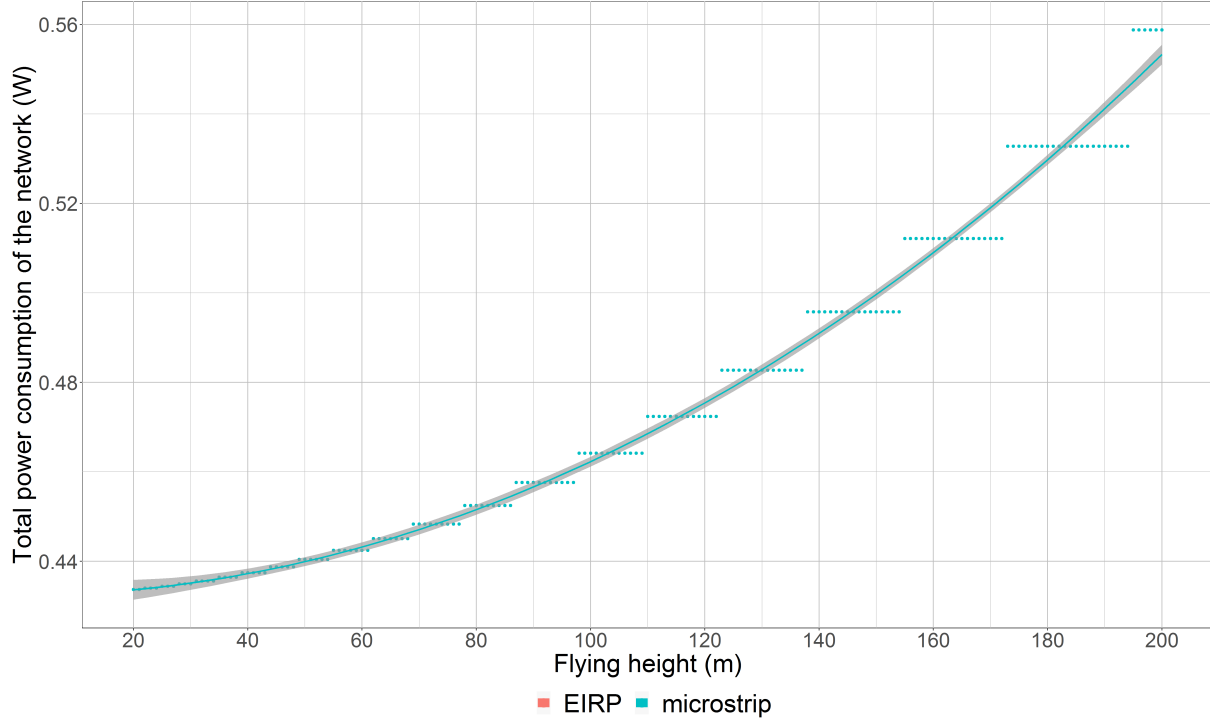


Figure 5.3: This figure shows the behaviour of the power consumption over the entire network at different flying heights. For this scenario, the power is used by only one UABS.

behaviour. The grey shadow behind the line represented the confidence interval.

## 5.2 Scenario II: Increased Population

This scenario has just like the previous scenario only one UAV available. However, more users will be present in the network. First, a variable flying altitude is investigated for a fixed number of 224 users. Secondly, the flying height is set to 100 metres with a variable number of users. When designing the network, there will be as much possible UAV locations as there are users in the network and the tool will consider all of them. Only when the program is finished, one UAV will remain. Each considered input value will be averaged over 20 simulations.

### 5.2.1 Influence of the Flying Altitude

The first evaluated parameter of this scenario investigates how the network, consisting out of one UABS, behaves when applied on an ordinary day during rush hours. Different fixed flying heights are considered while 224 active users are distributed uniformly over the city centre of Ghent. An example network is given in figure 5.4.



Figure 5.4: Example of an EIRP PwrC Opt network with only one UABS (yellow triangle). Only a very few users (green) are connected. All other users (red) remain uncovered.

Figure 5.5 presents the average DL exposure and average total power consumption. The grey area indicates the confidence interval. A power consumption optimized network with an EIRP antenna (green) has the highest exposure during the entire experiment. At the default flying height of 100 metres, an electromagnetic field radiation of  $10 \text{ mV/m}$  is measured. This is logical when comparing to an EIRP antenna in an exposure optimized network (red) with only  $8.5 \text{ mV/m}$ . However, when looking at figure 5.5.b, the power consumption in a power consumption optimized network is not necessarily less than in an exposure optimized network. For example, an EIRP and microstrip antenna will require at the default flying height respectively  $20 \text{ mW}$  and  $10 \text{ mW}$  more in a power consumption optimized network than in an exposure optimized network. To understand this, the behaviour of the deployment tool needs to be understood first. A power consumption optimized network will result in a few high powered UABSSs because increasing the input power of an antenna costs less than activating a new UAV. Likewise, an exposure optimized network generates a lot of low powered UABSSs because the lower the power of the antenna, the lower the exposure. This has the consequence that the cover radius is less and therefore requires more UAVs which costs more energy. When only a limited amount of UABSSs are available, like only one in this scenario, the tool will only keep those UABSSs that cover the most users. Therefore, the power consumption in a power consumption optimized network is often higher.

Figure 5.5 further also shows how the electromagnetic radiation from the UABS starts decreasing again at high altitude. A microstrip PwrC Opt network is at his highest point around 162 metres and an EIRP PwrC Opt is at his highest at 195 metres. This decline starts later

for exposure optimized networks and is situated outside the investigated flying range. The decreasing electromagnetic radiation at high flying altitudes is not caused by the obstructing buildings but by the distance in general.

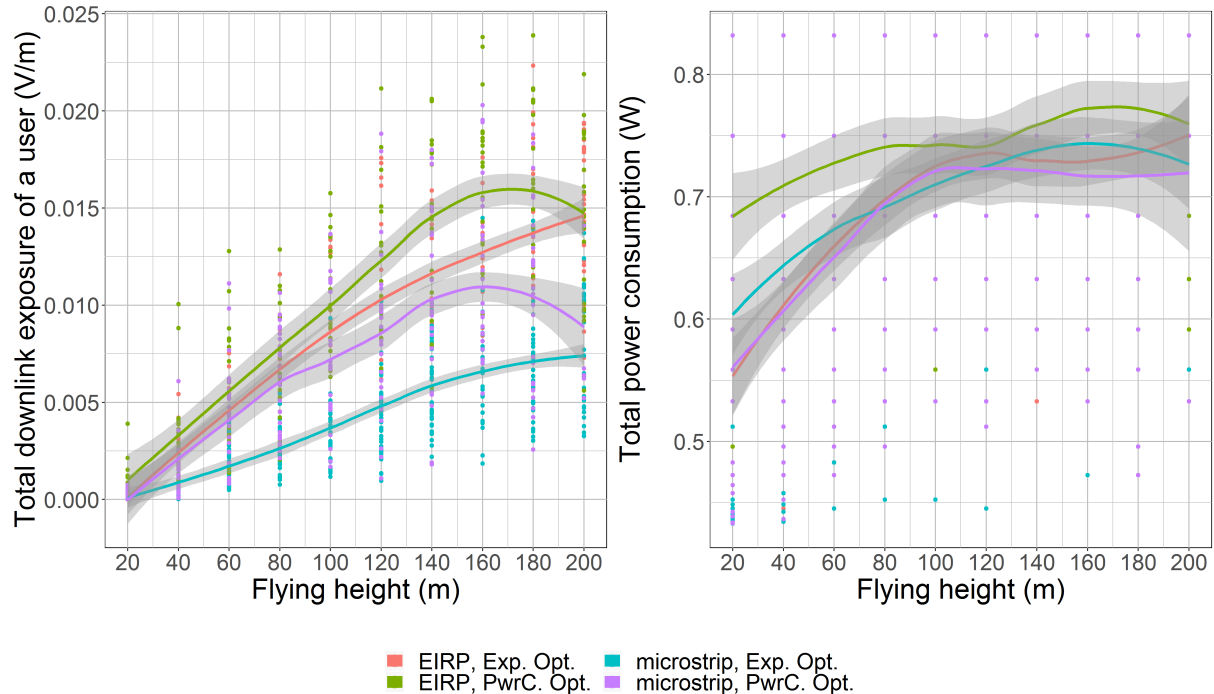


Figure 5.5: Fig. (a) show how the flying height influences the downlink electromagnetic radiation of the average user and fig. (b) the power consumption of the entire network for the only UABS available in the network.

The DL exposure in figure 5.5 increases along with the flying height. One might expect a more constant behaviour like it was the case in figure 5.2 of scenario I. To understand this, the scenario has been reduced to only two users and is illustrated in figure 5.6. The two users, who will be referred to by ‘red’ and ‘blue’, are 90 metres separated from each other with a building between them. scenario I already explained that the charts can be simplified and the blue line from fig. 5.7 remains in fact constant between zero and 130 metres. The chart shows that the UABS is positioned above the blue user. The red user is in NLOS as long as the UABS remains below 20 metres.

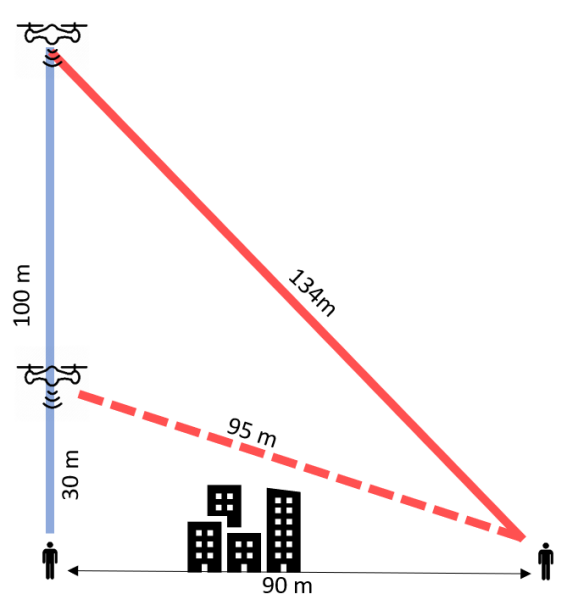


Figure 5.6: Schematic overview of scenario II with only 2 users.

Once the UABS increases its flying altitude, the red user comes into LOS but still remains uncovered. This is because the tool initially locates a possible UABS above each user and thereafter performs the fitness function. The applied fitness function must have decided that it is better to connect each user to the UABS above him. In a final stage, the tool checks whether the number of online UAVs does not exceed the capacity of the facility which is here the case. The tool therefore deactivates one UABS causing the red user to be uncovered. One could argue that the red user should be connected to the online UAV who is only 90 metres away. This would however require the online UAV to increase its power consumption which would make the decisions made by the optimization strategy obsolete. When the UAV flies higher, the difference in distance between both users and the base station decreases. In other words, the Pythagorean theorem shows that when the flying height of the UABS increases, the distance to the blue user increases faster compared to the distance between that same UABS and the red user. This is also illustrated in figure 5.6. At 130 metres, the tool decides to connect both users to the same UABS. Therefore, it increases its power consumption whereby the red user would have the minimal required electromagnetic exposure. This has of course a negative influence on the blue user who is much more closer and experiences now a much higher exposure level in fig 5.7. Around 180 metres, the red and blue line switch because the UAV changes position. As explained before, the tool assigns two possible UAVs, one above each user. The tool must have decided that connecting both users to the other UAVs improves the fitness function of the entire network even though that difference might be very little. Finally, this brings us back to the weighted average exposure from figure 5.5 where 223 users will behave like the red user and only one user behaves like the blue one. The red line therefore dominates the average exposure in figure 5.5.

Figure 5.5 showed that the electromagnetic exposure of the average user increases along with the flying height which reflects itself on better coverage as visible in figure 5.8. Increasing the flying height from 20 to 100 metres improves the coverage between 1% and 2% for all four configurations. When replacing the fictional EIRP antenna by a microstrip patch antenna, the percentage of covered users drops for both optimization strategies less than 1%. The difference is caused by users who have a higher horizontal distance between themselves and the UABS. Microstrip patch antennae have a smaller aperture angle than an equivalent isotropic radiator and have therefore a smaller range. When a microstrip patch antenna is positioned higher, the range of the antenna increases since the angle between the user and the UABS's main lobe decreases. The user will therefore experience less attenuation.

Eventually, figure 5.9 shows the whole body  $SAR_{10g}$  for the weighted average user, deducted from all electromagnetic sources. This combines the exposure of the only UABS available in the network, the UL exposure from the user's own device and the exposure of the devices from all

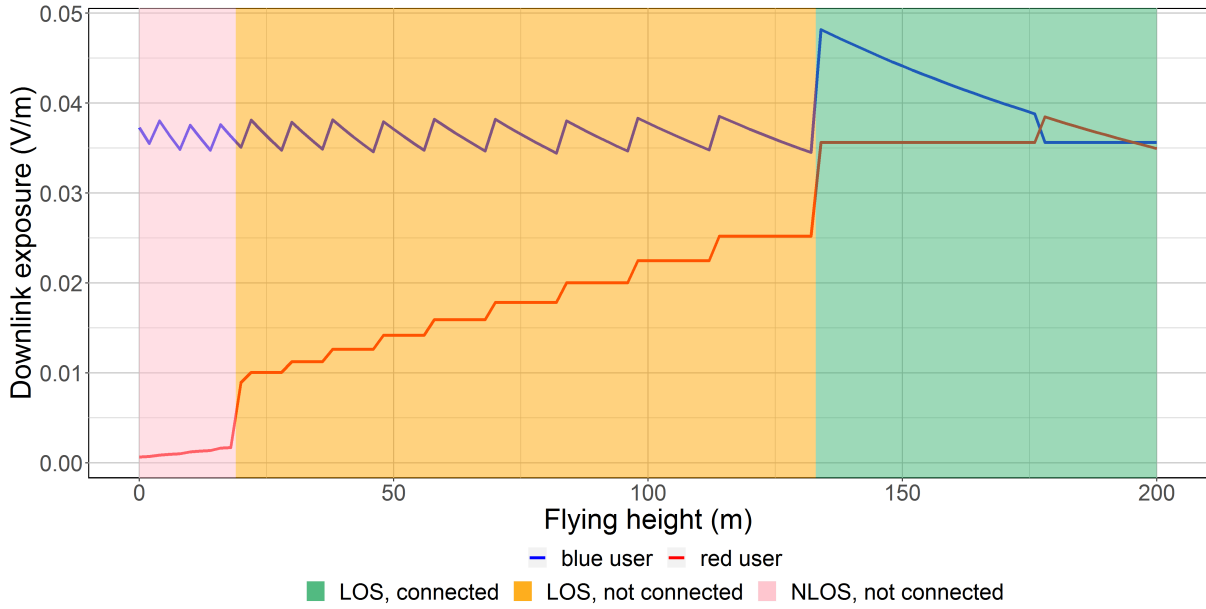


Figure 5.7: scenario II with only 2 users. The coloured areas are only applicable for the red user. The blue user is connected during the entire time.

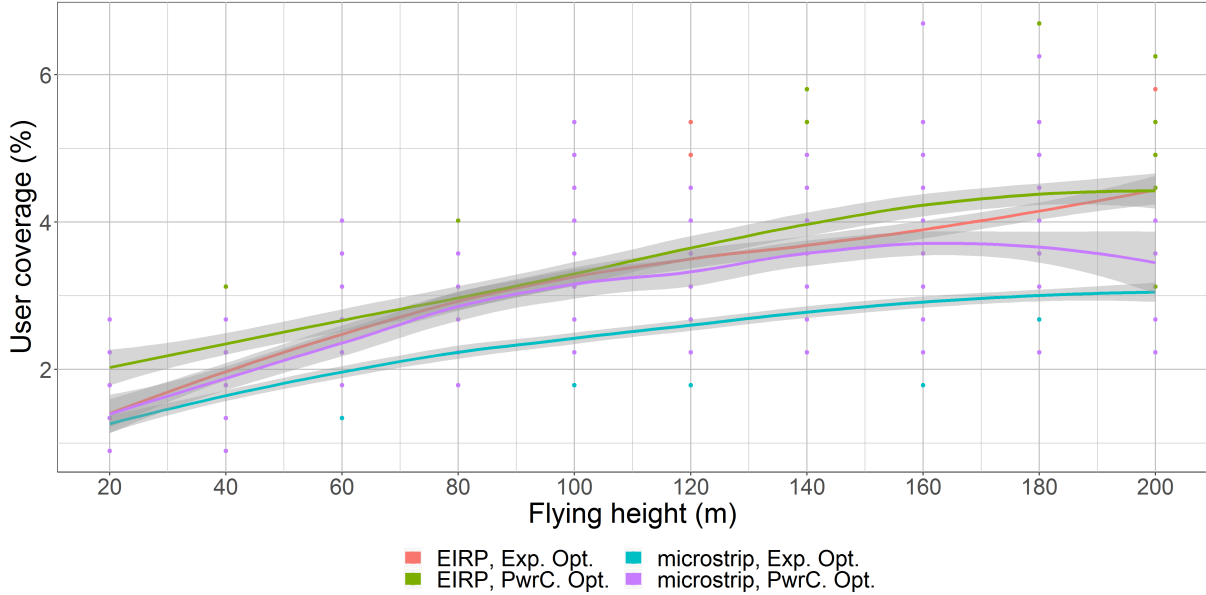


Figure 5.8: This graph shows the percentage of covered users for only one UABS at different flying heights.

other covered users. When investigating the three different sources, we see that the  $SAR^{myUABS}$  shows the same curve as it did with the electromagnetic exposure in figure 5.5.a. This is normal behaviour considering that equation 3.17 is able of converting the DL exposure to SAR by simply multiplying with a constant. During the entire time is  $SAR^{myUABS}$  the most dominant

factor followed by the near-field radiation from the user's own device. The far-field radiation from other UE barely has influence. As an illustration, when the UABS flies at 140 metres, the average user in an EIRP PwrC Opt network will experience around  $2.1 \text{ nW/kg}$  from the UABS and around  $0.2 \text{ nW/kg}$  from his own device. The exposure from other UE can be neglected with  $0.03 \text{ pW/kg}$ . A low but plausible value considering that most UE are not radiating anything since they are uncovered (hence the many red dots in fig. 5.4).

The weighted average  $SAR_{10g}^{ul}$  from the own device is zero in an exposure optimized network with a microstrip patch antenna which is even lower than the  $SAR_{10g}^{neighbours}$ . This is because the coverage in this scenario is so low that the weighted average only consists of uncovered users and the transmission power of an uncovered user is zero.

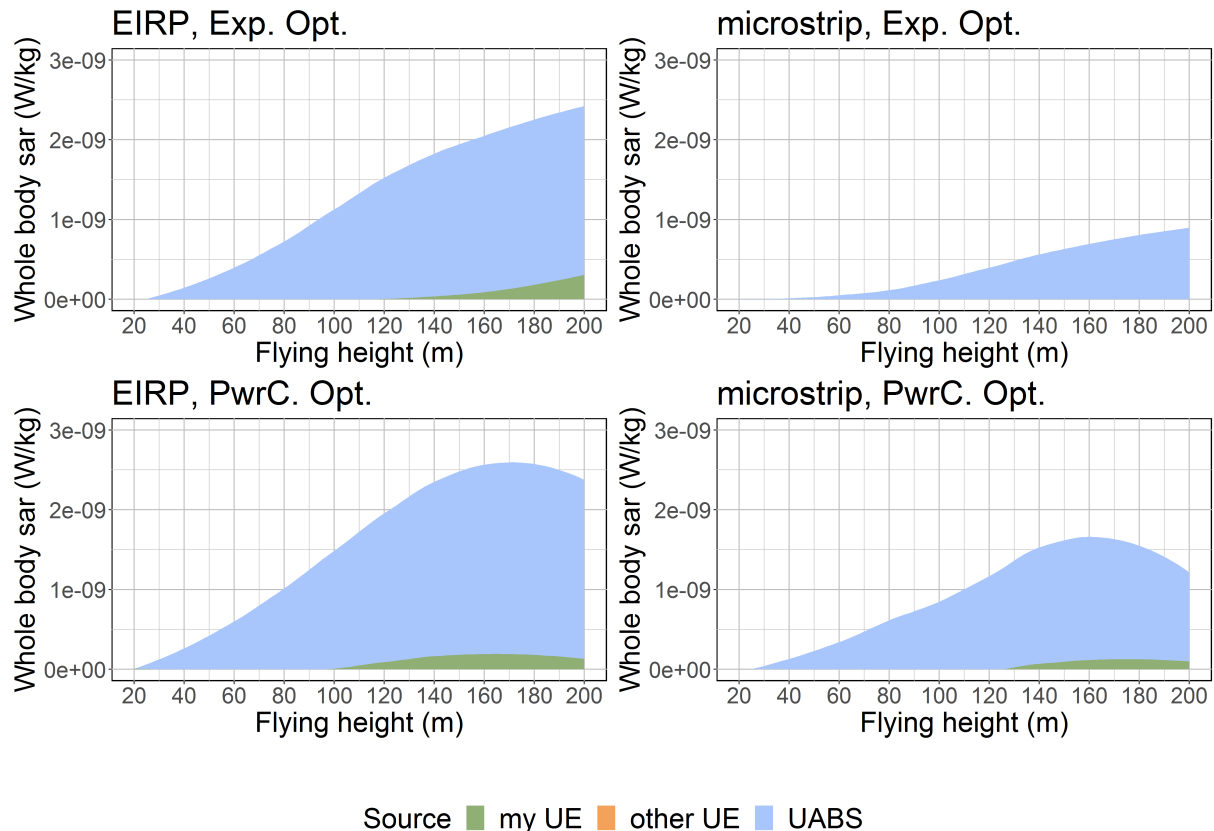


Figure 5.9: Each figure corresponds with a certain configuration and shows how the SAR from different sources are influenced by an increasing flying height.

### 5.2.2 Influence of the Number of Users

The number of covered users increases linearly compared to the number of users present in the network as shown in figure 5.10.b. It illustrates how an equivalent isotropic radiator is able to reach more users compared to a microstrip patch antenna. Just like an power consumption optimized network is able to reach more users than an exposure optimized network. For example, with 600 users, 5 to 7 additional people can be covered when replacing a microstrip patch antenna with an equivalent isotropic radiator. An changing an exposure optimized network with an power consumption optimized network will cover one or two additional users.

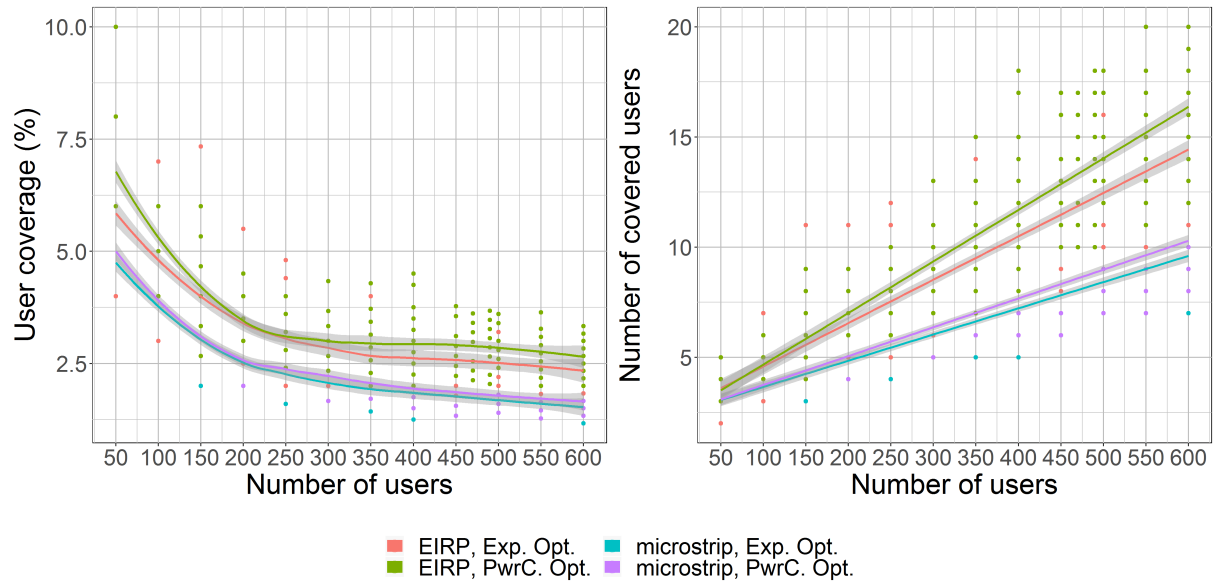


Figure 5.10: The influence of increasing traffic on the user coverage.

The linear regression lines from figure 5.10 can be predicted with the equations in 5.1.

$$\text{number of users} = \begin{cases} y = 0,0233x + 2,3553 & \text{if EIRP and PwrC Opt} \\ y = 0,0197x + 2,6144 & \text{if EIRP and Exp Opt} \\ y = 0,0131x + 2,4371 & \text{if microstrip and PwrC Opt} \\ y = 0,0119x + 2,4652 & \text{if microstrip and Exp Opt} \end{cases} \quad (5.1)$$

Figure 5.10.a shows the percentage of covered users that follow out of 5.10.b by taking the equations from 5.1 and dividing them by  $x$ . This results in a decreasing logarithmic behaviour because the regression lines from 5.10 have a slope of less than 0.5. This means that the percentage of covered users for a small populated network is more compared to the percentage of users in large populations. Figure 5.10 concludes that the increase in population causes a

decrease in coverage since only one UABS is available. While an EIRP PwrC Opt network with only 50 users knows a 6.75% coverage, a network with 600 users has no more than 2.75% coverage.

Figure 5.11.a is influenced by 5.10.a. When less users are covered, the exposure of the average user will decrease as well. For example, in an EIRP PwrC Opt network, 50 users have a 6.75% coverage which corresponds with a weighted average exposure of  $18 \text{ mV/m}$  while 600 users with 2.75% coverage only have  $9 \text{ mV/m}$ . Further, figure 5.11.b is directly influence by figure 5.10.b. When the UABS has to cover more users, the probability that some of these users have a worse path loss is higher. The UABS solves this problem by increasing the power consumption. Increasing the population from 50 to 600 will require between 0.05 and 0.1 W more. For this scenario, no clear difference in power consumption exists between the four configurations.

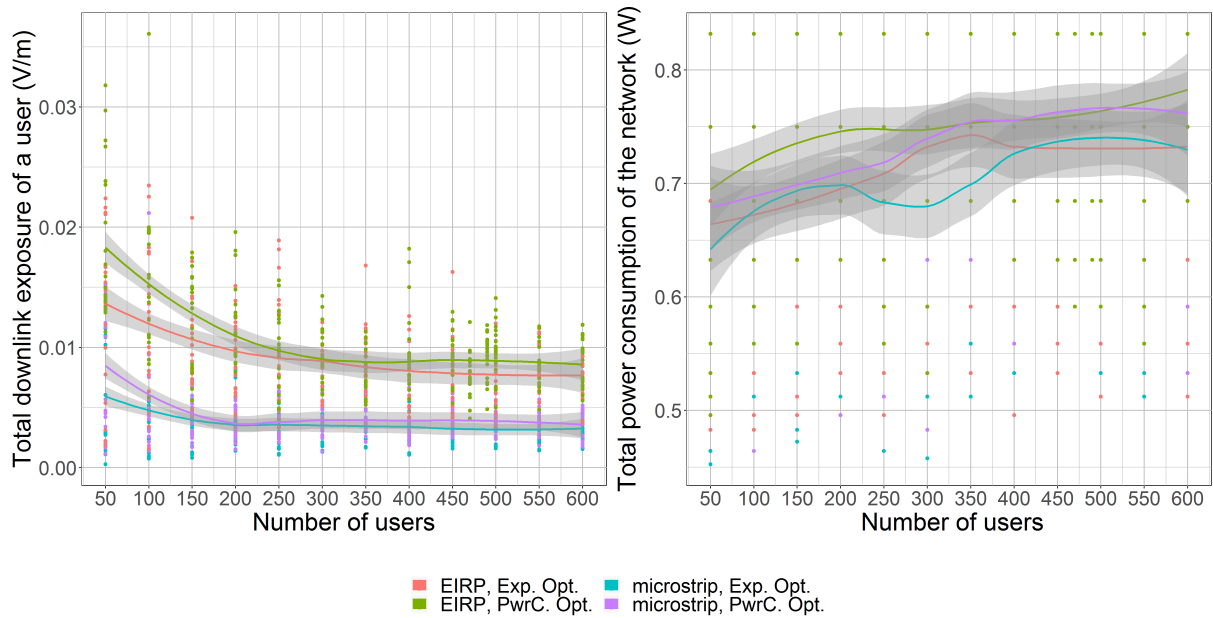


Figure 5.11: These two figures show how various sizes of population influence the downlink electromagnetic radiation of the average user (left) and power consumption of the entire network (rights) for one UABS available in the network.

Figure 5.12 investigates the assets of each source contributing to the total SAR. All four configurations show that base stations are the main source of electromagnetic radiation which remains almost constant. The equivalent isotropic radiator varies around  $1 \text{ nW/kg}$  for both optimizations and the microstrip antenna around  $0.16 \text{ nW/kg}$ . Figure 5.10 already showed that a sparsely populated network results in a higher coverage percentage which on his turn results in a higher  $SAR_{ownUE}^{ownUE}$ . The  $SAR_{ownUE}^{ownUE}$  for 50 users is for an equivalent isotropic radiator on average  $1.7 \text{ nW/kg}$  for both optimizations and the microstrip antenna around  $0.4 \text{ nW/kg}$ . The chart also proves once again that the far-field radiation from UE can be neglected. The SAR from neighbouring devices is not zero as it looks like in figure 5.12 but is just really low compared to the much higher SAR-values from other sources. While the population grows, more and more users become uncovered causing the average SAR to drop. However, this does not conclude that by increasing the population, the SAR of a user who is directly beneath a UABS would be less.

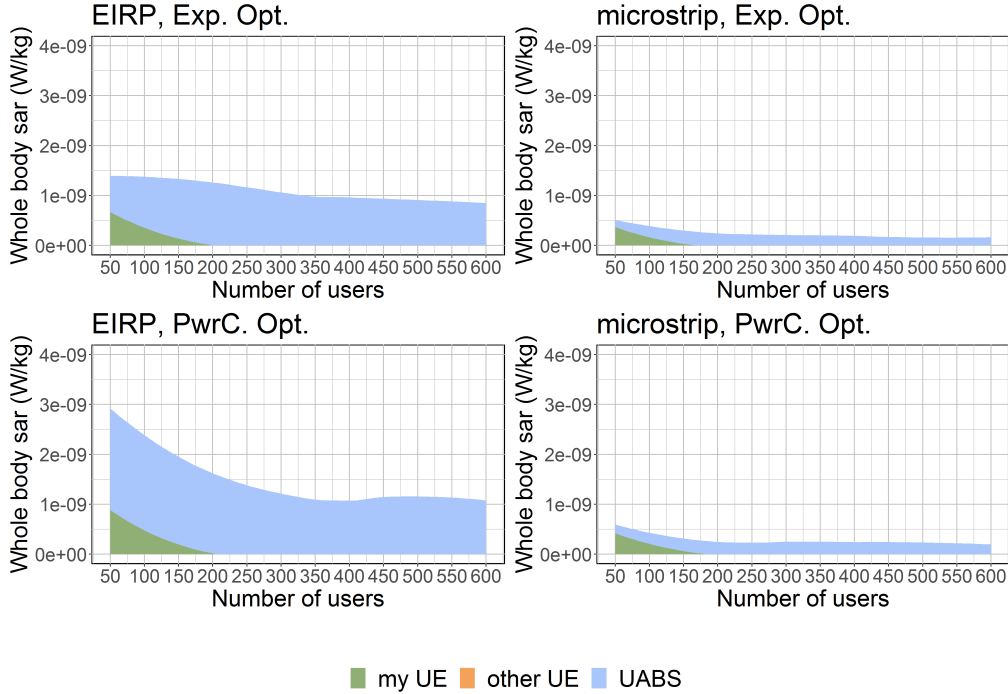


Figure 5.12: This figure shows how different sources are influenced by an increasing number of users.

To investigate this, a user is positioned in the middle of the city centre of Ghent and a UAV is positioned above him. Initially, only 49 people are active around him. The SAR of our central user is monitored while the population around him is growing. Figure 5.13 shows with the black lines which users are connected. Figure 5.13.a is for only 50 users and shows that only one user is connected besides our central user. Figure 5.13.b considers 600 users and shows much more connected users.

Scenario I already showed that the SAR from the user's own device is only influenced by the flying height. The flying height for this experiment is fixed and the UL SAR from his device should therefore also be a constant. A hypothesis that is confirmed by figure 5.14 where  $SAR^{myUE}$  is equal to  $0.15 \mu W/kg$ . The SAR from the UABS experiences a slight increase of  $0.005 \mu W/kg$ . When the population grows, more users become available and some will spawn near the central user. The UABS will likely decide to cover these users as well as visible in figure 5.13. These users might have a slightly worse path loss because of obstructing buildings or somewhat bigger distance. The UABS reacts to this by increasing his power consumption causing an increase in the DL SAR for the central user. The far-field radiation from UE is very low as mentioned before and therefore added separately in figure 5.13.b. It shows that the SAR from other UE increases from zero to  $0.15 pW/kg$ . This is normal behaviour considering that around the central user more and more people become available of which some will be connected to the UABS and

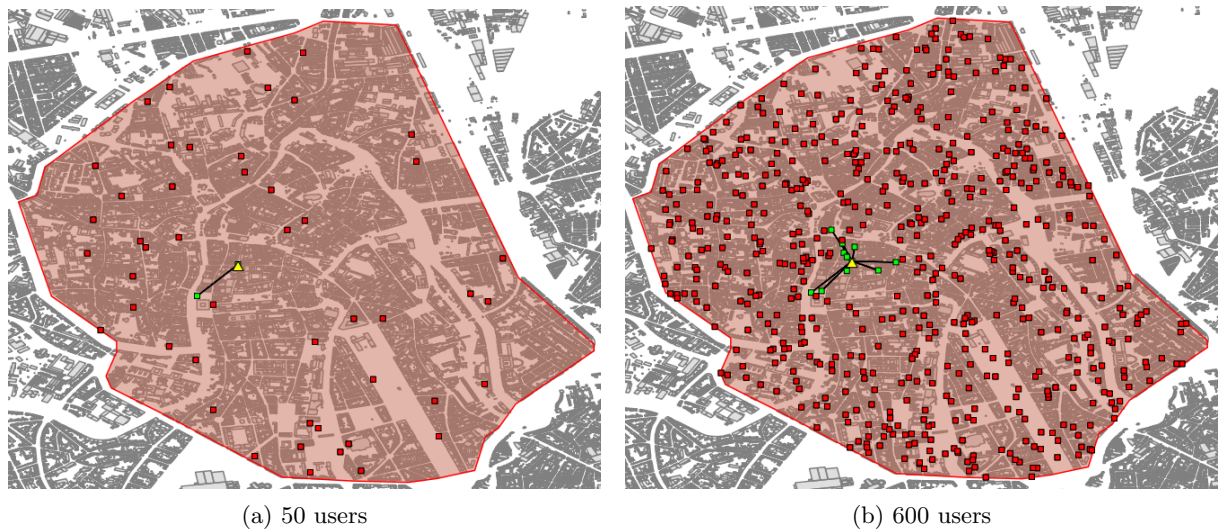


Figure 5.13: Overview of which users are connected to the UABS.

therefore also emitting radiation.

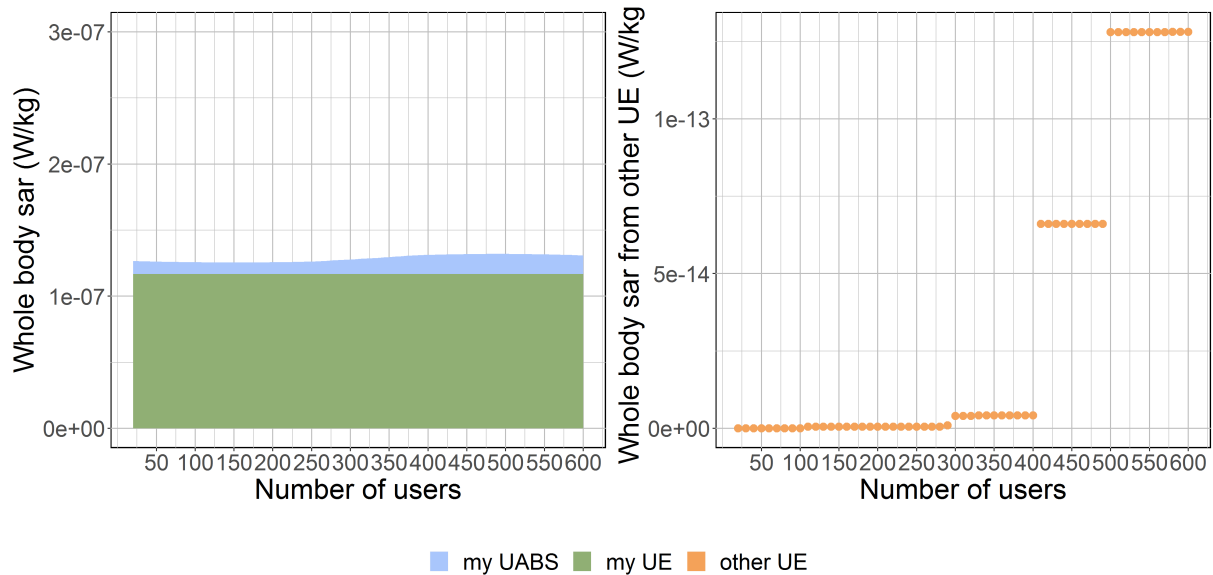


Figure 5.14: SAR-values for the user who is directly beneath the only UABS available.

### 5.3 Scenario III: Unlimited UAVs

This scenario, just like the previous one, has much more users in the network and investigates the same cases which include the variable flying height and the variable number of users. The only difference is that the restriction of only one UABS is dropped.

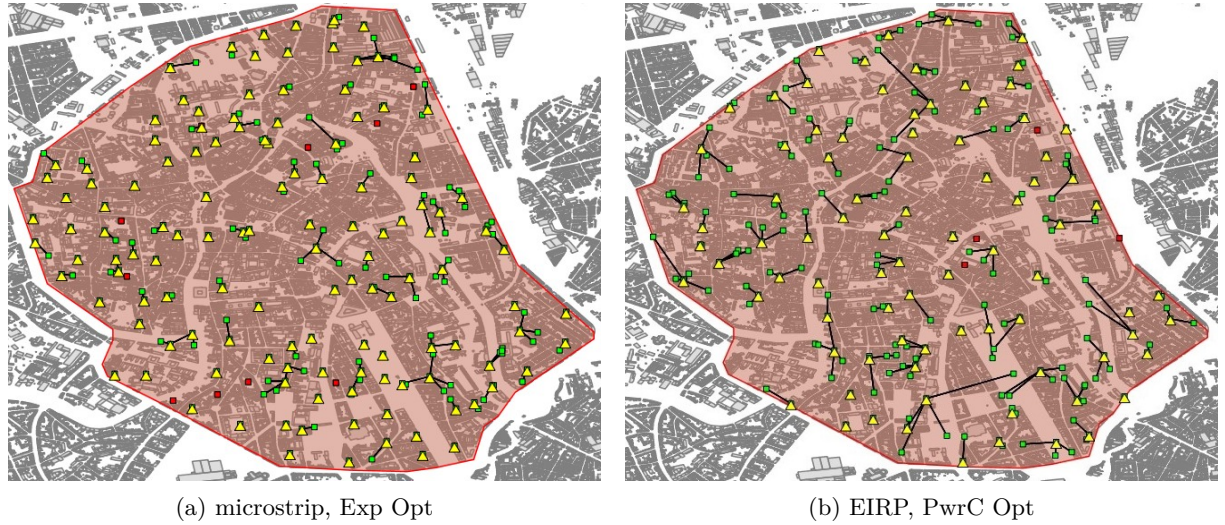


Figure 5.15: Example of two networks with users distributed over the area. Yellow triangles represent UABSSs and are connected with black lines to users in green. Uncovered users are coloured in red.

#### 5.3.1 Influence of the Flying Altitude

The first evaluated parameter of this scenario is the flying height with a fixed number of 224 users. Scenario II already explained that when only one UAV is available, a power consumption optimized network will not result in a low powered network. In this scenario, there is no limitation on the number of UAVs and the network remains thus unaltered after the decision algorithm is done. Figure 5.16 clearly proves that the different optimization strategies work as intended. Power consumption optimized networks have indeed a lower power consumption but therefore result in higher electromagnetic radiation. On the other hand, an exposure optimized network will reduce the electromagnetic exposure by using more UAVs and thence also increases the network's power consumption. A behaviour that was also concluded in [17]. For example, when comparing both optimization strategies for the same equivalent isotropic radiator and the same default flying height, we see that the power consumption optimized network requires 51 W and therefore exposes its users to 15 mV/m. When optimizing towards electromagnetic radiation, the exposure drops to 11.5 mV/m but at a cost of a higher power consumption of

54 W. Further, figure 5.16.a also shows that the exposure in an exposure optimized network increases logarithmically while in a power consumption optimized network the exposure has a concave relationship with the flying height, and has its lowest point at around 70 metres.

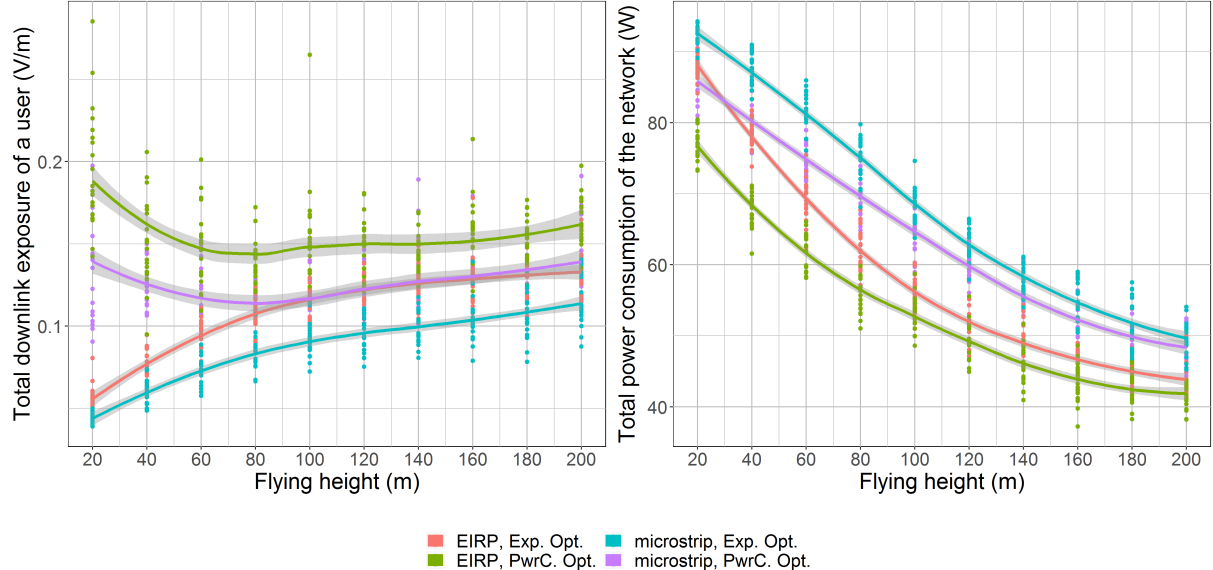


Figure 5.16: These two figures show how the flying height influences the downlink electromagnetic radiation of the average user (left) and power consumption of the entire network (right) for an unlimited number of drones.

Figure 5.17.a shows that the optimal coverage is achieved at a low flying height of 40 metres with around 99% coverage. However, there is a downside to this. Figure 5.17.b shows that the number of required UAVs increases when the flying altitude becomes lower; a behaviour which was also determined in [32]. For example, an microstrip Exp Opt network and an EIRP PwrC Opt network require respectively 84 and 64 UABSSs at a flying altitude of 200 m which increases respectively to 211 and 162 UABSSs at a much lower flying altitude of 20 m.

Scenario I already proved that for low flying UAVs, the main source of electromagnetic radiation are UABSSs. This changed around 80 metres where UL electromagnetic radiation of the UE exceeds DL radiation in order to still be able to reach the high flying UABSSs. When looking at the different individual sources of electromagnetic exposure presented in figure 5.18, we notice the same behaviour where the SAR from the own device indeed increases between 89 and 141 nW/kg by raising the flying altitude from 20 to 200 metres. However, a more logarithmic increase is shown despite the fact that figure 5.2 showed an exponential increase. This was however deducted with only one user present in the network as opposed to this scenario where 224 users are present. The electromagnetic radiation from the covered users will still behave like it did in scenario I. Moreover, the SAR shown in figure 5.2 is averaged over covered and uncovered users. In conclusion, the average UL SAR in figure 5.2 will not increase as fast as it

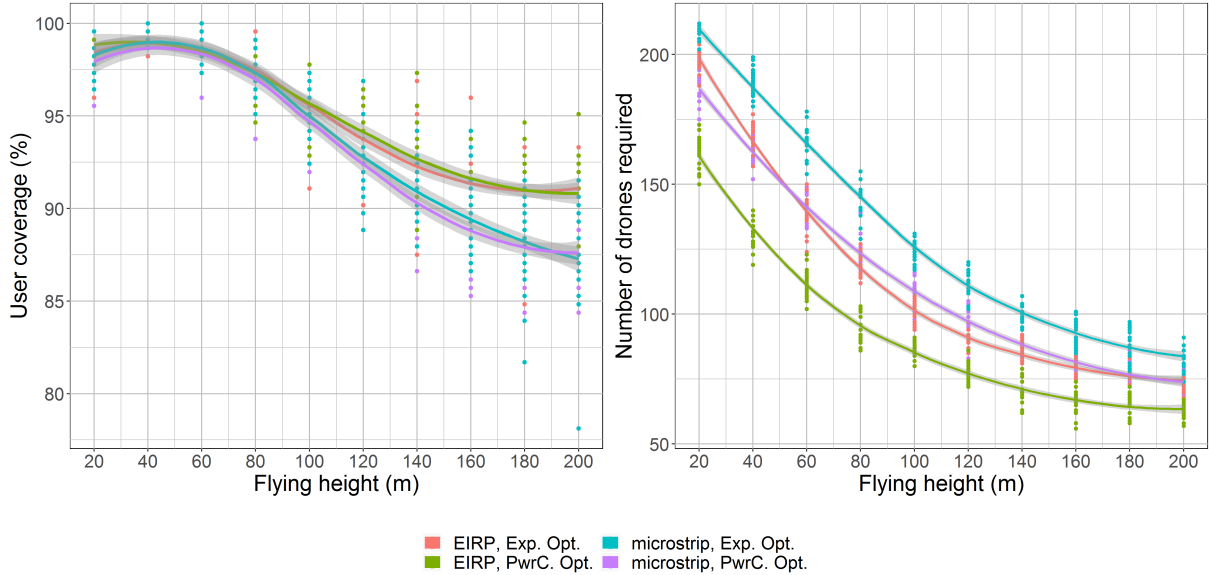


Figure 5.17: This graph shows how much UAVs are required at different flying heights while trying to achieve a 100% coverage.

did in Scenario I (fig. 5.2).

We can see from figure 5.18 that once the flying altitude surpasses the NLOS of the buildings, around 70 to 80 metres, the SAR from the serving UABS remains more or less constant for all configurations. The  $SAR^{myUABS}$  varies for flying heights between 80 and 200 metres around  $160 \text{ nW/kg}$  for microstrip PwrC Opt networks and around  $98 \text{ nW/kg}$  for microstrip Exp Opt and EIRP PwrC Opt networks. An EIRP Exp Opt network is situated around  $47 \text{ nW/kg}$ .

When looking at the exposure from ‘other UABSs’, an increase in electromagnetic radiation at higher flying altitudes is noticed. The lower path loss from less obstructing buildings will be the reason. The figures from 5.18 clearly show that this increase in electromagnetic radiation will be less for a microstrip patch antenna. The reason behind this is that energy will be more focused towards the ground and there is less sideways radiation because of attenuation. The results show that by raising the flying altitude from 20 to 200 metres, the  $SAR^{otherUABS}$  will increase between  $115$  and  $140 \text{ nW/kg}$  for EIRP antennae and between  $54$  and  $74 \text{ nW/kg}$  for microstrip patch antennae.

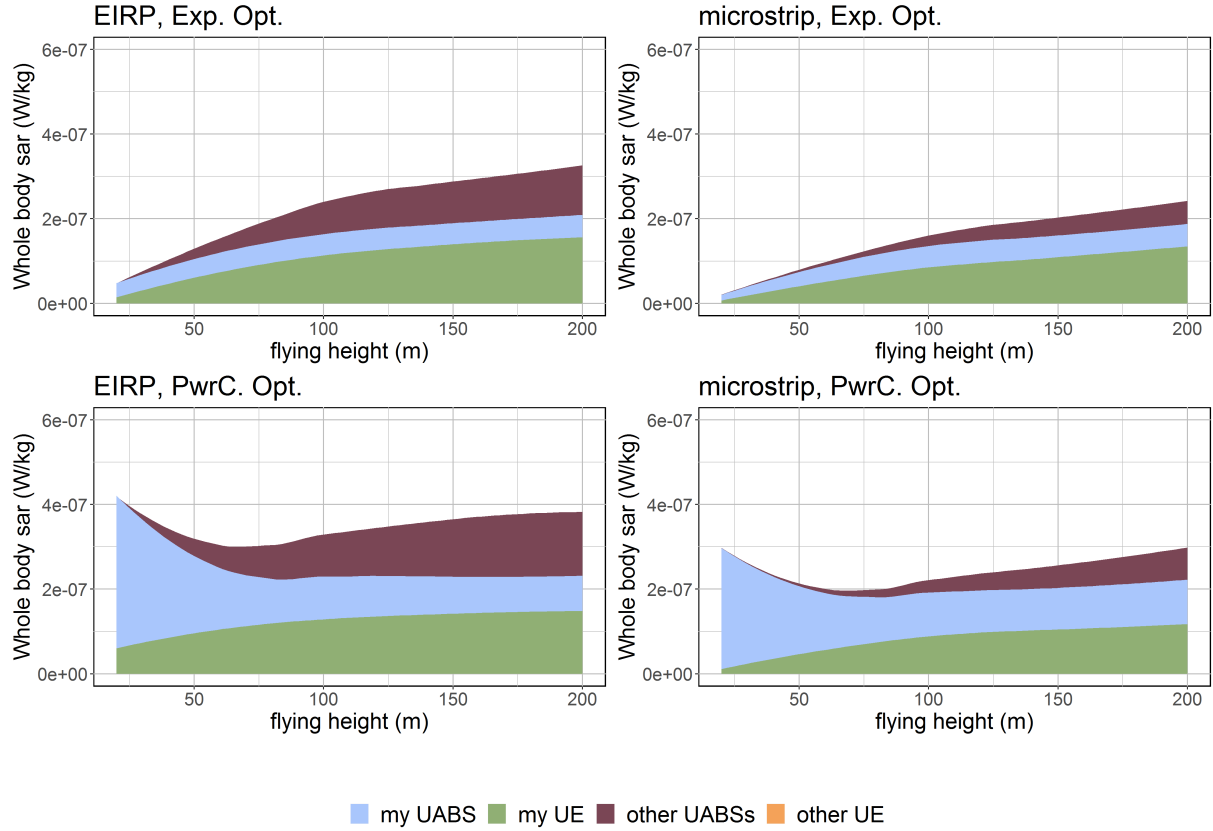


Figure 5.18: Each figure corresponds with a certain configuration and shows how the SAR from different sources are influenced by an increasing flying height.

### 5.3.2 Influence of the Number of Users

The second evaluated parameter of scenario III is a variable number of users while the flying height is fixed to 100 metres. Figure 5.19.a shows how the tool tries to reach a 100% coverage. The percentage of covered users is slightly less for smaller networks. For only 50 users, an average coverage of around 93% is achieved while a network with 600 users has a coverage of around 97%. Figure 5.19.b shows how the tool requires more UAVs for these large populations. The difference in optimization strategy is very little for a small amount of people but increases very quickly. When the population increases from 50 to 600 users, 200 more UABSSs are required by a microstrip Exp Opt network around 130 more UABSSs for an EIRP Exp Opt network or a microstrip PwrC Opt network and 110 more UABSSs for an EIRP PwrC Opt network. This is an expected behaviour when looking at scenario II where, with only one UABS available, the percentage of covered users decreases for these larger populations.

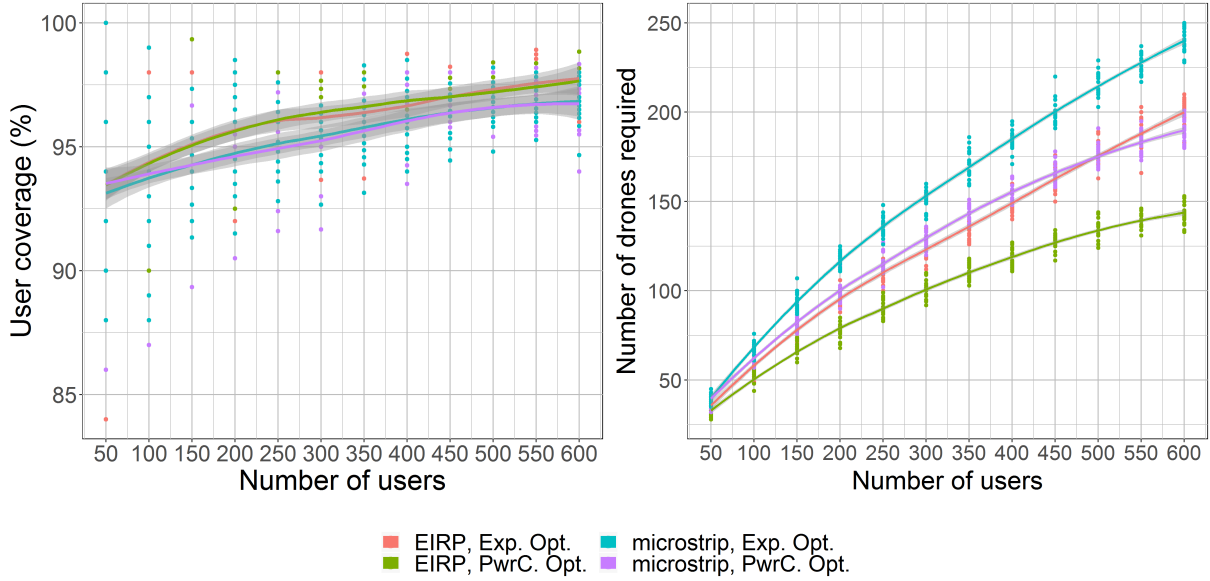


Figure 5.19: This graph shows how much UAVs are required for different flying heights while trying to achieve a 100% coverage.

Figure 5.20 shows that the electromagnetic radiation and power consumption increase for larger populations which is normal since more drones will be available. When the population increases from 50 to 600 users, the electromagnetic radiation increases between 80 and 130 mV/m depending on the configuration. The power consumption with 50 users is for all configurations around 20 W. Once the population is increased to 600 users, a microstrip Exp Opt network will require 130 W, a microstrip PwrC Opt network requires 117 W, EIRP Exp Opt networks require 107 W and EIRP PwrC Opt network requires 92 W.

The correct behaviour of the decision algorithm became already clear in the previous subsection 5.3.1 but is also confirmed here. When comparing both optimization strategies, a power consumption optimized network requires around 5 W less but exposes its users between 27 mV/m and 30 mV/m more than exposure optimized networks. Further, it is also noticed that equivalent isotropic radiators cause more electromagnetic radiation for less energy compared to microstrip patch antennae. When comparing the two types of antennae for a default number of 224 users, an equivalent isotropic radiator will expose the average user between 25 mV/m and 27 mV/m more while requiring around 12 W less than when the network would be using a microstrip patch antennae.

This means that scenario III confirms that a power consumption optimized network indeed results in less UAVs and a lower power consumption for the entire network. At the same time, scenario II showed that the active UABSS have a higher individual power consumption. We can therefore state that a power consumption optimized network will reduce its total power

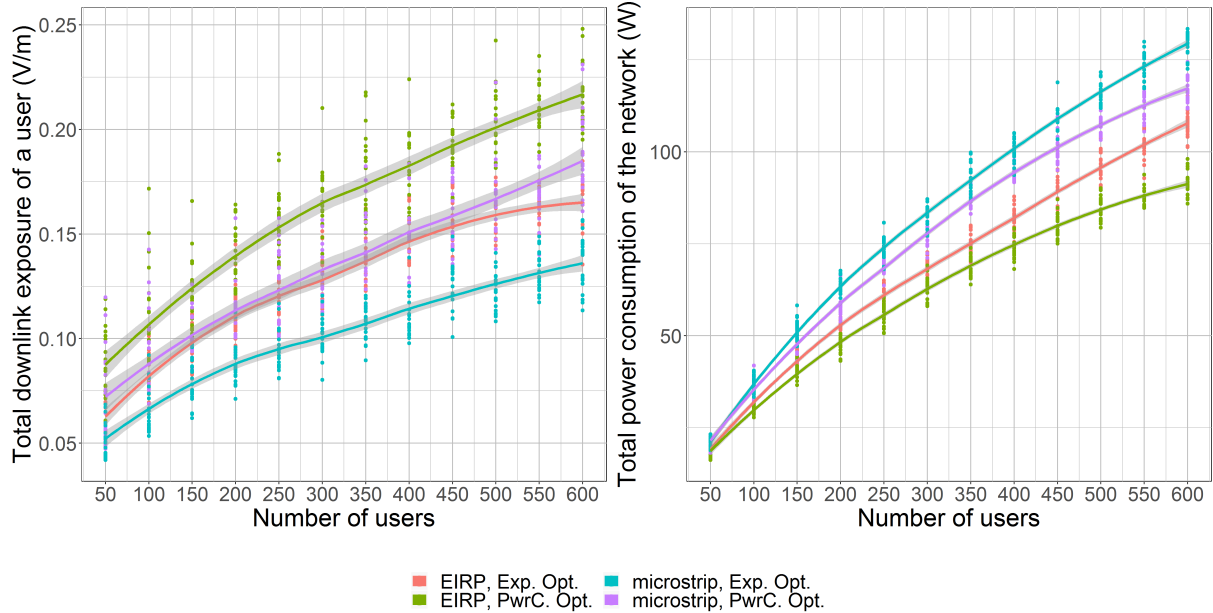


Figure 5.20: The influence of the population size on the downlink electromagnetic radiation (a) and power consumption (b).

consumption by using a few high powered UAVs. Likewise for an exposure optimized network, we can conclude that the network has indeed a lower electromagnetic exposure but the power consumption of the entire network is much higher. In scenario II became already clear that the active UABSs have a low power consumption in order to guarantee a low electromagnetic exposure towards the users. We can conclude that an exposure optimized network will reduce the exposure of an individual by deploying several low powered UABSs.

Figure 5.21 shows how the  $SAR^{ownUE}$  remains almost constant which is normal since the flying height remains the same and will vary between  $0.7 \mu W/kg$  and  $1.2 \mu W/kg$ . The  $SAR^{myUABS}$  barely increases in an exposure optimized network and is situated around  $0.5 \mu W/kg$  for both antennae. The power consumption optimized network also starts around  $0.5 \mu W/kg$  but increases when more users become online. A normal behaviour when considering that these UABSs try to cover much more users. Therefore, the  $SAR^{myUABS}$  with 600 users increases up to  $2 \mu W/kg$  depends on the configuration. The SAR value that increases the most is  $SAR^{otherUABS}$  which starts really low with less than  $0.1 \mu W/kg$  for 50 users for all configurations. The SAR increases however very fast. The biggest increase is noticed in an EIRP PwrC Opt network where  $3 \mu W/kg$  is measured for 600 users. The  $SAR^{otherUE}$  increases the least for microstrip Exp Opt with only  $1 \mu W/kg$  for 600 users.

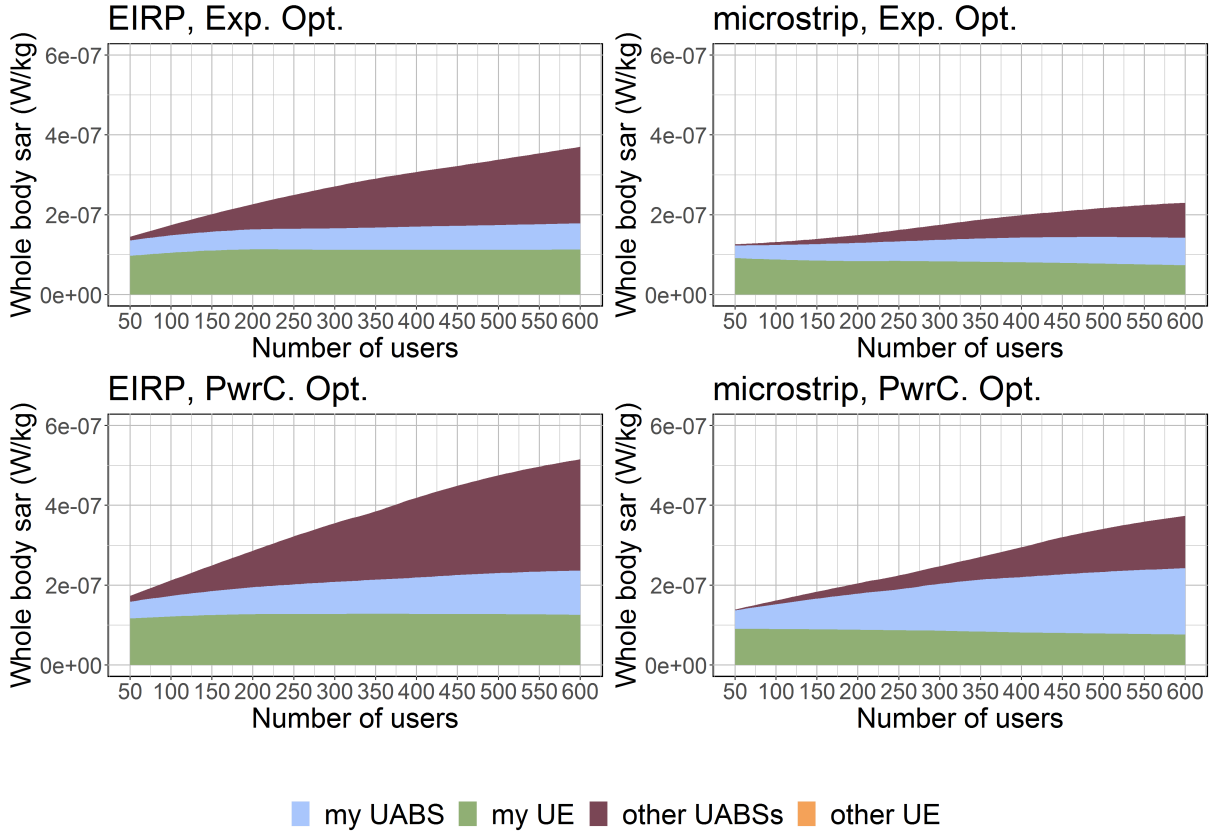


Figure 5.21: Each figure corresponds with a certain configuration and shows how the SAR from different sources are influenced by an increasing population density. An unlimited number of UABSs is available.

## 5.4 Summary

This chapter discusses the achieved results when applying the tool to the different scenarios. Scenario I concludes that the required transmission power increases logarithmically with the flying height. The results show how the user's device is the main source of electromagnetic radiation for all flying heights above 80 metres and grows exponentially along with the flying height. On the other hand, the electromagnetic radiation from the UABS remains constant around  $10 \text{ nW/kg}$ . Scenario II shows that electromagnetic exposure drops when the population size increases or when the flying height decreases and a lower user exposure corresponds with lower coverage. Users that are covered are, just like in scenario I, mainly exposed to their own device, followed by the UABS in second place. The results also show that the power consumption slightly increases when the UABS covers more users. The last scenario shows that less UABSs are required for higher flying altitudes and therefore result in a decreased power consumption. Exposure from the serving UABS remains almost constant above 80 meters while exposure

from other UABSs and UE increases. Scenario III also shows that more UABSs are required for larger populations and therefore increase power consumption and electromagnetic exposure. Finally, the results also confirm that the optimization algorithm works as intended and is able to optimize towards either electromagnetic exposure or overall power consumption.

# 6

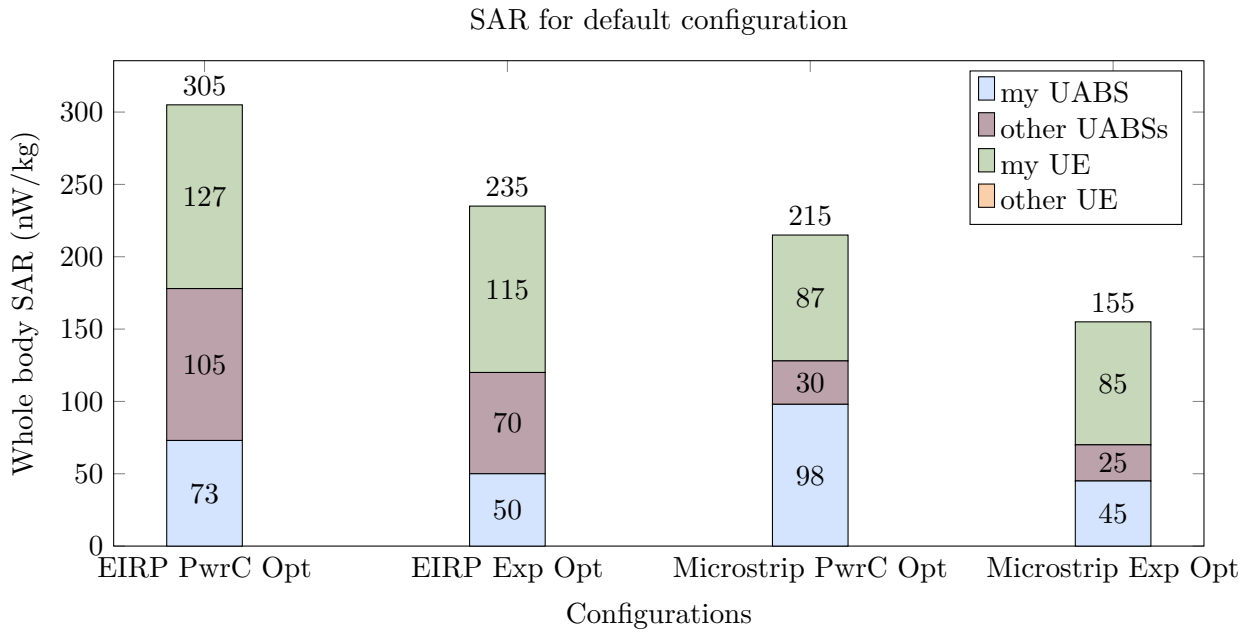
## Conclusions

The following section presents the conclusion where the impact of the flying height and users population in a UAV-aided network is investigated by examining electromagnetic exposure and power consumption. Also, optimization techniques towards both evaluation parameters have been applied and two different antenna types have been considered. All conclusions are based on the default configuration with a flying height of 100 metres and 224 active users to cover. The other parameters are described in table 4.1.

### 6.1 Conclusion

Literature showed that a network can be optimized towards either the power consumption of the entire network or the electromagnetic exposure of the average user using a fitness function. This is because the power required to activate a new base station is much higher than for raising the electromagnetic radiation and therefore increasing its range [17]. The fitness function was originally applied for fixed transmission towers but can also be used for UABSs as this research shows. However, the fitness function should be used with care considering that UABSs can be placed anywhere as opposed to the transmission towers from [17] who have a predetermined position. For default networks, the electromagnetic field radiation from a power consumption optimized network can be reduced up to 23% for equivalent isotropic radiators and 30% for

microstrip patch antennae by optimizing towards electromagnetic exposure. Doing so, decreases the range of the UABS and much more UABSSs will be needed. Therefore, exposure optimized networks will, on average, use 18 drones more than power consumption optimized networks and require therefore 5 W more energy. A power consumption optimized network on the other hand will try to limit the number of drones in order to save energy. So as a rule of thumb: an exposure optimized network will result in a lot of low powered devices (increasing the overall power consumption) while a power consumption optimized network results in a few high powered devices (increasing the exposure of the average user). The authors from [20] confirm this by stating that smaller cells will reduce electromagnetic radiation. If the goal is to remain in the air for a longer period of time, an exposure optimized network is recommended because the power consumption of an individual UABS is lower. On the other hand, a power consumption optimized network is cheaper because less drones are involved. Moreover, the results show that the electromagnetic radiation in a power consumption optimized network (with high powered UABSSs) is far below the thresholds enforced by the Flemish government with more than one millionth of the maximal allowed whole body SAR.



A directional microstrip patch antenna is introduced because it gives several advantages compared to omnidirectional antennae. Directional antennae are able to focus their energy there where it is needed, namely towards the ground. Microstrip patch antennae further benefit from their thin and lightweight design. The performance of this directional microstrip patch antenna has been compared to a fictional equivalent isotropic radiator. This equivalent isotropic radiator has higher exposure and coverage for less power compared to a microstrip patch antenna. For a default network, a microstrip patch antenna can reduce between 30% and 34% electromagnetic exposure from an equivalent isotropic radiator. Doing so will increase the power consumption

with 11 W. The fact that an equivalent isotropic radiator has higher electromagnetic exposure for less power is due to the absence of attenuation and can hypothetically be compared to an antenna with a very big aperture angle. A microstrip patch antenna with a more limited aperture angle of 90° requires more resources but causes less sideways radiation. So the exposure from other UABSs will also be less.

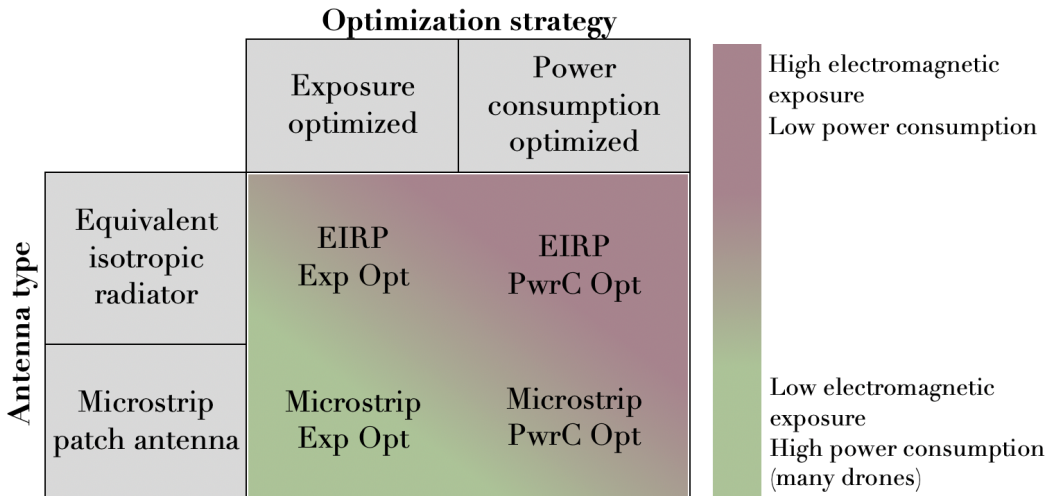


Figure 6.1: Matrix with the four possible configurations, colour-coded based on the results.

Figure 6.1 shows an overview based on the results from the two optimization strategies and the two types of antenna. Remarkable is that an EIRP exposure optimized network behaves very similar to a microstrip power consumption optimized network. Therefore, the microstrip patch antenna in a power consumption optimized network is recommended. The microstrip patch antenna will generate less electromagnetic radiation by design and the power consumption optimization reduces the number of required drones and power. A microstrip patch antenna with an aperture angle of 90° is considered as a good solution but if budget is more limited, an antenna with a larger aperture angle would further reduce cost without interfering with the Flemish legislation regarding electromagnetic exposure.

Figure 6.2 gives an overview of the contribution of SAR in percentage to the total exposure for a default network. The values have been averaged over all four possible configurations. The user's main source of exposure is clearly the user's own device which contributes 52% of the total experienced exposure. A conclusion that was also made by the authors of [20] where a 5G network is simulated and by the authors from [28] where a GSM and UMTS network is simulated. However, in [28] is also concluded that, thanks to power control, the electromagnetic radiation from the mobile phone comes really close to the exposure from the UABS. Also this is confirmed by the results. Figure 6.2 shows that the electromagnetic exposure from all UABSs together covers the remaining 48% of which 15 % is from the serving UABS. The electromagnetic exposure from devices belonging to other people can be ignored compared to the much higher

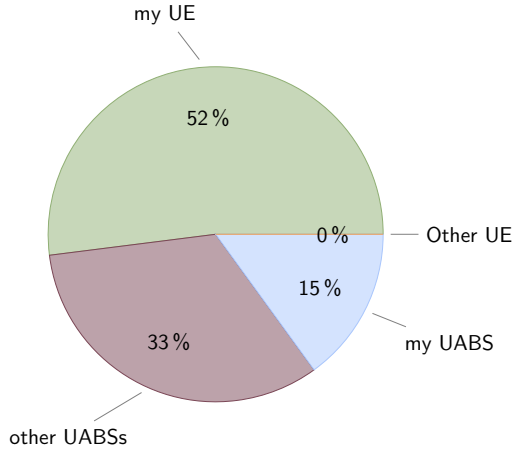


Figure 6.2: Contribution from each source towards the total SAR that is experienced by the weighted average user. The percentages are averaged over the four considered configurations.

electromagnetic exposure from the other sources and contributes only 0.0001%. It is important to notice that a rather low PUSCH value is used in equation 3.21 for determining the UL radiation and it is believed that a higher value will have a major effect on the SAR from the user's own device but also from neighbouring devices.

As last, the results confirm that the flying height and population size has a major influence on electromagnetic exposure and power consumption. It becomes clear that more UABSs are required when the population size increases. This comes with a higher power consumption and electromagnetic exposure. When the population increases from 50 to 600 users, the electromagnetic radiation increases between 80 and 130  $mV/m$  depending on the configuration. The power consumption increases with 110 W for all configurations. The main source that is influenced by the number of users is the SAR from other UABSs with an increase between 1 and 3  $\mu W/kg$ , depending on the configuration. Further, increasing the flying altitude has a positive influence on the number of required drones which on his turn has a positive influence on power consumption. Increasing the flying altitude from 50 m to 200 m, decreases the number of required drones around 59%. This decrease in number of UABSs was also concluded in [32]. Also authors from [20] made the conclusion that reduced path loss decreases electromagnetic exposure. The electromagnetic radiation from the UABSs does not change for flying altitudes between 80 and 200 metres. Most UABSs are in LOS and no more power will be used thanks to power control. However, the electromagnetic radiation from the user's own device does increase in order to reach the high flying drones. Around 80 metres, the exposure from the user's device surpasses the exposure from the serving UABS. When more UABSs are available in the network, electromagnetic exposure from other UABS will increase as well because more UABSs come into LOS. Raising the flying altitude from 50 to 200 m will increase the SAR from other UABSs between 49 and 46 times when using a EIRP antenna and between 70 and 85 times when using

a for microstrip patch antenna. It is therefore concluded that raising the flying height has a positive but is not unlimited. When also considering the results from [33] where a flying altitude of 80 metres is suggested for an optimal access and backhaul connectivity, a flying height of 80 metres is also here proposed for the city centre of Ghent.

## 6.2 Summary

The microstrip patch antenna with an aperture angle of  $90^\circ$  is a suitable starting point for an antenna. This directional antenna focusses electromagnetic radiation where it is needed. Unwanted sideways radiation is therefore reduced by design. The sufficiently large aperture angle covers enough users. The antenna is recommended to be deployed in a power consumption optimized network since less drones are required and therefore also less expensive. The optimal flying height for the city center of Ghent is believed to be situated at 80 metres since lower flying heights require much more UABS and higher flying heights has a negative influence on the electromagnetic exposure.

## 6.3 Future work

Despite the fact the many parameters has been examined, still some parameters require further investigations. The PUSCH value defines the minimal required signal strength received by the UABS and still need to be evaluated for different values. Also, the exposure caused by backhaul links has not been evaluated yet.

The chosen microstrip patch antenna is solely based on literature and performing an excessive research to various types of radiation patterns is outside the scope of this master dissertation. It is expected that the radiation can further be improved by using microstrip patch antennae in more complex array-configurations.

The tool provide support for any possible radiation pattern and applies this to any UABS. However, despite some minor changes, each UABS can has it's custom radiation pattern which makes 3D beamforming possible. Therefore, electromagnetic exposure can be determined for base stations where MiMo and massive MiMo is in use.

Also, the tool makes use of an exact algorithm. Despite the fact that several tactics have been introduced to improve performance, large populations still cause long runtimes. It might be useful to reduce the quality of the result in order to improve performance. Mozafari et al. discusses in [34] several other approaches besides exact algorithms like heuristic methods, machine learning and so on.

## Bibliography

- [1] “kaart van mobiel netwerkbereik.” <https://www.test-aankoop.be/hightech/gsms-en-smartphones/module/kaart-van-mobiel-netwerkbereik>. Accessed: 03-03-2020.
- [2] “Vijf jaar geleden sloeg het noodlot toe op pukkelpop,” *Het nieuwsblad*, 2016.
- [3] “Base overschreed stralingsnormen na aanslagen,” *De standaard*, 2019.
- [4] L. Hardell and C. Sage, “Biological effects from electromagnetic field exposure and public exposure standards,” *Biomedicine and Pharmacotherapy*, vol. 62, no. 2, pp. 104 – 109, 2008.
- [5] “What are electromagnetic fields.” <https://www.who.int/peh-emf/about/WhatisEMF/en/index1.html>. Accessed: 15-10-2019.
- [6] “Elektromagnetische velden en gezondheid: Uw wegwijzer in het elektromagnetische landschap,” *Federale overheidsdienst: volksgezondheid, veiligheid van de voedselketen en leefmilieu*, vol. 5, 2014.
- [7] “Normen zendantennes.” <https://omgeving.vlaanderen.be/normen-zendantennes>. Accessed: 19-03-2020.
- [8] A. Ahlbom, U. Bergqvist, J. Bernhardt, J. Cesarini, M. Grandolfo, M. Hietanen, A. McKinlay, M. Repacholi, D. H. Sliney, J. A. Stolwijk, *et al.*, “Guidelines for limiting exposure to time-varying electric, magnetic, and electromagnetic fields (up to 300 ghz),” *Health physics*, vol. 74, no. 4, pp. 494–521, 1998.
- [9] W. H. Bailey, R. Bodemann, J. Bushberg, C.-K. Chou, R. Cleveland, A. Faraone, K. R. Foster, K. E. Gettman, K. Graf, T. Harrington, *et al.*, “Synopsis of ieee std c95. 1<sup>TM</sup>-2019 “ieee standard for safety levels with respect to human exposure to electric, magnetic, and electromagnetic fields, 0 hz to 300 ghz”,” *IEEE Access*, vol. 7, pp. 171346–171356, 2019.
- [10] E. Commission, “Council recommendation of 12 july 1999 on the limitation of exposure of the general public to electromagnetic fields (0 hz to 300 ghz),” *Official Journal of the European Communities*, vol. 59, 1999.

- [11] “Wireless devices.” <https://www.health.belgium.be/en/wireless-devices>. Accessed: 13-05-2020.
- [12] A.-K. Lee, S.-E. Hong, M. Taki, K. Wake, and H. Do Choi, “Comparison of different sar limits in sam phantom for mobile phone exposure,” in *2018 Asia-Pacific Microwave Conference (APMC)*, pp. 687–689, IEEE, 2018.
- [13] “iphone 11 pro rf exposure information.” <https://www.apple.com/legal/rfexposure/iphone12,3/en/>. Accessed: 13-05-2020.
- [14] “Sar information.” <https://www.samsung.com/sar/sarMain>. Accessed: 13-05-2020.
- [15] “Bundesamt für strahlenschutz.” [http://www.bfs.de/SiteGlobals/Forms/Suche/BfS/EN/SARsuche\\_Formular.html](http://www.bfs.de/SiteGlobals/Forms/Suche/BfS/EN/SARsuche_Formular.html). Accessed: 14-10-2019.
- [16] D. Plets, W. Joseph, K. Vanhecke, and L. Martens, “Exposure optimization in indoor wireless networks by heuristic network planning,” *Progress In Electromagnetics Research*, vol. 139, pp. 445–478, 01 2013.
- [17] M. Deruyck, E. Tanghe, D. Plets, L. Martens, and W. Joseph, “Optimizing lte wireless access networks towards power consumption and electromagnetic exposure of human beings,” *Computer Networks*, vol. 94, 12 2015.
- [18] D. Plets, W. Joseph, S. Aerts, K. Vanhecke, G. Vermeeren, and L. Martens, “Prediction and comparison of downlink electric-field and uplink localised sar values for realistic indoor wireless planning,” *Radiation Protection Dosimetry*, vol. 162, no. 4, pp. 487–498, 2014.
- [19] D. Plets, W. Joseph, K. Vanhecke, and L. Martens, “Downlink electric-field and uplink sar prediction algorithm in indoor wireless network planner,” in *The 8th European Conference on Antennas and Propagation (EuCAP 2014)*, pp. 2457–2461, IEEE, 2014.
- [20] S. Kuehn, S. Pfeifer, B. Kochali, and N. Kuster, “Modelling of total exposure in hypothetical 5g mobile networks for varied topologies and user scenarios,” *Final Report of Project CRR-816, Available on line at: https://tinyurl. com/r6z2gqn*, 2019.
- [21] D. Plets, W. Joseph, K. Vanhecke, G. Vermeeren, J. Wiart, S. Aerts, N. Varsier, and L. Martens, “Joint minimization of uplink and downlink whole-body exposure dose in indoor wireless networks,” *BioMed research international*, vol. 2015, 2015.
- [22] Z. Mahfouz, A. Gati, D. Lautru, J. Wiart, and V. F. Hanna, “Sar assessment and analysis of cumulative body exposure to multi transmitters from a mobile phone,” in *2012 IEEE Topical Conference on Biomedical Wireless Technologies, Networks, and Sensing Systems (BioWirelessS)*, pp. 77–80, IEEE, 2012.
- [23] C. Lazarescu, I. Nica, and V. David, “Sar in human head due to mobile phone exposure,” in *2011 E-Health and Bioengineering Conference (EHB)*, pp. 1–4, IEEE, 2011.

- [24] G. Bit-Babik and A. Faraone, "Standardization of sar simulation techniques for rf exposure compliance in and around vehicles," in *2013 7th European Conference on Antennas and Propagation (EuCAP)*, pp. 1984–1986, IEEE, 2013.
- [25] E. Piuzzi, P. Bernardi, M. Cavagnaro, S. Pisa, and J. C. Lin, "Analysis of adult and child exposure to uniform plane waves at mobile communication systems frequencies (900 mhz–3 ghz)," *IEEE transactions on electromagnetic compatibility*, vol. 53, no. 1, pp. 38–47, 2010.
- [26] A. Hirata, O. Fujiwara, T. Nagaoka, and S. Watanabe, "Variability of whole-body average sar in human models for far-field exposures," in *2008 Asia-Pacific Microwave Conference*, pp. 1–4, IEEE, 2008.
- [27] T. Shiina and K. Yamazaki, "Assessment of human exposure to radiofrequency electromagnetic fields in the vicinity of smart meter at 920 mhz and 2.45 ghz," in *2019 Joint International Symposium on Electromagnetic Compatibility, Sapporo and Asia-Pacific International Symposium on Electromagnetic Compatibility (EMC Sapporo/APEMC)*, pp. 744–747, IEEE, 2019.
- [28] A. Gati, E. Conil, M.-F. Wong, and J. Wiart, "Duality between uplink local and down-link whole-body exposures in operating networks," *IEEE transactions on electromagnetic compatibility*, vol. 52, no. 4, pp. 829–836, 2010.
- [29] Y. Zeng, Q. Wu, and R. Zhang, "Accessing from the sky: A tutorial on uav communications for 5g and beyond," *Proceedings of the IEEE*, vol. 107, no. 12, pp. 2327–2375, 2019.
- [30] Y. Kawamoto, H. Nishiyama, N. Kato, F. Ono, and R. Miura, "Toward future unmanned aerial vehicle networks: Architecture, resource allocation and field experiments," *IEEE Wireless Communications*, vol. 26, no. 1, pp. 94–99, 2018.
- [31] R. Gangula, O. Esrafilian, D. Gesbert, C. Roux, F. Kaltenberger, and R. Knopp, "Flying robots: First results on an autonomous uav-based lte relay using open airinterface," in *2018 IEEE 19th International Workshop on Signal Processing Advances in Wireless Communications (SPAWC)*, pp. 1–5, IEEE, 2018.
- [32] M. Deruyck, J. Wyckmans, W. Joseph, and L. Martens, "Designing uav-aided emergency networks for large-scale disaster scenarios," *EURASIP Journal on Wireless Communications and Networking*, vol. 2018, 12 2018.
- [33] G. Castellanos, M. Deruyck, L. Martens, and W. Joseph, "Performance evaluation of direct-link backhaul for uav-aided emergency networks," *Sensors*, vol. 19, no. 15, p. 3342, 2019.
- [34] M. Mozaffari, W. Saad, M. Bennis, Y.-H. Nam, and M. Debbah, "A tutorial on uavs for wireless networks: Applications, challenges, and open problems," *IEEE communications surveys & tutorials*, vol. 21, no. 3, pp. 2334–2360, 2019.

- [35] M. Mozaffari, A. T. Z. Kasgari, W. Saad, M. Bennis, and M. Debbah, "Beyond 5g with uavs: Foundations of a 3d wireless cellular network," *IEEE Transactions on Wireless Communications*, vol. 18, no. 1, pp. 357–372, 2018.
- [36] M. Deruyck, A. Marri, S. Mignardi, L. Martens, W. Joseph, and R. Verdone, "Performance evaluation of the dynamic trajectory design for an unmanned aerial base station in a single frequency network," in *2017 IEEE 28th Annual International Symposium on Personal, Indoor, and Mobile Radio Communications (PIMRC)*, pp. 1–7, IEEE, 2017.
- [37] H. Huang and A. V. Savkin, "A method for optimized deployment of unmanned aerial vehicles for maximum coverage and minimum interference in cellular networks," *IEEE Transactions on Industrial Informatics*, vol. 15, no. 5, pp. 2638–2647, 2018.
- [38] A. V. Savkin and H. Huang, "Deployment of unmanned aerial vehicle base stations for optimal quality of coverage," *IEEE Wireless Communications Letters*, vol. 8, no. 1, pp. 321–324, 2018.
- [39] Q. Wu, L. Liu, and R. Zhang, "Fundamental trade-offs in communication and trajectory design for uav-enabled wireless network," *IEEE Wireless Communications*, vol. 26, no. 1, pp. 36–44, 2019.
- [40] C. T. Cicek, H. Gultekin, B. Tavli, and H. Yanikomeroglu, "Uav base station location optimization for next generation wireless networks: Overview and future research directions," in *2019 1st International Conference on Unmanned Vehicle Systems-Oman (UVS)*, pp. 1–6, IEEE, 2019.
- [41] J. Wyckmans, W. p. v. Joseph, and L. c. v. Martens, "Emergency ad hoc networks through mobile base stations," 2016.
- [42] A. Rizwan, D. Biswas, and V. Ramachandra, "Impact of uav structure on antenna radiation patterns at different frequencies," in *2017 IEEE International Conference on Antenna Innovations & Modern Technologies for Ground, Aircraft and Satellite Applications (iAIM)*, pp. 1–5, IEEE, 2017.
- [43] Y. Zheng, J. Zhou, W. Wang, and M. Chen, "A low-profile broadband circularly polarized antenna array for uav ground-to-air communication," in *2018 IEEE Asia-Pacific Conference on Antennas and Propagation (APCAP)*, pp. 219–220, IEEE, 2018.
- [44] C. Sairam, T. Khumanthem, S. Ahirwar, and S. Singh, "Broadband blade antenna for airborne applications," in *2011 Annual IEEE India Conference*, pp. 1–4, IEEE, 2011.
- [45] B. A. Arand, R. Shamsaei, and B. Yektakhah, "Design and fabrication of a broadband blade monopole antenna operating in 30 mhz–600 mhz frequency band," in *2013 21st Iranian Conference on Electrical Engineering (ICEE)*, pp. 1–3, IEEE, 2013.

- [46] M. Nosrati, A. Jafargholi, R. Pazoki, and N. Tavassolian, “Broadband slotted blade dipole antenna for airborne uav applications,” *IEEE Transactions on Antennas and Propagation*, vol. 66, no. 8, pp. 3857–3864, 2018.
- [47] M. Nosrati, A. Jafargholi, and N. Tavassolian, “A broadband blade dipole antenna for uav applications,” in *2016 IEEE International Symposium on Antennas and Propagation (APSURSI)*, pp. 1777–1778, IEEE, 2016.
- [48] L. Akhoondzadeh-Asl, J. Hill, J.-J. Laurin, and M. Riel, “Novel low profile wideband monopole antenna for avionics applications,” *IEEE transactions on antennas and propagation*, vol. 61, no. 11, pp. 5766–5770, 2013.
- [49] M. Park and J. Jung, “An analysis of communication performance according to antenna directionality in uav operation environment,” in *2010 2nd IEEE International Conference on Network Infrastructure and Digital Content*, pp. 854–857, IEEE, 2010.
- [50] I. Singh and V. Tripathi, “Micro strip patch antenna and its applications: a survey,” *Int. J. Comp. Tech. Appl.*, vol. 2, no. 5, pp. 1595–1599, 2011.
- [51] K. Kashwan, V. Rajeshkumar, T. Gunasekaran, and K. S. Kumar, “Design and characterization of pin fed microstrip patch antennae,” in *2011 Eighth International Conference on Fuzzy Systems and Knowledge Discovery (FSKD)*, vol. 4, pp. 2258–2262, IEEE, 2011.
- [52] S. S. Siddiq, G. Karthikeya, T. Tanjavur, and N. Agnihotri, “Microstrip dual band millimeter-wave antenna array for uav applications,” in *2016 21st International Conference on Microwave, Radar and Wireless Communications (MIKON)*, pp. 1–4, IEEE, 2016.
- [53] X. Sun, R. Blázquez-García, A. García-Tejero, J. M. Fernández-González, M. Burgos-García, and M. Sierra-Castañer, “Circular array antenna tor uav-uav communications,” in *2017 11th European Conference on Antennas and Propagation (EUCAP)*, pp. 2025–2028, IEEE, 2017.
- [54] A. Sudarsan and A. Prabhu, “Design and development of microstrip patch antenna,” *International Journal of Antennas (JANT) Vol*, vol. 3, 2017.
- [55] T. K. Sarkar, Zhong Ji, Kyungjung Kim, A. Medouri, and M. Salazar-Palma, “A survey of various propagation models for mobile communication,” *IEEE Antennas and Propagation Magazine*, vol. 45, no. 3, pp. 51–82, 2003.
- [56] “Specific absorption rate (sar) for cellular telephones.” <https://www.fcc.gov/general/specific-absorption-rate-sar-cellular-telephones>. Accessed: 27-03-2020.
- [57] A. Christ, M.-C. Gosselin, M. Christopoulou, S. Kühn, and N. Kuster, “Age-dependent tissue-specific exposure of cell phone users,” *Physics in Medicine & Biology*, vol. 55, no. 7, p. 1767, 2010.

- [58] P. Joshi, D. Colombi, B. Thors, L.-E. Larsson, and C. Törnevik, “Output power levels of 4g user equipment and implications on realistic rf emf exposure assessments,” *IEEE Access*, vol. 5, pp. 4545–4550, 2017.
- [59] R. Mullner, C. F. Ball, K. Ivanov, J. Lienhart, and P. Hric, “Contrasting open-loop and closed-loop power control performance in utran lte uplink by ue trace analysis,” in *2009 IEEE International Conference on Communications*, pp. 1–6, IEEE, 2009.
- [60] M. Lauridsen, A. R. Jensen, and P. Mogensen, “Reducing lte uplink transmission energy by allocating resources,” in *2011 IEEE Vehicular Technology Conference (VTC Fall)*, pp. 1–5, 2011.
- [61] N. Bhatia *et al.*, “Survey of nearest neighbor techniques,” *arXiv preprint arXiv:1007.0085*, 2010.
- [62] S. Dhanabal and S. Chandramathi, “A review of various k-nearest neighbor query processing techniques,” *International Journal of Computer Applications*, vol. 31, no. 7, pp. 14–22, 2011.
- [63] J. L. Bentley, “Multidimensional binary search trees used for associative searching,” *Communications of the ACM*, vol. 18, no. 9, pp. 509–517, 1975.

# Appendices

# A

## Radiation Patterns: Datasheet

Table A.1 gives an overview of the attenuation in the E and H plane. The first radiation pattern has a square groundplane with an edge of 0.060 meter while the second pattern is more of a rectangular shape with a width of 0.0524m and a length of 0.0438m. All other settings are equal as defined in 3.2.1

Table A.1: Overview of attenuation in dBm.

angle	pattern 1		pattern 2	
	E	H	E	H
0	0	0	0	0
10	-0,17	-0,14	-0.1561	-0.158
20	-0,67	-0,57	-0.5797	-0.6257
30	-1,48	-1,27	-1.263	-1.386
40	-2,57	-2,22	-2.193	-2.412
50	-3,90	-3,39	-3.357	-3.665
60	-5,40	-4,73	-4.741	-5.099
70	-7,09	-6,23	-6.337	-6.658
80	-8,82	-7,87	-8.136	-8.278
90	-10,54	-9,70	-10.11	-9.88
100	-12,20	-11,84	-12.14	-11.34
110	-13,73	-14,37	-13.81	-12.47
120	-15,04	-17,65	-14.42	-13.00
130	-16,01	-21,83	-13.72	-12.82
140	-16,47	-23,63	-12.41	-12.08
150	-16,42	-20,37	-11.15	-11.15
160	-16,05	-17,49	-10.21	-10.33
170	-15,69	-15,93	-9.683	-9.786
180	-15,54	-15,54	-9.596	-9.596
190	-15,69	-16,30	-9.963	-9.784
200	-16,05	-18,44	-10.79	-10.33
210	-16,42	-22,85	-12.07	-11.15
220	-16,47	-31,23	-13.71	-12.07
230	-16,00	-24,07	-15.25	-12.80
240	-15,03	-18,05	-15.65	-12.99
250	-13,72	-14,42	-14.3	-12.45
260	-12,20	-11,81	-12.11	-11.33
270	-10,54	-9,70	-9.882	-9.866
280	-8,82	-7,87	-7.859	-8.267
290	-7,09	-6,23	-6.069	-6.649
300	-5,40	-4,73	-4.502	-5.093
310	-3,90	-3,39	-3.154	-3.661
320	-2,57	-2,22	-2.029	-2.409
330	-1,48	-1,27	-1.138	-1.384
340	-0,67	-0,57	-0.4963	-0.6246
350	-0,17	-0,14	-1143	-0.1575

# B

## Radiation patterns: Example Configuration

In listing 2, a possible configuration for a radiation pattern is described. It is important to notice that this example configuration does not represent the used configuration in this master dissertation. The `radiationPattern`-tag consists of a `slices`-tag. This tag can contain as much slices as desired. In this example, 3 slices are defined indicated with the `attenuation`-tag. This tag contains a mandatory attribute `az` which defines the azimuth angle to which all underlying attenuation values belong. Inside the `attenuation`-tag, all attenuation values are written in a `value`-tag. Each `attenuation`-tag must contain an equal amount of `value`-tags.

The tool distributes all values equally over the  $180^\circ$  of that slice. In the example below, each `attenuation`-tag contains 10 values meaning that the exact attenuation is known every  $20^\circ$ .

The highlighted value of  $-14, 42$  is therefore measured at an azimuth angle of  $0^\circ$  and an elevation angle of  $120^\circ$  (counterclockwise).

```

1 <radiationPattern>
2   <slices>
3     <attenuation az="0">
4       <value>0</value>
5       <value>-0.5797</value>
6       <value>-2.193</value>
7       <value>-4.741</value>
8       <value>-8.136</value>
9       <value>-12.14</value>
10      <value>-14.42</value>
11      <value>-12.41</value>
12      <value>-10.21</value>
13      <value>-9.596</value>
14    </attenuation>
15    <attenuation az="90">
16      <value>0</value>
17      <value>-0.6257</value>
18      <value>-2.412</value>
19      <value>-5.099</value>
20      <value>-8.278</value>
21      <value>-11.34</value>
22      <value>-13.00</value>
23      <value>-12.08</value>
24      <value>-10.33</value>
25      <value>-9.596</value>
26    </attenuation>
27    <attenuation az="180">
28      <value>0</value>
29      <value>-0.4963</value>
30      <value>-2.029</value>
31      <value>-4.502</value>
32      <value>-7.859</value>
33      <value>-12.11</value>
34      <value>-15.65</value>
35      <value>-13.71</value>
36      <value>-10.79</value>
37      <value>-9.596</value>
38    </attenuation>
39  </slices>
40 </radiationPattern>

```

Listing 2: Example configuration of a radiation pattern.